FEATURE EXTRACTION OF MUSICAL CONTENT FOR AUTOMATIC MUSIC TRANSCRIPTION

THÈSE N^{O} 3638 (2006)

PRÉSENTÉE LE 17 OCTOBRE 2006
À LA FACULTÉ DES SCIENCES ET TECHNIQUES DE L'INGÉNIEUR
Laboratoire de traitement des signaux 3
SECTION DE GÉNIE ÉLECTRIQUE ET ÉLECTRONIQUE

ÉCOLE POLYTECHNIQUE FÉDÉRALE DE LAUSANNE

POUR L'OBTENTION DU GRADE DE DOCTEUR ÈS SCIENCES

PAR

Ruohua ZHOU

Master of Engineering, Chinese Academy of Science, Beijing, Chine
de nationalité chinoise

acceptée sur proposition du jury:

Prof. J. R. Mosig, président du jury
Dr M. Mattavelli, directeur de thèse
Prof. C. Bornand, rapporteur
Prof. M. Kunt, rapporteur
Prof. R. Rabenstein, rapporteur

ÉCOLE POLYTECHNIQUE
FÉDÉRALE DE LAUSANNE
Lausanne, EPFL
2006

ACKNOWLEDGMENTS

First of all, I wish to express my genuine gratitude and respect to Dr Marco Mattavelli, my director of the thesis. Time passes so quickly, it has been more than five years since I at the first time wrote to Dr Mattavelli and looked for a chance to pursue PhD. I also remember that he kindly welcomed me in his office and introduced me to other colleagues when I came to EPFL for the first time. I admire his broad interdisciplinary expertise. Dr Mattavelli spent much time for instructing my experiment and provided me many valuable suggestions for my thesis. He also shows me some creative ideas for future research.

I wish to express my special gratitude to Dr Giorgio Zoia. We have worked together for nearly five years. Dr Zoia is my project leader and also gives me instruction for my research work. He is a very excellent project manager and creates a nice work environment for me. I never forget that he once gave me much help. Dr Zoia introduced me into the challenging field of automatic music analysis. He spent much time on helping me improve my thesis. Thank Dr Zoia very much for his continuous support and encouragement during past several years.

I am very grateful to Prof. Daniel Mlynek. As the director of our laboratory, he makes it possible for me to work and study here. He once spent his precious time on checking my PhD work and gave me guidance. He also gave me more time for my PhD work.

I would like to express my whole-hearted gratitude to Prof. Murat Kunt, Prof. Rudolf Rabenstein, Prof. Cedric Bornand, Professor Auke Jan Ijspeert, who do me the honor of accepting to take part in the jury of my thesis. As the director of Signal Processing Institute, Prof. Murat Kunt creates a nice academic atmosphere for us. Prof. Rudolf Rabenstein once provided me useful suggestions for my PhD work. When working in STILE project, Prof. Cedric Bornand gave me much encouragement. Professor Auke Jan Ijspeert kindly accepted to be president of the jury for my oral examination.

I would like to thank Mack Vincent for his help in accomplishing the abstract of French version.

I also grateful to my colleagues: Beilu Shao, Aleksandar Simeonov, Robert Lluis Gracia, Massimo Ravasi, Graziano Varotto and Christophe Clerc, Nicolas Scaringella. And thank all the former and present colleagues in LTS3.

Finally, I am greatly grateful to my parents, sister and brother for their support and encouragement.

TABLE OF CONTENTS

ACKNOWLEDGMENTS II

TABLE OF CONTENTS IV

LIST OF FIGURES VIII

LIST OF TABLES X

ABBREVIATIONS XI

ABSTRACT XII

RESUME XIV

CHAPTER 1 INTRODUCTION 1

1.1 Definition of Automatic Music Transcription 1

1.2 Objectives 1

1.3 Motivations 1

1.4 Main Results of the Thesis 3

1.5 Organization of the Thesis 7

CHAPTER 2 TIME-FREQUENCY ANALYSIS FOR MUSIC SIGNAL: STATE OF THE ART 9

2.1 Introduction 9

2.2 STFT and Spectrogram 10

2.3 Wavelet Analysis 12

2.4 Wigner Distribution 19

2.5 Auditory Filter Bank 22

2.6 Review of Joint Time-Frequency Analysis for Music Signals 25

CHAPTER 3 LEARING THEORY: STATE OF THE ART 29

3.1 Empirical Risk Minimization and Structure Risk Minimization Inductive Principle 29

3.2 Maximum-Margin Support Vector Machine 34

3.3 Soft Margin Support Vector Machine 37

3.4 Nonlinear Support Vector Machine 38

3.5 Multi-Class Support Vector Machine 40
  3.5.1 One-against-rest Multi-class Classifier 40
  3.5.2 One-against-one Multi-class Classifier 41

CHAPTER 4 A FREQUENCY-DEPENDENT TIME-FREQUENCY ANALYSIS TOOL: RESONATOR TIME-FREQUENCY IMAGE 43

4.1 Frequency-Dependent Time-Frequency Analysis 43

4.2 Resonator Time-Frequency Image for Musical Signals 45
  4.2.1 Energy and Frequency-difference Spectrum of RTFI 49

4.3 Discrete Resonator Time-Frequency Image 52
  4.3.1 Definition of Discrete RTFI 52
  4.3.2 Implementation of Discrete RTFI 53
  4.3.3 An Example of Discrete RTFI 61
  4.3.4 Multiresolution Fast Implementation of Discrete RTFI 62
    4.3.4.1 Proposed Multiresolution Fast Implementation 62
    4.3.4.2 Comparison with other Multiresolution Fast Implementations 65

CHAPTER 5 MUSIC ONSET DETECTION 67

5.1 Introduction 67

5.2 Reviews of Related Work 68
  5.2.1 Time-Frequency Processing 69
  5.2.2 Detection Function Producing 70
    5.2.2.1 Energy-Based Detection 70
    5.2.2.2 Phase-Based Detection 71
    5.2.2.3 Pitch-Based Detection 73
    5.2.2.4 Onset Detection Using Neural Network 73

5.3 Onset Detection System 74
  5.3.1 System Overview 74
  5.3.2 Time-Frequency Processing 75
  5.3.3 Detection Algorithms and Experiments 80
    5.3.3.1 Performance Evaluation, Tuning Database and Test Database 80
    5.3.3.2 Proposed Energy-based Detection Algorithm 81
    5.3.3.3 Proposed Pitch-based Detection Algorithm 87

5.4 Results of Database 93

5.4.1 Results 93
5.4.2 Discussion 98

CHAPTER 6 INTRODUCTION TO POLYPHONIC PITCH ESTIMATION.. 101

6.1 Introduction 101

6.2 Reviews of Related Work 101
6.2.1 Auditory Model of Pitch Perception 101
6.2.2 Blackboard System 104
6.2.3 Machine-learning Methods 105
6.2.4 Iterative Methods 106
6.2.5 Estimation Using Instrument Model 108

6.3 Problems in Polyphonic Pitch Estimation 109

CHAPTER 7 A NEW POLYPHONIC PITCH ESTIMATION METHOD: METHOD I 113

7.1 System Overview 113

7.2 Time-frequency Processing Based on the RTFI Analysis 114

7.3 Extracting Harmonic Components 116

7.4 Making Preliminary Estimation of Possible Multiple Pitches 116

7.5 Cancelling Extra Pitches by Checking Harmonic Components 119

7.6 Judging the Existence of the Pitch Candidate by the Spectral Smoothing Principle 120

CHAPTER 8 A NEW POLYPHONIC PITCH ESTIMATION METHOD COMBINING SVM AND SIGNAL PROCESSING: METHOD II 123

8.1 System Overview 123

8.2 Motivation for Selecting SVM Instead of Neural Network 124

8.3 Input Vectors and SVM Training 124

CHAPTER 9 EXPERIMENTAL RESULTS OF POLYPHONIC PITCH ESTIMATION METHODS 129

9.1 Performance Evaluation Criteria 129

9.2 Training/Tuning Database and Test Database 130

9.3 Test Results on the Test Database 1 (Polyphonic Mixtures) 133
9.3.1 Test Results of Method I on Polyphonic Mixtures 133
9.3.2 Test Results of Method II on Polyphonic Mixtures 138

9.4 Automatic Music Transcription Systems 143

9.5 Results on the Real Music Excerpts 148

CHAPTER 10 CONCLUSION AND FUTURE WORK 151

10.1 Conclusion 151
  10.1.1 An Original Time-Frequency Analysis Tool: Resonator Time-Frequency Image (RTFI) 151
  10.1.2 Music Onset Detection 151
  10.1.3 Polyphonic Pitch Estimation 152

10.2 Future Work 153
  10.2.1 Special-Purpose SVM Polyphonic Estimator 153
  10.2.2 Using Temporal Features for Polyphonic Pitch Estimation 153

10.3 Potential Commercial Applications 155

REFERENCES 157

CV 165

LIST OF FIGURES

Figure 1.1 : Essential Role of the Extracted Parameters: Onset Time and Polyphonic Pitch in Music Analysis……….. ...2

Figure 2.1 : Filter bank interpretation of STFT……………………………………………………………………...12

Figure 2.2 : Critical Band ……………………………………………………………………………………...23

Figure 2.3: Notched Noise Experiment……………………………………………………………………….....23

Figure 3.1: VC Dimension………………………………………………………….………………………...31

Figure 3.2: Implementation of Structure Risk Minimization…………………………………………………………33

Figure 3.3: Maximum-margin Classifier………………………………………………………………………...34

Figure 4.1: Comparison of Filter bank implementation of STFT and FDTF ……………………………………….....44

Figure 4.2: Under-sampling, over-sampling and critical-sampling …………………………………………………...54

Figure 4.3: Block Diagram for the Proposed Multi-resolution Fast Implementation……………………………………63

Figure 5.1: A General Onset Detection System…………………………………………………………………69

Figure 5.2: Proposed Onset Detection System …… ……………………………………………………………74

Figure 5.3: Comparing the Average Energy Spectrum with Adjusted Energy Spectrum ………………………………76

Figure 5.4: Difference Pitch Energy Spectrum……………………………………………………………………...78

Figure 5.5: Normal Pitch Energy Spectrum ……………………………………………………………………79

Figure 5.6: Energy-Based Detection Algorithm………………………………………………………………......83

Figure 5.7: Energy-Based Detection of Bow Violin with soft onset…………………………………………………...86

Figure 5.8: Normal Pitch Energy Spectrum for a classic string music sample ………………………………………...88

Figure 5.9: Searching of the pitch onsets in one frequency channel……………………………………………...…89

Figure 5.10: Pitch-Based Detection Algorithm ………………………………………………………….……91

Figure 5.11: Results Comparison between the Different Detection Algorithms …………………………………..….98

Figure 5.12: Precision Comparison of the Proposed Pitch-based and Energy-based Detection Algorithms……………100

Figure 6.1: General Four-Stages Pitch Perception Model ……………………………………………………….....103

Figure 6.2: Overview of Klapuri's Iterative Method…………………………………………………………….....107

Figure 6.3: A Harmonic Enhancement Based Pitch Estimation Algorithm ……………………………………………107

Figure 6.4: Inharmonic Spectral Structure of a Piano Note……………………………………………………...110

Figure 6.5: Coinciding Harmonic Components in Two Violin Notes ………………………………………………….111

Figure 7.1: Overview of Proposed Polyphonic Pitch Estimation Algorithm I……………………………………….113

Figure 7.2: RTFI Energy Spectrum, Relative Energy Spectrum and Extracted Harmonic Components ………………115

Figure 7.3: Relative Pitch Energy Spectrum of a violin example ……………………………………………….....118

Figure 7.4: Harmonic Component Energy Spectrum of Two Piano Samples……………………………………….121
Figure 8.1: System Architecture of Proposed Polyphonic Pitch Estimation II ……………………………………....123
Figure 8.2: A SVM input spectral peak vector ……………………………………………………………………125
Figure 8.3: SVM Polyphonic Estimator ……………………………………………………………………...…...126
Figure 8.4: Training Examples of Two Note Recognizers ……………………………………………………………..127
Figure 9.1: Training /Tuning Database and Test Database…………………………………………………………...127
Figure 9.2: FMeasure of Test Results of Method I with Clean signal or Added Noise ……………………………....135
Figure 9.3: Recall of Test Results of Method I with Clean signal or Added Noise …………………………………….135
Figure 9.4: Precision of Test Results of Method I with Clean signal or Added Noise …………………………………136
Figure 9.5: NER of Test Results of Method I with Clean signal or Added Noise ……………………………………....136
Figure 9.6: CER of Test Results of Method I with Clean signal or Added Noise……………………………………137
Figure 9.7: FMeasure, Recall and Precision of Test Result of Method I with different parameter values……………...137
Figure 9.8: Note Error Rate (NER) of Test Result of Method I with different parameter values……………………….138
Figure 9.9: F-Measure of Test Results of Method II (SVM) with Clean Signal or Added Noise………………………139
Figure 9.10: Recall of Test Results of Method II (SVM) with Clean signal or Added Noise…………………………..140
Figure 9.11: Precision of Test Results of Method II (SVM) with Clean signal or Added Noise………….....................140
Figure 9.12: NER of Test Results of Method II (SVM) with Clean signal or Added Noise……………………………141
Figure 9.13: CER of Test Results of Method II (SVM) with Clean signal or Added Noise…………………………….141
Figure 9.14: F-Measure, Recall and Precision of Method II (SVM) with different parameter values…………………..142
Figure 9.15: Note Error Rate (NER) of Test Result of Method II (SVM) with different parameter values…………… 143
Figure 9.16: Automatic Music Transcription System Using Method I……………………....……………….. ………..144
Figure 9.17: Automatic Music Transcription System Using the Method II ……………………………………………145
Figure 9.18: Time-Pitch Probability Output of a Piano Example ………………………………………... …………147
Figure 10.1: Energy Changes of Harmonic Components ……………………………...…………………………….154

LIST OF TABLES

Table 4.1 Fast Implementation of RTFI……………………………. ………………………………… ………….65

Table 5.1: Tuning Database…………………………………………………………………..81

Table 5.2 : Result of Energy Detection Algorithm with Best parameter ……………………………………………….84

Table 5.3 : Result of Energy Detection Algorithm with Global Best parameter ……………………………………..85

Table 5.4 : Result of Pitch-Based Detection Algorithm with Global Fitting parameter………………………………....92

Table 5.5: Result for Pluck String …………………………………………………………………………….......94

Table 5.6: Result for Solo Winds…..…………………………………………………………………………...95

Table 5.7: Result for Piano……..…..……………………………………………………………………………....95

Table 5.8: Result for Solo Brass……………………………………………………………………………………...96

Table 5.9: Result for Sustained String…………………………………………………………………………..96

Table 5.10: Result for Complex Music………………………………………………………………………………..97

Table 6.1: Small Integer Ratio and Note Interval ……………………………………………………………………...111

Table 7.1: Deviation between approximation and ideal value ………………………………………………………....124

Table 9.1 Test Database 2-(Real Music Excerpts from Music CDs)…………………………………………………...133

Table 9.2 : Test Result on the Test Database 2 (Real Music Excerpts) ………………………………………………. 148

Table 9.3: Recall and Precision of Different Methods on Testing Real Polyphonic Music Excerpts…………………...149

Table 9.4: NERof Different Methods on Testing Polyphonic Mixtures (Avoiding Deletions)………………………. 150

Table 9.5: NERof Different Methods on Testing Polyphonic Mixtures (Avoiding Insertions)………………………..150

ABBREVIATIONS

AES	**Adjusted energy spectrum**
CWM	**Common western music**
CWT	**Continuous wavelet transform**
DPES	**Difference pitch energy spectrum**
ERB	**Equivalent rectangular bandwidth**
ERM	**Empirical risk minimization**
FDTF	**Frequency-dependent time-frequency transform**
FFT	**Fast Fourier transform**
KKT	**Karush-Kuhn-Tucker**
MIDI	**Musical Instrument Digital Interface**
MIREX	**Music Information Retrieval Evaluation Exchange**
NPES	**Normal pitch energy spectrum**
NER	**Note error rate**
PES	**Pitch energy spectrum**
PWD	**Pseudo Wigner-Distribution**
QP	**Quadratic programming**
RBF	**Radial basis function**
RTFI	**Resonator time-frequency image**
SACF	**Summary autocorrelation function**
STFT	**Short Time Fourier Transform**
SNR	**Signal-to-noise ratio**
SVM	**Support vector machine**
TDNN	**Time-delay neural networks**
TFR	**Time-frequency representation**
TPP	**Time-pitch probability**
WT	**Wavelet Transform**
WVD	**Wigner-Ville Distribution**

ABSTRACT

The purpose of this thesis is to develop new methods for automatic transcription of melody and harmonic parts of real-life music signal. Music transcription is here defined as an act of analyzing a piece of music signal and writing down the parameter representations, which indicate the pitch, onset time and duration of each pitch, loudness and instrument applied in the analyzed music signal.The proposed algorithms and methods aim at resolving two key sub-problems in automatic music transcription: *music onset detection* and *polyphonic pitch estimation*. There are three original contributions in this thesis.

The first is an original frequency-dependent time-frequency analysis tool called the Resonator Time-Frequency Image (RTFI). By simply defining a parameterized function mapping frequency to the exponent decay factor of the complex resonator filter bank, the RTFI can easily and flexibly implement the time-frequency analysis with different time-frequency resolutions such as ear-like (similar to human ear frequency analyzer), constant-Q or uniform (evenly-spaced) time-frequency resolutions. The corresponding multi-resolution fast implementation of RTFI has also been developed.

The second original contribution consists of two new music onset detection algorithms: Energy-based detection algorithm and Pitch-based detection algorithm. The Energy-based detection algorithm performs well on the detection of hard onsets. The Pitch-based detection algorithm is the first one, which successfully exploits the pitch change clue for the onset detection in real polyphonic music, and achieves a much better performance than the other existing detection algorithms for the detection of soft onsets.

The third contribution is the development of two new polyphonic pitch estimation methods. They are based on the RTFI analysis. The first proposed estimation method mainly makes best of the harmonic relation and spectral smoothing principle, consequently achieves an excellent performance on the real polyphonic music signals. The second proposed polyphonic pitch estimation method is based on the combination of signal processing and machine learning. The basic idea behind this method is to transform the polyphonic pitch estimation as a pattern recognition problem. The proposed estimation method is mainly composed by a signal processing block followed by a learning machine. Multi-resolution fast RTFI analysis is used as a signal processing component, and support vector machine (SVM) is selected as learning machine. The experimental result of the first approach show clear improvement versus the other state of the art methods.

Keywords: Signal processing, music transcription, onset detection, polyphonic pitch estimation

RESUME

Cette thèse aborde le sujet de la transcription musicale, que l'on définit ici comme le fait d'analyser le signal d'un morceau de musique, et d'en tirer une représentation paramétrique qui indique le ton, l'instant de l'attaque, la durée de la note, sa force et l'instrument utilisé dans le signal musical analysé.

De nouvelles méthodes de transcription de la mélodie et des parties harmoniques d'un signal musical, tel qu'on en trouve dans la vie réelle, en résultent. Les algorithmes et les méthodes proposées sont axées sur la résolution de deux sous-problèmes clés dans la transcription de la musique: la détection de l'attaque et l'estimation des tons polyphoniques. Il y a trois apports inédits dans cette thèse:

Le premier est un outil d'analyse temps-fréquence: le RTFI (pour Resonator Time-Frequency Image). En définissant simplement une fonction paramétrée faisant correspondre une fréquence au facteur exponnentiel de declin du groupe de filtres complexes du résonnateur, le RTFI peut servir à implémenter facilement l'analyse temps-fréquence, avec différentes résolutions du domaine temps-fréquence, telles que celle de l'oreille humaine, avec un facteur Q constant, ou encore uniforme (espacée régulièrement). Une implémentation rapide avec plusieurs résolutions simultanées a également été développée.

Deux nouveaux algorithmes de détection de l'attaque constituent le deuxième apport: l'un basé sur l'énergie et l'autre sur le ton. Celui basé sur l'énergie se comporte bien sur de fortes attaques. Celui basé sur le ton est le premier à exploiter correctement le changement de ton dans la détection d'attaque d'une musique polyphonique réelle, et offre de bien meilleurs résultats que les autres algorithmes existants, quant il s'agit de détecter des attaques douces.

Enfin, deux nouvelles méthodes d'estimation des tons polyphoniques sont proposées: la première, basée sur l'analyse RTF, exploite au mieux la relation harmonique et le principe du lissage spectral. Elle fournit par conséquent d'excellentes performances quand elle est appliquée à des signaux de musiques polyphoniques réelles. La seconde est basée sur une combinaison de traitement de signal et d'apprentissage de la machine. L'idée fondamentale de cette méthode est de transformer l'estimation de tons polyphoniques en un problème de reconnaissance de modèles. L'analyse RTFI rapide avec plusieurs résolutions simultanées sert au traitement du signal et l'apprentissage de la machine est géré par SVM (Support Vector Machine). Les résultats des essais effectués avec cette méthode montrent de claires améliorations de l'état de l'art.

Liste des mots-clefs :

Traitement du signal, transcription de la musique, détection de notes, estimation de hauteur polyphonique

Chapter 1

INTRODUCTION

1.1 Definition of Automatic Music Transcription

Music transcription is here defined as an act of analyzing a piece of music signal and writing down the parameter representations, which indicate the pitch, onset time and duration of each pitch, loudness and instrument applied in the analyzed music signal. Automatic music transcription is a process to convert an acoustical waveform into a musical notation (such as the traditional western music notation) by computer programming. In most cases automatic transcription of common monophonic music can be considered as a matured filed, however the computational transcription of polyphonic music has less relative success. Transcription of polyphonic music is a very difficult task for the average human without training, however human can improve their transcription ability by learning. Skilled musicians are able to transcribe polyphonies with much better performance than computational transcription system can achieve in current research phases. The automatic music transcription is a critical step for some higher level music analysis tasks such as melody extraction, rhythm tracking, and harmony analysis.

1.2 Objectives

The purpose of this thesis is to develop new methods for automatic transcription of melody and harmonic parts of real-life music signal. The proposed algorithms and methods aim at resolving two key sub-problems in automatic music transcription: *music onset detection* and *polyphonic pitch estimation*. The music signal is often considered as the succession of the discrete acoustic events. The term *music onset detection* refers to the detection of the instant when a discrete event begins in acoustic signal. The term *polyphonic pitch estimation* refers to the estimation of possible pitches in the polyphonic music signal that several music notes may occur simultaneously.

1.3 Motivations

The music consists of some basic elements. These are rhythm, melody, harmony, and timbre. The aim of this thesis is to extract two important parameters: note onset time and polyphonic pitch. As shown in Figure 1.1, the extraction of the both parameters plays an essential role in a music analysis.

The extracted onset time of music notes can be used to chiefly determine rhythm. The extracted multiple pitches of music notes can be primarily employed for the detection of melody and harmony. Melodic lines are sequences of notes over time, and harmony is determined by the relationship between the multiple simultaneously occurring pitches of music notes.

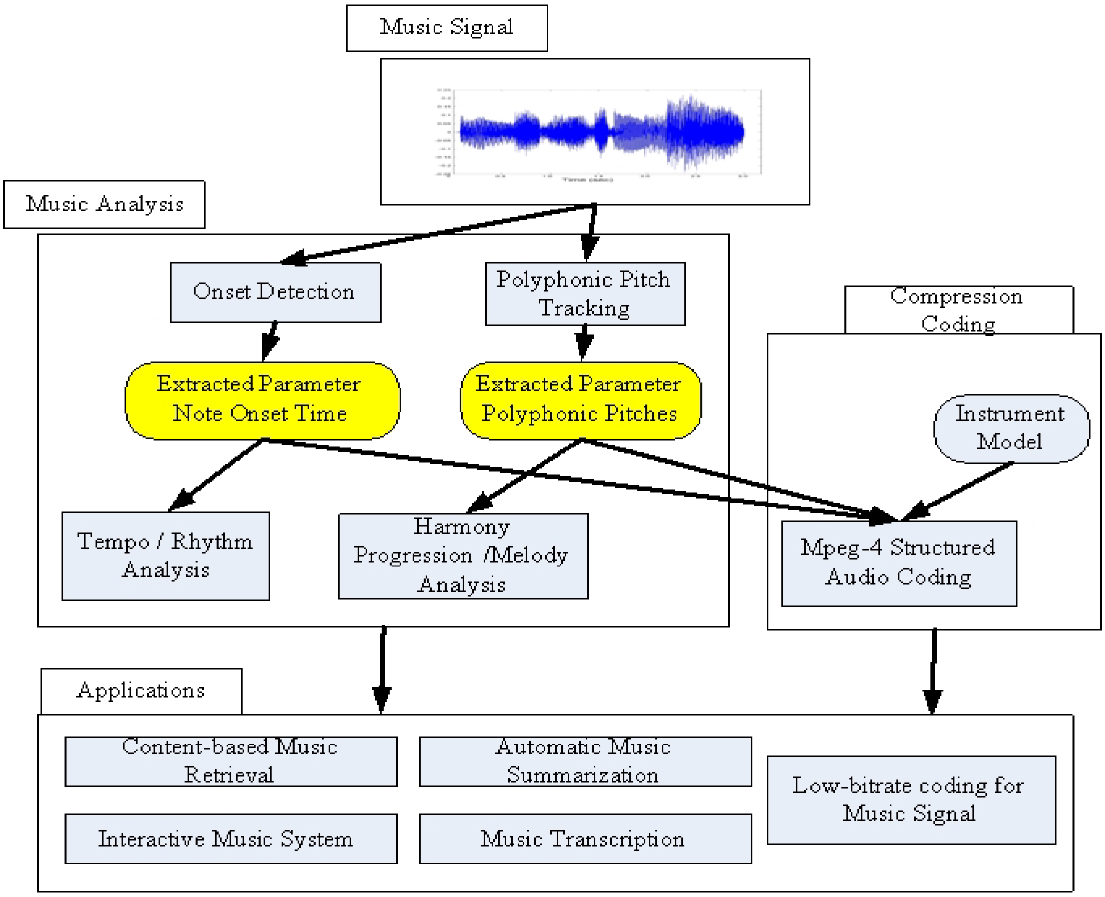
Music Signal
Music Analysis
Onset Detection
Polyphonic Pitch Tracking
Extracted Parameter Note Onset Time
Extracted Parameter Polyphonic Pitches
Tempo / Rhythm Analysis
Harmony Progression /Melody Analysis
Compression Coding
Instrument Model
Mpeg-4 Structured Audio Coding
Applications
Content-based Music Retrieval
Automatic Music Summarization
Interactive Music System
Music Transcription
Low-bitrate coding for Music Signal

Figure 1.1 Essential Role of the extracted parameters: Onset Time and Polyphonic Pitch in Music Analysis

Because the extraction of note onset time and polyphonic pitch is a fundamental stage of analyzing the basic elements of music signals, it can be utilized to support broad music applications. As shown in the Figure 1.1, except the automatic music transcription itself, the possible applications include content-based music retrieval, automatic music summarization, interactive music system, low-bitrate compression coding for music signal and so on. Multimedia music applications are nowadays rapidly moving from simple content related scenarios to more complex and sophisticated domains including content, interaction, related descriptions and annotations, item identification. The creation of huge databases coming from both restoration of existing analog content and new digital content is requiring more and more reliable and fast tools for content analysis and description, to be used for searches, content queries and interactive access. In the case of content-based music retrieval, automatic onset and harmonic information extraction is crucial. Not only it is interesting to build measures of harmonic similarity between musical excerpts, but it can further help some other kind of analysis such as rhythm or instrument detection by finding onset time points where such events or instrument note starts are more likely to be observed. . Another interesting point that is gaining importance in the domain is the automatic control of signal processing parameters according to content features and builds some music interactive systems. Another possible application of the extraction of polyphonic pitch is to assist for the low-bitrate coding for music signal. The MPEG-4 Structured Audio coding provides new methods for low-bitrate storage. In a framework of Structured Audio coding, automatic music transcription and music synthesis play chief role.

1.4 Main Results of the Thesis

The main three original contributions of this thesis can be summarized as follows:

1) An original frequency-dependent time-frequency analysis tool has been proposed and formalized: the Resonator Time-Frequency Image (RTFI).

Music signal is time-varying, and most of the music related tasks need a joint time-frequency analysis. An important time-frequency representation (TFR) is the Wigner-Ville Distribution (WD) which satisfies a number of desirable mathematical properties and provides high time-frequency resolution. However, the serious cross term interference in the WD prevents it from the practical application. A number of existing TFRs can be considered as the smooth version of WD to reduce the cross term interference. According to their covariance property, these existing TFRs can be categorized into several main classes such as the Cohen's class of time-frequency distributions, the Affine class of time-frequency distributions. For example, in the commonly-used TFRs for music analysis, the spectrogram (STFT analysis) is a particular example of the Cohen's class of time-frequency distribution, and the scalogram (wavelet analysis) belongs to the Affine class of time-frequency distribution.

The Cohen's class of time-frequency distributions perform the time-frequency analysis with a uniform time-frequency resolution in the time-frequency plane ("uniform analysis"), on the other hand the Affine class of time-frequency distributions have the "constant-Q" time-frequency resolution ("constant-Q analysis"). Most of the current existing TFRs show similar limitations, and their time-frequency resolutions are either uniform or "constant-Q". However, it is well known that time-frequency resolution of human ear frequency analyzer is neither uniform nor “constant-Q”. This motives me to develop a more general and flexible class of TFRs whose time-frequency resolutions are not limited in the uniform or “constant-Q” analysis. I extend the spectrogram into a broader class of TFRs and make the window function dependent on analysis frequency. Base on this idea, I propose and formulate a particular time-frequency representation: the Resonator Time-Frequency Image (RTFI) for music signal analysis. The RTFI is implemented by the one-order complex IIR-filter bank, so it is computation-efficient. By simply defining a parameterized function mapping frequency to the exponent decay factor of the complex resonator filter bank, the RTFI can easily and flexibly implement the time-frequency analysis with different time-frequency resolutions such as ear-like (similar to human ear frequency analyzer), constant-Q or uniform (evenly-spaced) time-frequency resolutions. The corresponding multi-resolution fast implementation of RTFI has also been developed. The practical application examples of RTFI analysis are the proposed music onset detection algorithms and polyphonic pitch estimation methods. In all these algorithms and methods, the RTFI become the common time-frequency analysis tool.

2) Two music onset detection algorithms have been proposed and developed: Energy-based detection algorithm and Pitch-based detection algorithm.

The note onsets may be classified into “soft” or “hard” onsets according to slow or fast transitions between the two successive notes in the analyzed music signal. The note transition with hard onset is accompanied with the sharp change in energy, and the note transition with soft onset shows a gradual change. Based on the RTFI analysis, I propose an energy-based onset detection algorithm which is simple and performs very well on the detection of hard onsets. However, the detection of soft onset has been proved to be very difficult task, because the real-life music signal often contains the noise and vibration associated with frequency and amplitude modulation. The energy-change in the vibration probably surpasses the energy-change of soft onset, and this makes it very hard to distinguish the true onsets from the vibration only based on the energy-change clue.

Pitch change is the most salient clue for note onset detection of the music signal with soft onset. On the one hand, there exist many onset detection systems that use energy change and/or phase change as the source of information, on the other hand, only few pitch-based onset detection systems exist. One important reason for this is that pitch-tracking itself is an challenging task.

The proposed Pitch-based detection algorithm uses RTFI analysis and produces a pitch energy spectrum that makes the pitch change more obvious; and then makes best use of pitch change clues to separate the music signal into transient and stable part, and finally searches the possible note onsets only in the transient part. This method greatly reduced the false positives that caused by the salient energy-change in the stable part of the music note, and greatly improve the detection performance on the music signal with many soft onsets or vibration.

Both of the energy-based and pitch-based detection algorithms have been tested on broad real-life music excerpts and the test results are encouraging. Especially, for the detection of the soft onsets, the proposed Pitch-based detection algorithm achieves a much better performance compared to the other existing onset detection algorithms.

3) Two polyphonic pitch estimation methods have been proposed and developed: polyphonic pitch estimation method I and polyphonic pitch estimation method II. Polyphonic pitch estimation is a very challenging task because of the wide pitch range, much variety of the spectral structures of the different instrument sound and the coinciding harmonic components frequently occurring in the polyphonic sound.

The proposed polyphonic pitch estimation method I mainly makes best of the harmonic relation and spectral smoothing principle. The harmonic relation means that the ratio between frequency components of a real monophonic music note and its fundamental frequency is integer or nearly integer. The spectral smoothing principle refers to the fact that the corresponding harmonic spectral envelop of a real monophonic music note often is gradually change. The proposed method I first produces the energy spectrum by RTFI analysis, and then uses the harmonic grouping principle to transform the RTFI energy spectrum into the pitch energy spectrum. The preliminary pitch candidates are estimated by picking the peaks in the pitch energy spectrum. The extraneous estimations in the pitch candidates are to be cancelled by the spectral smoothing principle. The detail description of the proposed estimation method I can be found in the Chapter 5.

The proposed polyphonic pitch estimation method II is based on the combination of signal processing and machine learning. The basic idea behind this method is to transform the polyphonic pitch estimation as a pattern recognition problem. The proposed estimation method is mainly composed by a signal processing block followed by a learning machine. Compared to the human listening system, the signal processing stage is a time-frequency signal analysis tool similar to cochlear filters, whereas the learning machine plays a role similar to human brain. Multi-resolution fast RTFI analysis is used as a signal processing component, and support vector machine

(SVM) is selected as learning machine. The detail description of the proposed estimation method II also can be found in the Chapter 5.

Additionally, with the combination of the proposed onset detection algorithms and polyphonic pitch estimation methods, the real automatic music transcription prototype systems have also been proposed and developed.

The both proposed polyphonic pitch estimation methods have been tested on the real music excerpts from the music CDs, clean polyphonic mixtures and the polyphonic mixtures with different level pink noise. The polyphonic mixtures is produced by the mixing the monophonic samples of 23 different music instrument types. The test results of the both proposed methods are competitive and encouraging, compared to the existing methods. On the one hand, the proposed method I presents better overall performance than the proposed method II (SVM). On the other hand, the method II (SVM) can produce time-pitch probability output, which is useful for some real applications.

1.5 Organization of the Thesis

This thesis is organized as follows. Chapter 2 summarizes the existing time-frequency analysis methods and presents their specific advantages and problems in their usages. Chapter 3 has an introduction of support vector machines. The original work is introduced in the Chapter 4-9. Chapter 4 presents and formalizes an original time-frequency analysis method: the Resonator Time-Frequency Image (RTFI), which is especially designed for music signal analysis. The corresponding multi-resolution fast implementation and application examples of RTFI are also introduced. As a basic time-frequency analysis tool, the RTFI is exploited in the later proposed music onset detection algorithms (introduced in Chapter 5) and polyphonic estimation methods (introduced in Chapter 6-9).Chapter 5 presents two proposed music onset detection algorithms: Energy-based detection algorithm and Pitch-based detection algorithm, and both algorithms employ the RTFI as the time-frequency analysis tool. Chapter 6-9 proposes two polyphonic pitch estimation methods, Polyphonic pitch method I and Polyphonic pitch method II. The method I also uses the RTFI as the time-frequency analysis tool, and time-frequency analysis of method II uses the RTFI multi-resolution fast implementation (introduced in Chapter 4). Additionally, Chapter 9 presents two real music transcription systems which combine the proposed polyphonic pitch methods and the music onset detection algorithms (introduced in Chapter 5). Chapter 10 presents the main conclusions and discusses the future work.

Chapter 2

TIME-FREQUENCY ANALYSIS FOR MUSIC SIGNAL: STATE OF THE ART

2.1 Introduction

The classic Fourier Transform is a very useful tool for frequency analysis of a stationary signal that maintains the same period over an infinite duration time. The Fourier Transform can show if a frequency component exists, but not tell when the frequency component occurs. The music signal is time-varying and non-stationary, its frequency components change with time, so music signal frequency analysis should better be a joint time-frequency analysis, which shows how the signal's frequency content evolves in time.

Because of the uncertainty principle, it is impossible for a time-frequency analysis to have both the best time and frequency resolution at the same time: there is a tradeoff between time and frequency resolution. To select a suitable time-frequency resolution for a joint time-frequency analysis of the music signal, there are two different approaches. The first one is to learn more about how human ear makes a time-frequency analysis by research in audio physiology and psychology, because the ear has very excellent performance as a music signal processing component (in fact, the auditory filter bank can be seen as a time-frequency analysis tool that simulates the cochlear function.). Another one is to learn more about the time-frequency energy density distribution of the most typical music signals. In the end, both approaches should be considered together to select a suitable time-frequency analysis.

One commonly-used time-frequency analysis tool is Short Time Fourier Transform (STFT), which cuts the signal into different slices and calculates the Fourier Transform on each slice to obtain a local time-frequency analysis. A different approach to get the local time-frequency analysis is the Wigner distribution, but its non-linearity causes cross interference, and at the same time the computation cost is very expensive; the above two reasons make Wigner distribution rarely used in practical applications. Wavelets are of course another alternative way to joint time-frequency analysis, and moreover they have a constant-Q frequency resolution that is similar to cochlear frequency resolution distribution at high frequencies, so the wavelet analysis is more adaptable to music signal processing than the STFT, which has the same time-frequency resolution in all the time-frequency domain; but the wavelet analysis still shows a similar limitation as STFT, as it always keeps the constant-Q frequency resolution: it can not flexibly set the time-frequency resolution in the time-frequency domain. On the other hand, the known cochlear filter only has similar constant-Q frequency resolution at high frequency, and it has a nearly equal frequency resolution at low frequency. The next sections will review the above mentioned tools in more detail and present their actual and possible uses in the context of music sound analysis.

2.2 STFT and Spectrogram

Fourier Transform and its inverse can transform signals between the time and frequency domains, and it becomes a very useful tool for stationary signal processing. It can make it possible to view the signal characteristics either in time or frequency domain, but not to combine both domains. In order to obtain a joint time-frequency analysis for non-stationary signals, STFT cuts the time signal into different frames and then perform a Fourier Transform in each frame. The STFT and its power spectrum named spectrogram, can be defined like in equations (2.1) and (2.2)

$$STFT(t,\omega)=\int_{-\infty}^{\infty} f(\tau)w(\tau-t)e^{-j\omega\tau}d\tau \qquad (2.1)$$

$$Power(t,\omega)=\left|STFT(t,\omega)\right|^2 \qquad (2.2)$$

The STFT at time *t* is the Fourier Transform of a local signal, which is obtained by multiplication of a signal $f(t)$ and a short window function $w(\tau-t)$ centered at time *t*. When moving the window along the signal time axis, we can calculate the STFT at different time instants and obtain a joint time-frequency analysis. Since STFT can be easily and efficiently implemented by fast algorithms of Fast Fourier Transform (FFT), it and the spectrogram have been early used in speech and music signal analysis. To construct a STFT, the effective length and shape of the window function is a key factor to determine the STFT characteristics. The shape of the window function is the first important factor; the default window is the rectangle widow, which causes the well-known frequency leakage problem because the signal's phase discontinuity at the edge of the window. To reduce the frequency leakage, some other windows are often selected such as the Hanning window. The other very important factor is the length of the window; the longer the window, the better frequency resolution the STFT has, but unfortunately at the price of poorer temporal resolution according to the uncertainty principle. Given a window function $w(t)$ and its Fourier Transform $W(\omega)$, the commonly used measure of the time and frequency resolution is the window's effective length Δt and bandwidth $\Delta\omega$, defined as in the following formulas:

$$\Delta t^2 = \frac{\int (t - t^{'})^2 \left|w(t)\right|^2 dt}{\int \left|w(t)\right|^2 dt} \qquad (2.3)$$

$$\Delta\omega^2 = \frac{\int (\omega - \omega^{'})^2 \left|W(\omega)\right|^2 d\omega}{\int \left|W(\omega)\right|^2 d\omega} \qquad (2.4)$$

where

$$t^{'} = \frac{\int t\left|w(t)\right|^2 dt}{\int \left|w(t)\right|^2 dt} \qquad (2.5)$$

$$\omega^{'} = \frac{\int t\left|W(\omega)\right|^2 dt}{\int \left|W(\omega)\right|^2 dt} \qquad (2.6)$$

According to the time-bandwidth uncertainty principle, Δt and $\Delta\omega$ must meet the following inequality:

$$\Delta\omega^{'} \bullet \Delta t \geq \frac{1}{2} \qquad (2.7)$$

According to this inequality, the STFT time and frequency resolutions can not be optimal at the same time, and there is a trade-off to be found between them. To make the (2.7) be an equality the window must be the Gaussian window.

One can simply transform the definition (2.1) into another equivalent definition as follows [Hlaw92]:

$$STFT(t,\omega) = (f(t) * (\gamma(t)e^{-j\omega t}))e^{-j\omega t} \qquad (2.8) \quad \text{or}$$

$$STFT(t,\omega) = (f(t) \bullet e^{-j\omega t}) * \gamma(t)) \qquad (2.9)$$

where $\gamma(t) = w(-t)$ (2.10)

From the formulas (2.8) and (2.9), there exist two different filter bank interpretations for the STFT as illustrated in the Figure 2.1.

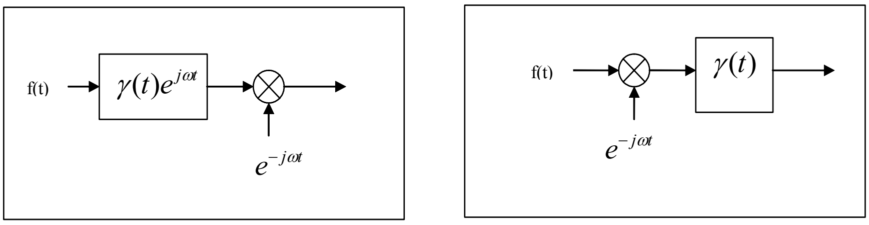

Figure 2.1 Filter bank interpretation of STFT

The left part of Figure 2.1 shows the STFT implementation by the band pass filter bank; at any angle frequency ω, first the signal passes through the band pass filter centered at ω and then it is demodulated to zero frequency. The right part of the Figure 2.1 shows the STFT implementation by a low pass filter; at any angle frequency, first the signal is demodulated to zero frequency and then passes through the low pass filter.

As described in the definition of STFT at (2.1), the window function is independent from the frequency ω, so the time-frequency resolution of STFT is the same in all the time frequency plane. This makes STFT able to have limited application in music signal processing, because the real music signal processing often needs to provide better time resolution at high frequencies and better frequency resolution at low frequencies.

2.3 Wavelet Analysis

Differently from the case of STFT, the Wavelet Analysis (WT) provides a varying time-frequency resolution in the time frequency plane. During the last twenty years, the WT has been developed and explored in many different research fields. The Wavelet Transform (WT) can be defined as the following formula:

$$WT(s,t) = \int_{-\infty}^{\infty} f(\tau) \frac{1}{\sqrt{s}} \phi^{*}(\frac{\tau - t}{s}) d\tau \qquad (2.11)$$

In the equation the Φ^* is the conjugate of the Φ. As shown by this definition, WT can be described in terms of the signal's decomposition over the wavelet $\phi_{s,t}(\tau)$, which is defined as the dilation and translation of the mother wavelet $\phi(\tau)$:

$$\phi_{s,t}(\tau) = \frac{1}{\sqrt{s}}\phi(\frac{\tau - t}{s}) \qquad (2.12)$$

In (2.12), t is the translation factor; s is the scale factor and $1/\sqrt{s}$ is used to normalize the wavelets. In (2.11), t, s, and τ are continuous variables; this wavelet transform is commonly named the Continuous Wavelet Transform (CWT). Differently from other transforms such as FT, the wavelet basis function is not specified. To make the reverse transform possible, the wavelet function must meet the so-called *admission condition*:

$$C_\phi = \int_{-\infty}^{+\infty} \frac{|\Phi(\omega)|^2}{|\omega|} d\omega < +\infty \qquad (2.13)$$

Where $\Phi(\omega)$ is the Fourier Transform of the wavelet function $\phi(\tau)$:

$$\Phi(\omega) = \int_{-\infty}^{+\infty} \phi(\tau) e^{-j\omega\tau} d\tau \qquad (2.14)$$

With the condition (2.13), the signal $f(\tau)$ can be reconstructed by the inverse transform of CWT [Cohen96]:

$$f(\tau) = \int_0^{+\infty} \frac{ds}{s^2} \int_{-\infty}^{+\infty} WT(t,s)\phi_{t,s}(\tau)dt \qquad (2.15)$$

The condition (2.13) also implies the following property of wavelet exists:

$$\int_{-\infty}^{+\infty} \phi(\tau) d\tau = \Phi(0) = 0 \qquad (2.16)$$

$\Phi(0)$ is 0, so the wavelet $\phi(\tau)$ should be oscillating. Sometimes another additional requirement, the so-called *regularity condition*, is also imposed for some application that need better detect the singularity of the analyzed signal. The *regularity condition* of wavelets can be described as follows:

$$\int_{-\infty}^{+\infty} \tau^p \phi(\tau) d\tau = 0 \qquad p = 0,1,2 \cdots N \quad (2.17)$$

Under the *regularity condition*, the values of $WT(t,s)$ are influenced by the regularity of the analyzed signal $f(\tau)$ and can be used to detect the signal's local singularity [Cohen96, Mallat98].

Another equal frequency definition of (2.11) is as following:

$$WT(t,s) = \int_{-\infty}^{\infty} F(\omega) \frac{\sqrt{s}}{2\pi} \Phi^*(s\omega) e^{j\omega t} d\omega \qquad (2.18)$$

In the (2.18) $F(\omega)$ and $\Phi(\omega)$ are the Fourier Transform of the signal $f(\tau)$ and the wavelet function $\phi(\tau)$ respectively, and the $WT(t,s)$ can be considered as the filtering result of the signal by the band pass filter bank. The filter bandwidth in the filter bank increases as the frequency increases (the scale factor s decreases), but the ratio between bandwidth and centre frequency keeps constant..

The CWT decomposes the signal into a time-frequency domain according to a continuously varying scale and translation and represents the signal with high redundancy, so it is reasonable to calculate the wavelet coefficient at discrete scale and time grids for a more efficient representation. Such a discrete sampling wavelet transform can been described as follows:

$$WT(j,k) = \int_{-\infty}^{\infty} f(\tau) \phi^*{}_{t,s}(\tau) d\tau \qquad (2.19)$$

where $$\phi_{j,k}(\tau) = \frac{1}{\sqrt{s_0^j}} \phi\left(\frac{\tau - k\tau_0 s_0^j}{s_0^j}\right) \quad (2.20)$$

It is common use to select $s_0 = 2$ and make a dyadic sampling on the frequency axis. The wavelet transform decompose the one-dimension signal into the 2 dimensions discrete wavelet coefficients. At this point it is important to consider if such wavelet coefficients give a complete and stable signal representation.

The frame theory is an important mathematics tool to resolve a problem of this kind. A sequence $\{\phi_n\}_{n\in z}$ in a Hilbert space H is called a frame if and only if there exists two constants $B \geq A > 0$ such that for all $f \in H$,

$$A\|f\|^2 \leq \sum_{n\in z} |(f,\phi_n)|^2 \leq B\|f\|^2 \quad (2.21)$$

When $B = A$, the frame is said to be tight (Mallat98). A frame is invertible and defines a complete and stable signal representation. If one wants to make the wavelet coefficients an efficient and invertible representation, a wavelet function sequence need to be a frame. Daubechies derives the admission and sufficient condition to construct a wavelet frame (Daub92). When a wavelet function sequence is a tight frame, it is an orthonormal base.

A new multi-resolution theory was formulated in 1989 and this provided also new view for wavelets [Mallat89]. The main concept is that wavelet analysis can be considered to approximate the analyzed signal from a coarse approximation to a more detailed approximation.

According to this multi-resolution theory wavelets can be formulated as a sequence of approximation subspaces $\{V_j\}_{j\in z}$ of $L_2(R)$ [Mallat98]:

$$\forall(j,k) \in Z^2, f(t) \in V_j \Leftrightarrow f(t-2^j k) \in V_j \quad (2.22)$$

$$\forall j \in Z, V_{j+1} \subset V_{j,} \quad (2.23)$$

$$f(t) \in V_j \Leftrightarrow f(t/2) \in V_{j+1} \quad (2.24)$$

$$\lim_{j\to+\infty} V_j = \bigcap_{j=-\infty}^{+\infty} V_j = \{0\}, \quad (2.25)$$

$$\lim_{j\to-\infty} V_j = Closure(\bigcup_{j=-\infty}^{\infty}) = L^2(R), \quad (2.26)$$

and there exists a $\{\varphi(t-n)\}_{n\in z}$ which is a Riesz basis of V_0

One can define that the function $\varphi_{j,n}$ as follows:

$$\varphi_{j,n}(t)=\{2^{-j/2}\varphi(2^{-j}t-n)\}_{n\in z}$$

From the definition it has been proved that $\varphi_{j,n}$ is also the Riesz basis of the subspace V_j and all $\varphi_{j,n}$ are collectively called scaling function, which needs to meet the following so-called scaling equation:

$$\varphi(t)=2\sum h(n)\varphi(2t-n) \quad (2.27)$$

Because $\varphi_{j,n}$ is the Riesz basis of the subspace V_j, so the $\varphi_{j,n}$ can be an orthonormal or biorthormal basis of the subspace V_j. One can define an approximation operator A_j that approximates a $L_2(R)$ function *f* by the basis of subspace V_j. In the case that $\varphi_{j,n}$ is an orthonormal function, A_j is expressed as follows:

$$A_j f=\sum_{n\in z}\left\langle f,\varphi_{j,n}\right\rangle\varphi_{j,n} \quad (2.28)$$

In case that $\varphi(2^j t-n)$ is biorthormal basis of the subspace V_j, A_j is expressed as follows:

$$A_j f=\sum_{n\in z}\left\langle f,\overline{\varphi}_{j,n}\right\rangle\varphi_{j,n} \quad (2.29)$$

where $\overline{\varphi}_{j,n}$ is a dual scaling function: $\left\langle\varphi_{j,m},\overline{\varphi}_{j,n}\right\rangle=\delta_{0,m-n}$. The dual scaling function also needs to meet the scaling equation:

$$\overline{\varphi}(t)=2\sum\overline{h}(n)\overline{\varphi}(2t-n) \quad (2.30)$$

One can derive a wavelet function from the scaling function as follows:

$$\phi(t) = 2\sum g(n)\varphi(2t-n)\,,\ \bar{\phi}(t) = 2\sum \bar{g}(n)\bar{\varphi}(2t-n) \quad (2.31)$$

where

$$g(n) = (-1)^n \bar{h}(1-n)\,,\ \bar{g}(n) = (-1)^n h(1-n) \quad (2.32)$$

such that :

$$\Delta f_j = A_{j-1}f - A_j f = \sum_{n\in z}\left\langle f, \bar{\phi}_{j,n}\right\rangle \phi_{j,n} \quad (2.33)$$

As shown in (2.32) wavelet functions can be use to demonstrate the detail information according to the corresponding scale. The wavelets $\{\phi_{j,n}\}_{n\in z}$ with fixed scale j constitutes a Reisz basis of the subspace W_j and the wavelets at all the scales $\{\phi_{j,n}\}_{j,n\in z}$ together constitute a Reisz basis of $L_2(R)$: $\left\langle \varphi_{i,m}, \bar{\varphi}_{j,n}\right\rangle = \delta_{i-j,m-n}$. Here it is preferred to explain the wavelet multi-resolution interpretation by signal processing terminology rather than introducing too much mathematics in detail. In the multi-resolution analysis, the scaling function is the low pass filter; the subspace V_j corresponds to a different frequency band. More specifically, for example there is a band-limited real signal f with frequency bandwidth range $[-\omega_0 \quad \omega_0]$, in the case that the scaling function of the subspace V_0 covers all the signal frequency $[-\omega_0 \quad \omega_0]$ band, then A_0f is a complete approximation of f; the scaling function of the subspace V_j has a compressed frequency band $[-\omega_0/2^j \quad \omega_0/2^j]$, so $A_j f$ has lost the high frequency information $[-\omega_0 \quad -\omega_0/2^j] \cup [\omega_0/2^j \quad \omega_0]$. From $A_{j-1}f$ to $A_j f$, the frequency information $[-\omega_0/2^{j-1} \quad -\omega_0/2^j] \cup [\omega_0/2^j \quad \omega_0/2^{j-1}]$ has been lost; the wavelets of the subspace W_j are the band pass filer with frequency band exactly in $[-\omega_0/2^{j-1} \quad -\omega_0/2^j] \cup [\omega_0/2^j \quad \omega_0/2^{j-1}]$, and used to detect the lost detail information Δf_j from $A_{j-1}f$ to $A_j f$; from the scaling equation (2.27) and equation (2.31), the scaling function and wavelet function at scale *j* can be calculated from the scaling function at scale 2^{j-1}; it is obvious that *h(n)* should be a low pass filter and *g(n)*should be a high pass filter.

If $\varphi_{j,n}$ and $\phi_{j,n}$ constitute an orthonormal base of subspaces V_j and W_j, $A_j f$ and Δf_j are characterized by $a_j = \langle f, \varphi_{j,n} \rangle$ and $d_j = \langle f, \phi_{j,n} \rangle$. It has been proved that [Mallat98]:

$$a_{j+1}[p] = \sum_{n \in z} h(n-2p) a_j(n) = a_j * h(-2p) \quad (2.34)$$

$$d_{j+1}[p] = \sum_{n \in z} g(n-2p) a_j(n) = a_j * g(-2p) \quad (2.35)$$

and the corresponding reconstruction :

$$a_j[p] = \breve{a}_{j+1} * h(p) + \breve{d}_{j+1} * g[p] \quad (2.36)$$

with the definition :

$$\breve{y}(n) = \begin{cases} y(2p) & if \quad n = 2p \\ 0 & if \quad n = 2p+1 \end{cases} \quad (2.37)$$

One can first get a discrete series a_0 that characterized the approximation of signal at the subspace V_0, then a_0 is first decomposed into two channels by low and high pass filters and then dyadic subsampling at each channel to get the wavelet coefficient d_1 for the high pass channel and a_1 for the low pass channel. This process can be iterated again and again and get a_j and d_j step by step. A corresponding fast reverse wavelet transform can be used to reconstruct the approximation series a_0 from the a_j and $\{d_k, d_{k-1}, \cdots, d_1\}$

In practical applications the analyzed signal is often a discrete series, and the discrete series *b(n)* can be considered as an approximation of *f(t)* in the subspace V_j; the above fast algorithm can then be used to calculate the wavelet transform. One one hand it is natural to derive the low pass filter *h(n)* and high pass filter *g(n)* from the scaling function φ, and then use *h(n)* and *g(n)* to perform fast wavelet transform; on the other hand in practical cases *h(n)* and *g(n)* are often designed first, and then the scaling function and wavelet function may be derived if necessary. One basic unit in the fast wavelet transform is the 2-channel muli-rate filter bank that decompose the signal into high and low frequency component following by the dyadic subsampling in each channel, and a corresponding multi-rate filter bank perform the reverse wavelet transform to reconstruct the original input. Such a reconstructive analysis-synthesis filter bank is a perfect reconstruction filter bank. The commonly used perfect reconstruction filter banks are a quadrature mirror filter (QMR) and a conjugate mirror filter (CMF). The perfect reconstruction condition (PR condition) for a 2-channel filter bank can be described in the *z* domain as follows:

$$H(-z)\hat{H}(z) + G(-z)\hat{G}(z) = 0 \quad (2.38)$$

$$H\ \ (z)\hat{H}(z) + G\ \ (z)\hat{G}(z) = 2z^{-k} \quad (2.39)$$

Since in the 2-channel multi-rate filter bank the dyadic subsampling may cause frequency aliasing, (2.38) is intended to clear the aliasing in the reconstructed output. And (2.39) makes sure that the reconstructed output equals the input delayed by k. For fast wavelet transform there are many different 2-channel filter bank implementations that have been explored under the PR condition and some other additional requirements. But such a dyadic sampling wavelet analysis shows a fixed limitation for some practical applications, because it always selects the scaling factor as 2 and the frequency band width of the high frequency channel is twice the frequency band of the neighboring low frequency channel. The wavelet packet analysis provides a much more flexible and detailed time-frequency resolution in the time-frequency plane. In many case it is much better if one performs an adaptive time-frequency analysis according to the signal content. The wavelet packet analysis provides an adaptive analysis according to the frequency axis, and makes it possible to flexibly select a time-frequency resolution for difference frequency bands. And the local cosine packet analysis can flexibly select a time-frequency resolution in the time axis.

2.4 Wigner Distribution

As mentioned in previous sections, the STFT-based time-frequency analysis is closely dependent on a window function, and the wavelet analysis depends on the wavelet function. Differently from them, the Wigner Distribution (WD) characterizes the time-frequency information by the autocorrelation of the analyzed signal and provides a better time-frequency energy concentration than STFT and WT. The WD can be described as follows:

Given a signal $s(t)$,

$$WD(t,\omega) = \int_{-\infty}^{+\infty} s^*(t - \frac{1}{2}\tau)s(t + \frac{1}{2}\tau)e^{j\tau\omega}d\tau \quad (2.40)$$

or given the spectrum $S(\omega)$, that is frequency transform of signal $s(t)$

$$WD(t,\omega) = \int_{-\infty}^{+\infty} S^*(\omega - \frac{1}{2}\theta)S(\omega + \frac{1}{2}\theta)e^{jt\theta}d\theta \quad (2.41)$$

The WD shows many attractive mathematics properties as an appropriate time-frequency representation [Hlaw92]:

1) WD preserves the frequency and time shift:

$$\tilde{s}(t) = s(t - t_0) \Rightarrow WD_{\tilde{s}}(t,\omega) = WD_s(t - t_0, \omega)$$
$$\tilde{s}(t) = e^{j\omega_0 t}s(t) \Rightarrow WD_{\tilde{s}}(t,\omega) = WD_s(t, \omega - \omega_0)$$

2) WD is a real distribution:

$$WD_s^{\,*}(t,\omega) = WD_s(t,\omega)$$

3) WD preserves the signal energy. The integration of WD over the time-frequency domain equals the total energy of the signal:

$$\iint WD_s(t,\omega)dtd\omega = \int |s(t)|^2 dt = \int |S(\omega)|^2 d\omega$$

4) WD has the marginal property. Integration of WD over time equals the energy spectrum, while integration of WD over frequency equals the instantaneous energy:

$$\int WD_s(t,\omega)dt = |S(\omega)|^2 \quad \int WD_s(t,\omega)d\omega = |s(t)|^2$$

5) WD is also a finite support if the signal is a finite support in the time domain or in the frequency domain. If the signal is zero out of a given time interval, correspondingly the WD is also zero, and the same if the signal is zero out of a given frequency interval, the corresponding the WD is zero:

$$\forall t \notin [t_1 \quad t_2] \;\; s(t) = 0 \;\; \Rightarrow \;\; \forall t \notin [t_1 \quad t_2] \;\; WD_s(t,\omega) = 0$$
$$\forall t \notin [\omega_1 \quad \omega_2] \;\; S(\omega) = 0 \;\; \Rightarrow \;\; \forall \omega \notin [\omega_1 \quad \omega_2] \;\; WD_s(t,\omega) = 0$$

6) For a monocomponent analytical signal, the group delay GD of the signal can be achieved by calculating the first moment in time of WD, while the instantaneous frequency IF of the signal can be obtained by calculating the first moment in frequency of WD

$$GD(\omega) = \frac{\int tWD_s(t,\omega)dt}{\int WD_s(t,\omega)dt} \qquad IF(t) = \frac{\int \omega WD_s(t,\omega)d\omega}{\int WD_s(t,\omega)d\omega}$$

The WD reveals then many desirable mathematics properties as a time-frequency representation, but WD has been seriously limited in the practical application by the presence of cross terms inference.

$$\begin{aligned} &for \quad s(t) = x(t) + y(t) \\ &WD_s(t,\omega) = WD_x(t,\omega) + WD_y(t,\omega) + 2\,\mathrm{Re}\,WD_{x,y}(t,\omega) \\ &where \quad WD_{x,y}(t,\omega) = \frac{1}{2\pi}\int_{-\infty}^{+\infty} x^*(t-\frac{1}{2}\tau)y(t+\frac{1}{2}\tau)e^{j\tau\omega}d\tau \end{aligned}$$

As shown in the above equations, the WD of the sum of two signals does not equal the sum of the two signal's WD, but has an additional term $WD_{x,y}$ that represents the so-called cross term. The cross term lies in the center of the two auto-components and oscillates; the frequency of its oscillation increases as the distance between the two auto-component increases. If the signal has N components, then the signal's WD contains $N(N+1)/2$ cross interference terms. These interferences make the WD much more complex and very difficult for the analysis of an actual signal that often is multi-component. Because the cross interference terms oscillate, it is a natural idea to remove the cross interference of the WD by low pass filtering it. The pseudo Wigner-Distribution (PWD) is defined as:

$$PWD(t,\omega) = \int_{-\infty}^{+\infty} s^*(t-\frac{1}{2}\tau)s(t+\frac{1}{2}\tau)h(\tau)e^{j\tau\omega}d\tau \quad (2.42)$$

where the *h* is a finite length window function. In terms of WD, the PWD is the frequency smooth of the WD by the *h* that introduces a frequency convolution [Doug92]:

$$PWD(t,\omega) = \int_{-\infty}^{+\infty} H(\omega - \eta) WD(t,\eta) d\eta \quad (2.43)$$

The PWD smooth the WD in the frequency axis, while the Cohen's class smooth the WD in both time and frequency direction by 2-D low pass filter. The Cohen's class reduces the cross term inferences in the time-frequency plane. Cohen's class can be defined as follows in term of WD:

$$C(t,\omega) = \int_{-\infty}^{+\infty} \phi(\eta,\tau) WD(t-\tau, \omega-\eta) d\eta d\tau \quad (2.44)$$

2.5 Auditory Filter Bank

There are many music analysis tasks that are closely related to human perception. Understanding how the auditory system works is especially useful to the music analysis, as it is the best existing example of analysis "tool".

The human ear consists of outer ear, middle ear and inner ear. Sounds go through the outer ear, middle ear, inner ear, nervous fibers and finally into the brain. The sound wave is picked up in outer ear, and then transformed into a mechanical vibration in the middle ear. In the inner ear, the cochlear transforms the mechanical vibration into neural impulse by a complex process. Cochlear plays an important role, similar to a frequency analyzer. The auditory frequency analyzer is often modeled by a band pass filter bank, which is the so-called auditory filter bank. The masking experiment is commonly used to detect the bandwidth and shape of the auditory filter. Masking refers to a psychoacoustics phenomena: a sound becomes inaudible when another louder sound is present within certain time-frequency intervals. Another important notion relative to the auditory filter bank is the 'critical band' introduced by Fletcher in 1940. As illustrated in Figure 2.2, one sinusoid signal, with power P_s at frequency F, is masked by the wideband noise that is centered at F and has equal power spectrum density in band △F; and the threshold of hearing of the sinusoid signal increases when the noise band △F is increased; however, when the noise band △F is up to a certain value △B, the threshold is not increased significantly even if the noise band △F is further enlarged. This value △B is called critical band centered at F. This detection of the band width is based on the assumption that the audio filter's shape is approximately rectangle and the signal is detectable if the signal-noise-ratio (SNR) is equal or greater than 1.

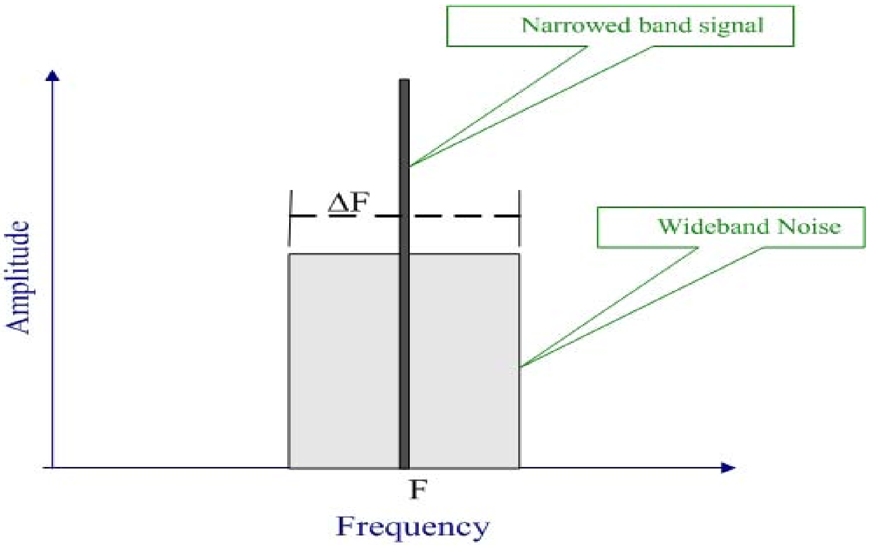

Figure 2.2 Critical Bandwidth

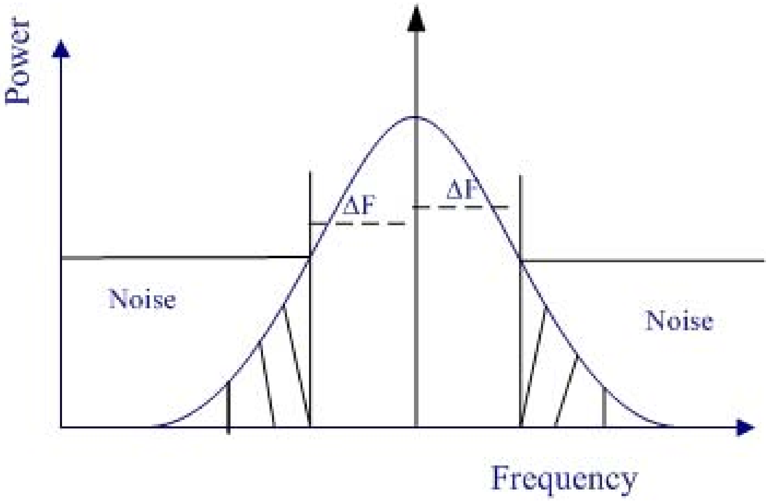

Figure 2.3 Notched Noise Experiment

Another generalized critical band concept for the auditory filter is the Equivalent Rectangular Bandwidth (ERB) defined as follows:

$$B_{EB} = \int_0^{\infty} |H(f)|^2 df \quad (2.45)$$

where H(f) is the frequency response of a auditory filter and the value of |H(f)| is normalized at 1. The real power response shape of the auditory filter is not a rectangle and it can be measured with some special assumptions. The notched-noise experiment is commonly used to define the possible shape of auditory filter power response. Illustrated in Figure 2.3, a sinusoid signal is masked by the wideband noise with the spectral notch centered at the signal frequency. The threshold of hearing of the sinusoid signal can be measured in function of the notch width, 2△F, and the measured threshold is proportional to the noise power leaking into the auditory filter, so the power response shape of the auditor filter can be deduced by the function relation between the measured threshold and the notch width. The easiest way is to approximate the auditory filter power response by some parameterized function family. The rounded-exponential function is introduced to approximate the shape of auditory filter power response. The rounded-exponential auditor filter power response can be defined as follows:

$$|H(f)|^2 = (1 + pg)e^{-pg} \quad (2.46)$$

where

$$g = \left| \frac{f - f_c}{f_c} \right| \quad (2.47)$$

There is only one parameter p in the definition (2.46). To measure the shape of the power response of the auditory filter, it is necessary to make an assumption that the threshold to hear the signal is proportional to the noise power leaking into the auditory filter. If the measured power threshold of hearing the signal is P_S, the noise power is P_N, the noise spectrum density is N_0 and K is a constant, the following equations apply (Hart97):

$$P_N(\Delta g) = 2N_0 f_c \left(\int_{\Delta g}^{1} |H(g)|^2 dg + \int_{\Delta g}^{\infty} |H(g)|^2 dg \right) \quad (2.48)$$

$$P_S(\Delta g) = KP_N(\Delta g) \quad (2.49)$$

In the two equations there are 2 parameters that need to be calculated, so two measurements are enough for the calculation. However in practical experiments there are many measurements and it is possible to select the parameters that make the parameterized function the best approximation of the power response of the filter.

Another commonly used auditory bank is the gammatone filter bank that can be defined by its impulse response. A gammatone filter's impulse response is described as follows:

$$h(t) = at^{n-1}\exp(2\pi bt)\cos(2\pi f_c t + \phi) \quad t > 0 \quad (2.50)$$

The impulse response is the product of a cosine carrier and a gamma envelope; the parameter f_c is the center frequency of the filter, b determines the frequency bandwidth, n is the filter order. Compared to the other auditory filter bank, the gammatone filter bank has some advantages. First, as shown in the definition, it is expressed as a casual impulse response, so it is realizable and computation-efficient implementations are available. Secondly it is reported that the magnitude response of the gammatone filter bank matches very well with many results from psychoacoustic research. It is well known in fact that the human ear filter seems symmetric at low level input, asymmetric with increasing frequency, and behaves like a level-dependent nonlinear filter.

Recently it was reported [Irino97] that gammachirp auditory filter bank is a better candidate for an asymmetric, level-dependent auditory filter bank, and matches very well with many notched-noised masking data. The gammachirp auditor filter may be defined according to its impulse response as follows:

$$h(t) = at^{n-1}\exp(2\pi bt)\cos(2\pi f_c t + c\ln t + \phi) \quad t > 0 \quad (2.51)$$

Compared to gammatone filter, the gammachirp impulse response adds a new log-time phase term $c\ln t$. The additional phase term controls the filter's asymmetry.

2.6 Review of Joint Time-Frequency Analysis for Music Signals

Music signal analysis is closely related to most of modern music research tasks such as timbre analysis, sound compression, auditory modelling and automatic music transcription. Helmholtz analyzed the timbre of instruments by Fourier analysis based on limited spectral analysis tools, including acoustic resonators, tuning forks, and reeds; but Fourier analysis only can provide some information about the amplitudes of the harmonic components without any time-varying character information; this is probably the reason why Helmholtz believed that the fundamental frequency of the harmonic series determined the pitch and the pattern of magnitudes of the remaining components determined the timbre [Will96]. In fact it is well known now that both things are not completely true. The timbre perception is also relative to the time-varying character of the harmonic components, and most of the music related tasks need a joint time-frequency analysis, though the autocorrelation analysis may be enough to detect a fundamental frequency of simple monophonic music [Mont00].

As a traditional and convenient time-frequency analysis tool, STFT is still broadly exploited for music analysis; for example, Pertusa recently used the STFT as the front-end processing for his polyphonic transcription tool [Pert03, Pert04]. But as mentioned STFT only provides the same time-frequency resolution in all the time-frequency plane, this conflicts with the requirement that music signal analysis need a better time resolution at high frequency and better frequency resolution at low frequency. STFT is then commonly combined with some other frequency analysis tool to reduce its main disadvantage. In his signal analysis system, Peeters first use a Mel filter bank to separate the input signal into different frequency bands and then STFT is used to extract detailed frequency information for every frequency band; the STFT window-size can be flexibly set according to signal analysis requirements [Peet02]. In another polyphonic transcription system, Klapuri first calculates the STFT of the input signal and gets the frequency information, then directly in the frequency domain he separates the signal into 18 different frequency bands, each of which comprises a 2/3-octave region of the spectrum; and then local regions of the spectrum are further processed separately [Klapuri04]. Hainsworth introduces the Time-Frequency Reassignment technology, which is considered as a refinement of STFT and makes best use of the phase information of STFT to reduce the smearing of the energy of the standard STFT [Hains01-1]; he tries to use this technology in real-word examples and shows some advantages over the standard STFT [Hains01-2]. Keren proposes Multiresolution Fourier Transform (MFT) as a computation-efficient time-frequency analysis tool for polyphonic music transcription; the basic idea behind the MFT almost is to separate the signal into different frequency bands by subsampling, then perform the different window-size STFT in every frequency band, and achieve different time-frequency resolution in the time-frequency plane with high improved computation efficiency [Keren98]. Jang introduces a multiresolution time-frequency analysis for sinusoid models; in his analysis-synthesis processing, the signal is first separated into different octave-spaced subbands by dyadic sampling multirate filter bank, and then in every subband an optimal analysis-synthesis frame size is chosen adapting to its time-frequency character, then sinusoid component is extracted in every frame by matching pursuit algorithm.

Another multiresolution time-frequency analysis, wavelet analysis, can provide a constant-Q frequency resolution that almost matches the requirement of music signal analysis. But the commonly used dyadic sampling DWT can only provide very coarse frequency resolution that is far from the frequency resolution requirement of music signal analysis. The wavelet packet analysis provides a more flexible and detailed resolution in the time-frequency plane and also provides an orthonormal or biorthonormal base, so it shows strong attraction in music applications especially for feature extraction and compression. Srinivasan incorporates the psychoacoustic models with an adaptive wavelet packet scheme and achieve high-quality compression in audio signal [Srin98]. Jones tries to summarize a general relation between the number of vanishing moments of the wavelet and sparseness of the DWT coefficient for application in the music signals compression [Jone04]. Grimaldi applies the Discrete Wavelet Packet Transform (DWPT) to extract time and frequency features from music signal for music genre classification [Grim02]. Tzanetakis developes a system to track the music beat by the DWT [Tzane01]. Dörfler tries to provide a mathematical tool for time-frequency analysis of music signal by introducing the Gabor analysis, which is mathematically well-defined and can help understanding many issues in the time-frequency processing of audio signals [Dorf01].

As mentioned before, the Wigner-Distribution has a good time-frequency energy concentration, but it is the cross-term interference and high computation cost that prevents Wigner-Distribution from applying as a general time-frequency analysis tool in practical music analysis. Cohen's class has been explored for music signal analysis by several researchers. Donovan develops a perceptual joint time-frequency tool in the framework of Cohen's class that combines a smooth kernel and Wigner-Distribution to incorporate a joint model of both temporal and spectral mask [Dono05]. Modal distribution is a member of Cohen's class specifically designed for music signal analysis. Steran designs an automatic transcription system, which uses the modal distribution as time-frequency analysis front end [Ster96]. And Mellody applies the modal distribution as time-frequency analysis tool in exploring the characteristics of violin vibratos [Mell00].

As mentioned in the previous sections, the auditory filter bank is commonly used to model the human ear as a frequency analyzer, so the auditory filter bank is often designed to match as far as possible with the human ear's frequency analysis function based on the existing data from the psychoacoustics and physiology research; for a perception-relative music processing, the auditory filter bank can be considered as one phase of the time-frequency analysis. If a practical music processing task (such as polyphonic transcription) needs relatively high frequency resolution, the audio-model-based time-frequency analysis often includes two phases; first the input signal is separated into the different frequency bands by auditory filter bank, and then more detail frequency information need to be obtained in every frequency band in some other ways. In polyphonic transcription systems, Marolt combines the gammatone filter bank and an adaptive oscillator to perform the frequency analysis; first the music signal is separated into different frequency bands by a gammatone filter bank, and then an adaptive oscillator is used to track partials [Maro04].

Chapter 3

LEARING THEORY: STATE OF THE ART

There are many common and practical tasks such as feature recognition and classification, that are very difficult to be resolved by traditional computational means, but that are usually not difficult for the human being once educated by learning and experience; it is then a natural idea to mimic the natural behavior by implementing some kind of learning machine to deal with similar problems. In this section, a two-class classifier is discussed in the context of machine learning associated to signal processing for the solution of classification tasks related to music. With this, a short introduction to Support Vector Machines will be given.

3.1 Empirical Risk Minimization and Structure Risk Minimization Inductive Principle

Considering a two-class classifier, a machine learning process may be described as follows:
There exist m samples with n dimensional input vector ***x*** and known output label ***y***,

$$x_m \in R^n\,,\; y_m \in \{-1,1\} \quad (3.1)$$

and the decision function set,

$$S = \{f(x,\alpha) : \alpha \in \Lambda\},\quad f : R^n \to \{-1,1\}$$

where Λ is a set of the parameters.

From the above decision function set, one wants to find a specific function f(x,α^*), which can be used to estimate the output values for the new input samples with minimal real errors; in other words, a machine learning processing consists of adjusting the parameter α for minimizing expected risk R(α) on bad classification of new unknown samples. If a function ***L*** is selected as loss function, P(x,y) is the probability distribution, and assumed the example data is independently and identically distributed (i.i.d.) , it can be written that:

$$R(\alpha) = \int L(y, f(x,\alpha))dP(x,y) \qquad (3.2)$$

Usually the *P(x,y)* is unknown, R(α) can not be directly computed, and only the limited number of m samples following the *P(x, y)* is known; consequently the empirical risk $R_{emp}(\alpha)$ is usually used to train the learning machine (in place of $R(\alpha)$) by the empirical risk minimization (ERM) inductive principle, which plays an important role in the learning theory.

$R_{emp}(\alpha)$ can be calculated according to the following definition:

$$R_{emp}(\alpha)=\frac{1}{m}\sum_{i=1}^{m}L(y_i,f(x_i,\alpha,)) \quad (3.3)$$

The least-squares method is often chosen as the loss function; in this case the empirical risk is therefore:

$$R_{emp}(\alpha)=\frac{1}{m}\sum_{i=1}^{m}(y_i-f(\alpha,x_i))^2 \quad (3.4)$$

The goal of the learning process is to minimize the expected risk (real risk) instead of empirical risk, so if a learning processing is based on the empirical risk minimization inductive principle, it must be considered when such a learning process can also achieve a small expected risk (real risk) and when it cannot; in other words, it must be explored if the minimization of the empirical risk is consistent with the minimization of real risk. Vapnik [[Vapnik99] uses the uniform convergence framework to resolve such an issue. It is claimed that expected risk $R_{emp}(\alpha)$ uniformly converge to real risk $R(\alpha)$ if the following equation is valid :

$$\lim_{l\to\infty}P\left\{\sup_{\alpha\in A}(R(\alpha)-R_{emp}(\alpha))>\varepsilon\right\}=0,\quad \varepsilon>0 \quad (3.5)$$

with the condition $A\le R(\alpha)\le B$

The equation (3.5) is also a sufficient and necessary condition for the ERM principle to be consistent. The theory of uniform convergence can provide some bounds on the deviation of empirical risk from expected risk. As an example, one commonly-used bound, with the probability $1-\eta$, can be described as follows:

$$R(\alpha)\le R_{emp}(\alpha)+\sqrt{\frac{h(\ln\frac{2l}{h}+1)-\ln\frac{\eta}{4}}{l}} \quad (3.6)$$

where h is the Vapnik-Chervonenkis (VC) dimension of the decision function set *S*. The above inequality can also be rewritten in general as:

$$R(\alpha)\le R_{emp}(\alpha)+\phi(\frac{l}{h}) \quad (3.7)$$

where the $\phi(l/h)$ is so-called confidence interval.

For a certain training set, the bound in (3.6) provides a way to estimate the real risk on future data based only on the empirical risk and the VC dimension. The VC dimension represents a crucial concept in the statistic learning theory and can be used to estimate the capacity of a learning machine. The VC dimension of a set of indicator functions (the function with only two values) f(x, α) can be defined as the maximum number h of vectors $x_1, x_2 \ldots x_h,$ that can be separated into two classes in all 2^h possible ways using functions of the set [Vapnik99]. The VC dimension is independent from the sample distribution and only depends on the set of the decision function.

For example, a two-dimension two-class linear classifier has the decision function like,

$$f(z,\alpha)=\left\{\begin{matrix}1 & if:\alpha_1 z_1+\alpha_2 z_2+\alpha_0\ge 0\\ 0 & if:\alpha_1 z_1+\alpha_2 z_2+\alpha_0<0\end{matrix}\right\} \quad (3.8)$$

in the two-dimension coordinate space $Z=(z_1,z_2)$, the VC dimension of this classifier equals 3 (as illustrated in Figure 3.1).

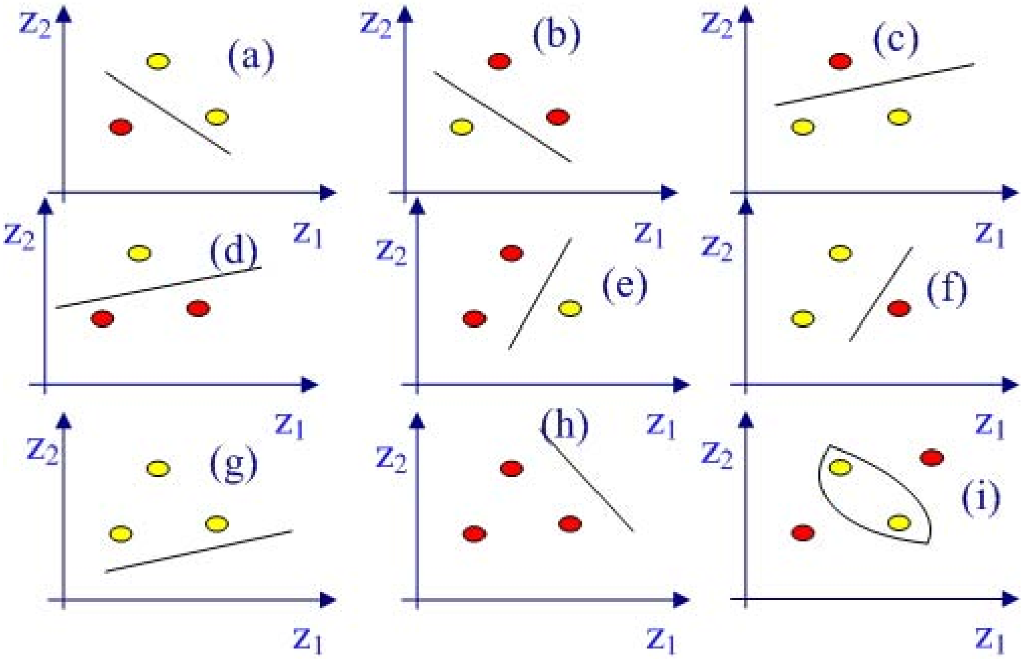

Figure 3.1 VC dimension

As *shown in sub-image (a-h), given 3 input samples* $z^1, z^2 z^3,$ *and the corresponding output label* y_1, y_2, y_3 *can be arranged at most in eight different ways, in each of which the samples* $(z^1, y_1), (z^2, y_2), (z^3, y_3)$ *can be always correct classified into two classes by 2-dimension linear decision function (in equation 3.8) with selection of 3 approximate parameters; given 4 input samples with the output labels as shown in sub-image (i) , the linear decision function can not correctly classify the 4 samples anymore, so the VC dimension of this classifier equals 3.*

From the bound (3.6), it is also evident that the deviation of empirical risk from expected risk is negligible if the ratio between the sample size and the VC dimension *l/h* is large enough. For the case with a small sample size (e.g. *l/h<20*), the second term in the right side of (3.6) is not negligible anymore and the learning process should consider both the empirical risk and capacity of the decision function set; such a learning process is commonly based on the Structural Risk Minimization (SRM) inductive principle, which is proposed and developed by Vapnik. To implement the SRM inductive principle, an important issue is how to construct the decision function set with controllable capacity; in other words, the VC dimension h of the decision function set is a controllable variable. With the assumption that the capacity of the decision function set is controllable, the learning process of a classifier may be described as follows:

First, one nested structure of the decision function sets need be designed like:

$$S_1 \subset S_2 \ldots \subset S_k \subset S_N \quad (3.9)$$

where $h_k<h_{k+1}$ and h_k is the corresponding VC dimension of the decision function subset S_k. And then for a given *l* samples, the decision function $f_k(x,\alpha^*)$ is obtained with the minimal empirical risk $R_k(\alpha^*)$ in each decision function subset S_k; at the same time another term confidence interval $\phi(l/h_k)$ can also be calculated for the subset S_k. With the subset index increasing, usually the empirical risk $R_k(\alpha^*)$ decreases and the confidence interval increases. As illustrated in Figure 3.2, the subset S_n is finally considered as the best decision function subset for learning if n=k minimizes the sum of empirical risk $R_k(\alpha^*)$ and confidence interval $\phi(l/h_k)$; correspondingly, the specified decision function $f_n(x,\alpha^*)$ is considered as the optimal solution and has a minimum expected risk on the future unknown input samples.

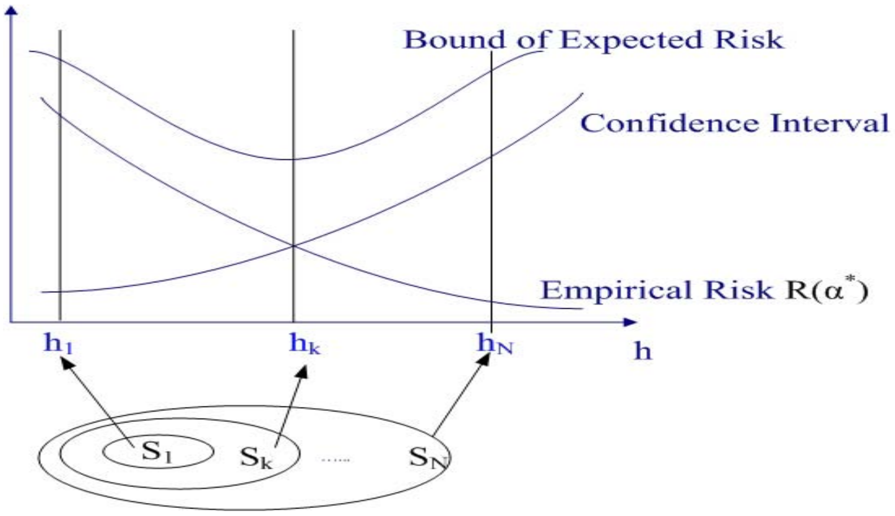

Figure 3.2 Implementation of Structure Risk Minimization

In summary, based on the same training data set, sometimes one low-capacity learning machine with more training error may perform better than another high-capacity with small training error on the future data. This is the so-called overfitting problem relative to the generalization ability of a learning machine. To control the generalization ability of machine learning, Vapnik provides the structure risk minimization (SRM) inductive principle, which minimizes the expected risk function in term of both empirical risk and capacity of machine learning. According to SRM, to minimize the expected risk both empirical risk and machine capacity need to be considered. Although SRM inductive principle has been founded well in theory, its practical implementation still is very challenging, because it is not clear how to compute the VC dimension for most of the practical implementations of learning machines; only a few of these machines have a known computation method for VC dimension, and secondly it is not easy to control the capacity of the learning machine in the training phase. The support vector machine (SVM) provides an excellent implementation of learning machine based on the SRM inductive principle, and can minimize the empirical risk and control the capacity of a learning machine at the same time. SVM are introduced in the next section.

3.2 Maximum-Margin Support Vector Machine

Given the samples listed in (3.1), one can separate them into two classes by a linear hyperplane

$$w \cdot x - b = 0 \quad (3.10)$$

If the samples are linearly separable, there are many hyperplanes that can separate the data without error, and the separating hyperplane with maximum margin is considered as the optimal hyperplane or maximum-margin hyperplane. The margin means the distance between hyperplane to the closest vector as shown in Figure 3.3.

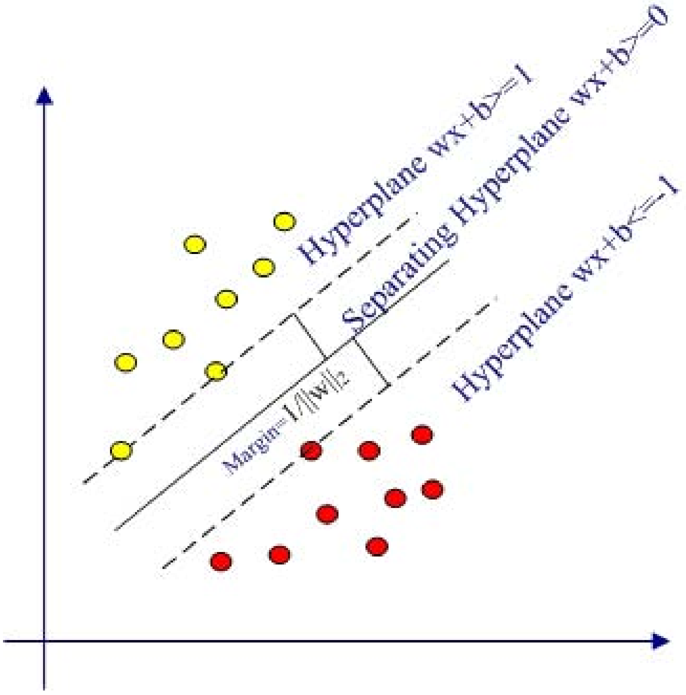

Figure 3.3 Maximum-margin Classifier

The classifier with the maximum-margin separating hyperplane may be described in the following way:

$$y_i = 1 \quad if: wx_i + b \geq 1 \text{ and } y_i = -1 \quad if: wx_i + b \leq -1 \quad (3.11)$$

and the (3.11) can be expressed more simply by one inequality as follows:

$$y_i(wx_i + b) \geq 1 \quad (3.12)$$

where *w* is the weight vector and *b* is the bias.

Once the classifier expressed according to (3.12), the corresponding margin γ can be calculated as follows (Figure 3.3):

$$\gamma = \frac{1}{\|w\|} \quad (3.13)$$

There exists a bound for the VC dimension h of the n-dimension linear classifier with a certain margin γ:

$$h \leq \min(\left\lfloor \frac{R^2}{\gamma^2} \right\rfloor, n) = \min(R^2 \|w\|^2, n) + 1 \quad (3.14)$$

where R is minimal radius of the sphere that includes all the input vectors x. According to (3.14), the classifier with the maximum-margin hyperplane has the smallest VC dimension bound, that is to say, has the best generalization ability. As mentioned in the previous section, a learning process based on SRM inductive principle considers both the empirical risk and capacity of the learning machine. In the linearly separable case, the support vector machine keeps the empirical risk is not changed (always equal to zero), and select the maximum-margin hyperplane as the separating hyperplane, which is considered to have the lowest capacity.

As shown in equation (3.13), maximizing the margin corresponds to minimizing the ||w||, so the process to search the maximum-margin hyperplane can be described as follows:

$$\textit{Minimizing}_{w,b} < w \cdot w > \quad (3.15)$$

$$\textit{subjecting to } y_i(wx_i + b) \geq 1 \quad i = 1,2,3..m;$$

The above problem can be solved according to the standard Quadratic Programming optimization techniques. Using these techniques, a Lagrange functional has to be calculated:

$$L(w,b,\alpha) = \frac{1}{2}(w \cdot w) - \sum_{i=1}^{m} \alpha_i \{[(x_i \cdot w) - b]y_i - 1\} \quad (3.16)$$

And then the Lagrange functional is minimized with respect to *w* and *b* with the w, b meeting the following constraints:

$$\frac{\partial L(w,b,\alpha)}{\partial w} = w - \sum_{i=1}^{m} y_i \alpha_i x_i = 0; \quad (3.17)$$

$$\frac{\partial L(w,b,\alpha)}{\partial b} = \sum_{i=1}^{m} y_i \alpha_i = 0; \quad (3.18)$$

The equation (3.16) is commonly called the primal representation of Lagrange functional, and substituting the equation (3.17) and (3.18) into (3.16), one can get the dual representation,

$$L(w,b,\alpha) = M(\alpha) = \sum_{i=1}^{m} \alpha_i - \frac{1}{2}\sum_{i,j=1}^{m} y_i y_j \alpha_i \alpha_j < x_i \cdot x_j > \quad (3.19)$$

According to the Quadratic Programming optimization theory, the solution of the problem in (3.15) can be achieved by resolve the following problem:

$$\textit{Maximizing}\;\; M(\alpha) = \sum_{i=1}^{m} \alpha_i - \frac{1}{2}\sum_{i,j=1}^{m} y_i y_j \alpha_i \alpha_j < x_i \cdot x_j > \quad (3.20)$$

$$\textit{subjecting to} \sum_{i}^{m} \alpha_i y_i = 0; \;\textit{and}\; \alpha_i \geq 0 \;\; i = 1,2,3..m;$$

Suppose that α^* is the solution of the problem in (3.20), the solution w^* of the problem in (3.15) can be calculated according to relation equation (3.17):

$$w^* = \sum_{i=1}^{m} y_i \alpha_i^* x_i; \quad (3.21)$$

According to the Karush-Kuhn-Tucker complementary condition, the solution α^* and (w^*,b^*) meet the following relationship:

$$\alpha_i^* \{y_i[(w^* \cdot x_i) - b_0] - 1\} = 0 \; (3.22)$$

From equation (3.22), only the support vector can have nonzero α_i^* in the w^* expansion. Support vectors are the input vectors satisfying the equality condition

$$y_i[(w_0 \cdot x_i) - b_0] = 1 \quad (3.23)$$

The equation (3.21) can be rewritten as:

$$w^* = \sum_{i \in SV} y_i \alpha_i^* x_i, \; \alpha_i^* \geq 0 \; (3.24)$$

and the decision function of the classifier with maximum-margin separating hyperplane is therefore:

$$f(x) = sign(\sum_{i \in SV} y_i \alpha_i^* (x_i \cdot x) - b^*) \quad (3.25)$$

$$b^* = \frac{1}{2}[(w^* \cdot x^*(-1) + w^* \cdot x^*(1))] \quad (3.26)$$

where x*(-1) is any support vector with the target label –1, and x*(1) is any support vector with target value 1.

3.3 Soft Margin Support Vector Machine

On one hand, and as an important concept, the maximal margin classifier is a good starting point to construct a more complex Support Vector Machine; on the other hand it only can be used in the linearly separable case; however, practical data often contain noise, and it is not linearly separable. For this reason, the optimization problem is replaced by a so-called soft margin optimization that may be described as follows:

$$Minimizing_{w,b} \ < w \cdot w > +C\sum_{i=1}^{m} \xi_i^k \quad (3.27)$$

$$subjecting\ to \ \ y_i(wx_i+b)\geq 1-\xi_i \ \ i=1,2,3..m$$

$$\xi_i \geq 0 \ \ i=1,2,3..m;$$

In the above optimization problem, the introduced new variable ξ_i is the slack variable to allow the margin constraints to be violated, and the parameters C and k define the cost of the constraint violation. As mentioned before, for a linearly separable case the support vector machine always makes the empirical risk equal to zero, and then select the classifier with the lowest capacity; this is a special case for the implementation of the SRM inductive principle. But if the sample data are not linearly separable, a linear SVM can not separate the sample data without error, then minimizing the second term of the objective function of the optimization problem in (3.27) is relative to control the empirical risk, and minimizing the first term is used for minimization of the VC dimension of the learning machine, so this approach is a typical implementation of SRM inductive principle.

For an example, to solve the problem in (3.27) with parameter k=1 (1-Norm Soft Margin), the primal representation of the constructed Lagrange functional can be expressed as follows:

$$L(w,b,\xi,\alpha,r)=\frac{1}{2}(w\cdot w)+C\sum_{i=1}^{m}\xi_i-\sum_{i=1}^{m}\alpha_i\{[(x_i\cdot w)-b]y_i-1+\xi_i\}-\sum_{i=1}^{m}r_i\xi_i \quad (3.28)$$

where $\alpha_i \geqslant 0$ and $r_i \geqslant 0$. And then the Lagrange functional is minimized with respect to *w* and *b* with the w, b meeting the following constraints:

$$\frac{\partial L(w,b,\xi,\alpha,r)}{\partial w}=w-\sum_{i=1}^{m} y_i\alpha_i x_i=0; \ (3.29)$$

$$\frac{\partial L(w,b,\xi,\alpha,r)}{\partial \xi_i}=C-\alpha_i-r_i=0; \ (3.30)$$

$$\frac{\partial L(w,b,\xi,\alpha,r)}{\partial b}=\sum_{i=1}^{m} y_i\alpha_i=0; \ (3.31)$$

Substituting the above equations into the primal Lagrange functional, one can get the dual representation as follows:

$$L(w,b,\xi,\alpha,r) = M(\alpha) = \sum_{i=1}^{m} \alpha_i - \frac{1}{2}\sum_{i,j=1}^{m} y_i y_j \alpha_i \alpha_j < x_i \cdot x_j > \quad (3.32)$$

And resolving a 1-norm soft margin problem is equivalent to resolving the following problem:

$$\textit{Maximizing} \;\; M(\alpha) = \sum_{i=1}^{m} \alpha_i - \frac{1}{2}\sum_{i,j=1}^{m} y_i y_j \alpha_i \alpha_j < x_i \cdot x_j > \quad (3.33)$$

$$\textit{subjecting to} \sum_{i}^{m} \alpha_i y_i = 0; \textit{and } C \geq \alpha_i \geq 0; \;\; i = 1,2,3..m;$$

Suppose that the α^* is the solution of the problem in (3.33), then the solution w^* of the problem in (3.27) can be calculated according to relation equation (3.29):

$$w^* = \sum_{i=1}^{m} y_i \alpha_i^* x_i; \quad (3.34)$$

Similar to the linearly separable case, only some coefficients have the non-zero value in the expansion (3.34), and the vectors with non-zero coefficients are called support vectors.

Compared to the maximum-margin optimization, the 1-norm soft margin optimization has the same object function, and the only difference is that there exists an upper bound C for α in the constraint. The upper bound C intuitively limits the influence of the outliers that often have large Lagrange multipliers.

3.4 Nonlinear Support Vector Machine

For many practical applications, the ideal decision functions of the classifiers are probably not linear.

In the introduced algorithms for maximum-margin classifier and 1-norm soft margin classifier, there is an important characteristic. The final decision function and the solution of the quadratic optimization problem both only depend on the inner product of input vectors. This characteristic makes it possible to solve some nonlinear problems by SVM. The basic idea is to first nonlinearly map the input data to another high dimension feature space, where the nonlinear problem may become a linear problem, and then use the above linear algorithm to solve the problem. Because the algorithm only depends on the inner product, it is not necessary to know the exact mapping function if the inner product of the mapping function is known. For example, a nonlinear mapping function can be:

$\phi : \Re^n -> G$, where G is the feature space. And a kernel function is as follows:

$$k(x, y) =< \phi(x) \cdot \phi(y) > \quad (3.35)$$

When searching a 1-norm soft margin hyperplane in the feature space, every input sample x_i will be replaced by the $\phi(x_i)$, finally the decision function and corresponding quadratic optimization problem become as follows:

$$f(x) = sign(\sum_{i \in SV} y_i \alpha_i^* k(x_i, x) + b^*) \quad (3.36) \text{ and}$$

$$Maximizing \ M(\alpha) = \sum_{i=1}^{m} \alpha_i - \frac{1}{2} \sum_{i,j=1}^{m} y_i y_j \alpha_i \alpha_j k(x_i, x_j) \quad (3.37)$$

$$subjecting \ to \ \sum_{i}^{m} \alpha_i y_i = 0; \ and \ C \geq \alpha_i \geq 0 \ \ i = 1,2,3..m;$$

As shown in equation (3.36) and equation (3.37), a maximum margin hyperplane classification in the feature space can be achieved only depending on the computation in the input data space by the kernel function.

The determination of a kernel usually involves two cases. First, if the mapping function from the input space to the feature space is known, the kernel function can be derived from the map function according equation (3.35); in another case, the mapping function is implicit and the kernel can not be derived and need to be defined directly. One issue is how to judge if a function can be expressed like in (3.35) without the explicit form of a map function. The answer lies in the Mercers condition. According to Mercers theorem, if $K : X \times X -> R$ is a continuous symmetric function, the input space X is a compact subset of R^n, and the K meets the following condition:

$$\int_{X \times X} K(x, z) f(x) f(z) dxdz \geq 0 \quad (3.38)$$

for all square integratable function f; then K can be expanded into a uniform convergence series like:

$$k(x, z) = \sum_{j=1}^{\infty} \lambda_i \varphi_i(x) \varphi_i(z) \quad \lambda_i \geq 0 \quad (3.39)$$

Let a map function $\phi : X -> R^{\infty}$:

$$\phi(x) = (\phi_1(x), \phi_2(x), .. \phi_n(x) ....), \text{ and } \phi_i(x) = \sqrt{\lambda_i} \varphi_i(x)$$

then the equality (3.39) can be rewritten as follows:

$$k(x,z) = \sum_{j=1}^{\infty} \phi_i(x)\phi_i(z) =< \phi(x) \cdot \phi(z) > \quad (3.40)$$

So if a function K meets the inequality constraint in (3.38), then K can be considered as a kernel function, which is the inner product of certain implicit map function.

The two commonly-used kernel functions are the Gaussian and the polynomial kernel:

$$\text{Polynomial kernel: } k(x,z) = (x \cdot z + 1)^p \quad (3.41)$$

$$\text{Gaussian kernel: } k(x,z) = e^{-\|x-z\|/2\sigma^2} \quad (3.42)$$

where p and σ are called the model parameters .

More complex kernel functions can be constructed by some known kernel functions according to the following proposition [Crist00].

Given the kernel function K_1 and K_2 over the X×X, $X \subseteq R^n$, a∈R^+, f(.) is a real-valued function on X, and B a symmetric positive semi-definite n×n matrix. Then the new kernels can be constructed as follows:

$$k(x,z) = k_1(x,z) + k_2(x,z) \quad (3.43)$$

$$k(x,z) = ak_1(x,z) \quad (3.44)$$

$$k(x,z) = k_1(x,z)k_2(x,z) \quad (3.45)$$

$$k(x,z) = f(x)f(z) \quad (3.46)$$

3.5 Multi-Class Support Vector Machine

The discussion about support vector machines in previous sections is based on the binary classifier; in practical applications the classifier need to be constructed for a multi-class classification problem. There exist several known proposed methods for multi-class support vector machines. These methods usually exploit two different strategies.

3.5.1 One-against-rest Multi-class Classifier

The first strategy is the so-called one-against-rest classifier, which is intuitive and simple. For a K-class problem, the one-against-rest multi-class classifier first builds K 2-class classifiers, each of which is responsible for every class respectively. For the n^th binary classifier, all training data need to be involved; the positive result is the data point in class n, and the negative result is the data point in the other n-1 classes. Each of the K binary classifiers is trained to find the decision function by a 2-class support vector machine, and then all the decision functions are combined to get the final decision function for multi-class classification problem:

$$f(x) = \arg\max_{n} \sum_{i \in SV} y_i \alpha_i^n k(x_i, x) + b^n) \quad (3.47)$$

where $\sum_{i \in SV} y_i \alpha_i^n k(x_i, x) + b^n)$ is the decision function of the n^{th} class binary classifier.

3.5.2 One-against-one Multi-class Classifier

The second strategy uses some schemes and combines pair-wise binary classifiers to resolve the multi-class classification problem; this is the so-classed one-against-one classifier [Hast96]. In this strategy, a binary classifier has to be built for each possible pair of classes and the total number of these binary classifiers is equals to K(K-1)/2. The training data of each binary pair classifier only includes the training data of the involved two classes. A one-against-rest multi-class classifier only can output the class decision but not the class probability. The probability estimation is important for some practical applications, in which the classifier is not used in isolation but integrated with some other higher level knowledge.

The class probability problem for the K-class classification (K>2) may be expressed more clearly and formally as follows. Given the a K-class classification training data set, observation X and label Y, the first problem is how to estimate the posterior probability $\mu_{i,j}$=P(Y=i|Y=i or j,, X) from the binary pair-wise classifier, and the second problem is how to estimate probability P(Y=i|X), i=1,…,K. based on the estimation of pair-wise probability $\mu_{i,j}$ for the new data. As shown in the above sections, the output of the SVM decision function is not a probability. This because directly training a binary SVM classifier with probability output is very difficult in practice. One commonly-used way is to solve the problem into two phases, first a standard binary SVM classifier is trained to get the decision function, and then estimation of the $\mu_{i,j}$ may be conversed to estimate a functional relation between the probability $\mu_{i,j}$ and the output of decision function. The probability $\mu_{i,j}$ can be described as follows:

$$\mu_{i,j}(x) = F(f_{i,j}(x)) \quad (3.48)$$

where $f_{i,j}(x)$ is the decision function of the pair-wise binary classifier involving the i^{th} class and j^{th} class. Direct estimation of the function F in (3.48) is still a difficult issue; usually with the assumption of F belonging to a parameterized function set, the estimation of F is reduced to estimate the parameters. For an example, in [Platt99] the sigmoid function is suggested as the model of F, and the equation (3.48) can be written as follows:

$$\mu_{i,j}(x) = \frac{1}{1+\exp(Af_{i,j}(x)+B)} \quad (3.49)$$

where A and B are the parameters and need be estimated by some ways.

With the assumption that the all the pair-wise probabilities $\mu_{i,j}$ are known , several methods are suggested to get the probability P(Y=i|X) based on the combination of the estimates of all the pair-wise probabilities $\mu_{i,j}$.

For example: an intuitive rule [Fried96] of the combination of the all binary classifiers is to use a voting scheme and assign to the class that wins the most pair-wise comparisons as like: let $r_{i,j}$ be the estimate of $\mu_{i,j}$, and the voting rule is

$$f_{\max}(x) = \arg\max_{i} \sum_{j:j\neq i} I(r_{i,j} > r_{j,i}) \quad (3.50)$$

where the *I* is a indicator function and *I(x)*=1,if x is true, otherwise *I(x)*=0. A simple estimation of class probabilities can be calculated according to equation (3.51):

$$P(Y=1\,|\,X) = \frac{2\arg\max_{i} \sum_{j:j\neq i} I(r_{i,j} > r_{j,i})}{K(K-1)} \quad (3.51)$$

Some other more refined methods can be found in the literatures [Wu04, Hast96]

Chapter 4

A FREQUENCY-DEPENDENT TIME-FREQUENCY ANALYSIS TOOL: RESONATOR TIME-FREQUENCY IMAGE

As mentioned before, because the length of the window function of the STFT is independent from frequency, the STFT always maintains the same resolution in the time-frequency plane, and such resolution distribution is not suitable for music signal analysis. Other analysis methods have also been reviewed presenting specific advantages and problems in their use. For these reasons an original frequency-dependent time-frequency analysis tool has been developed and proposed here: the Resonator Time-Frequency Image (RTFI), which is especially designed for music signal analysis.

4.1 Frequency-Dependent Time-Frequency Analysis

To better introduce RTFI, it is better to start from a generalized definition of frequency-dependent time-frequency analysis. It is proposed to define the Frequency-Dependent Time-Frequency Transform (FDTF) as follows:

$$FDTF(t,\omega) = \int_{-\infty}^{\infty} s(\tau) w(\tau - t,\omega) e^{-j\omega(\tau - t)} d\tau \quad (4.1)$$

Differently from STFT, the window function *w* of FDTF may depend on frequency *ω*; this means that time and frequency resolutions can be changed according to frequency. The energy of STFT is named a *spectrogram*, a name that has earlier been used for speech analysis. Similarly the energy of FDTF is named here *Musicgram*, which can be defined as follows:

$$MusicGram(t,\omega) = \left| FDTF(t,\omega) \right|^2 \quad (4.2)$$

At the same time, equation (4.1) can also be expressed like:

$$\begin{aligned} FDTF(t,\omega) &= \int_{-\infty}^{\infty} s(\tau) w(\tau - t,\omega) e^{-j\omega(\tau - t)} d\tau \\ &= s(t) * I(t,\omega) \qquad (4.3) \end{aligned}$$

with

$$I(t, \omega) = w(-t, \omega)e^{j\omega t} \qquad (4.4)$$

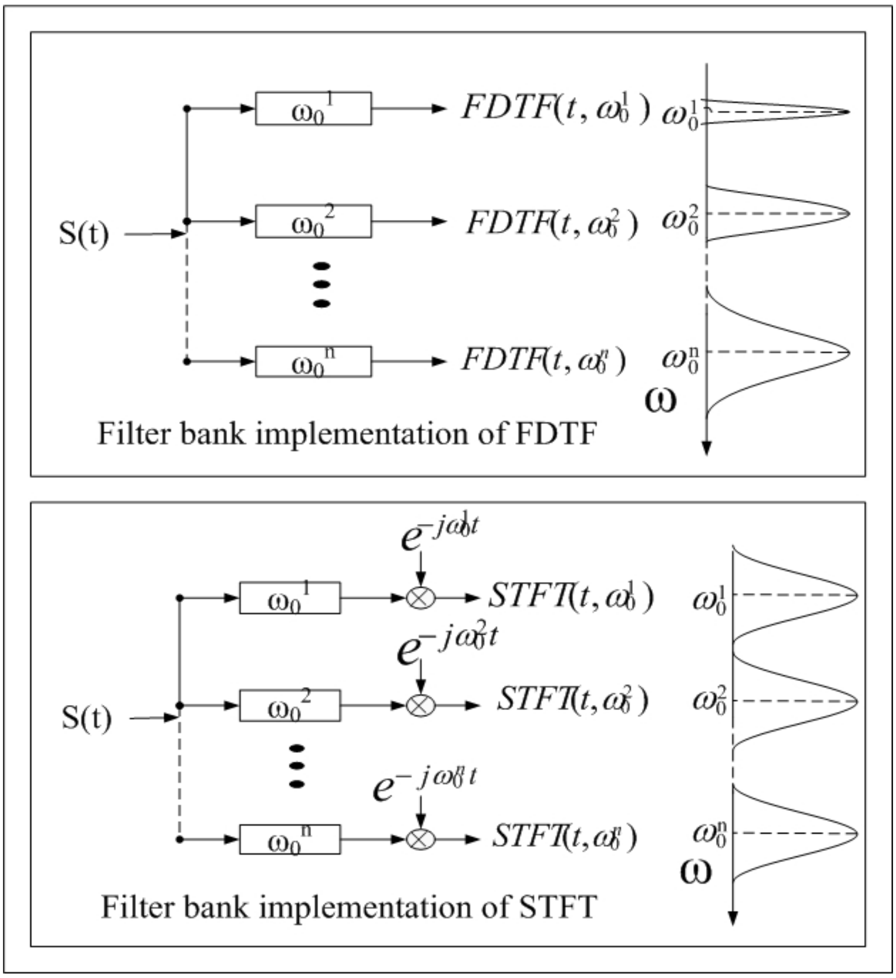

Figure 4.1 Comparison of Filter Bank Implementation of STFT and FDTF

Equation (4.1) is more suitable to express a transform-based implementation whereas equation (4.3) is more straightforward to implement a filter bank with impulse response functions expressed by equation (4.4). As introduced in a previous section (Chapter 2 Section 2), in the filter bank implementation of STFT, the signal passes first through the band bass filter centered at ω and then it is demodulated to zero frequency. As illustrated in Figure 4.1, there are two main differences between the band pass filter implementations of STFT and FDTF. One difference is that, in the implementation for STFT, the bandwidth of the band pass filter is kept fixed and independent on its centre frequency ω; instead for FDTF, the bandwidth of band filter can be changed according to centre frequency ω. Another difference is that, in the implementation of STFT, the output of every band pass filter centered at ω is then demodulated to zero frequency; such a demodulation process does not exist in the implementation of FDTF. As mentioned above, there are two different implementations of FDTF: transform-based implementation and filterbank-based implementation. The filterbank-based implementation may be further classified into IIR filter bank or FIR filter bank implementation. From the view of computational efficiency, the IIR filter-bank-based implementation is greatly advantageous over the other two implementations; the order of the filter bank needs to be as small as possible to reduce the computation cost.

For music signal analysis an original FDTF tool is especially developed: the Resonator Time-Frequency Image (RTFI), which selects a first-order complex resonator filter bank to implement a frequency-dependent time-frequency analysis.

4.2 Resonator Time-Frequency Image for Musical Signals

The Resonator Time-Frequency Image (RTFI) can be described as follows:

$$RTFI\ (t,\omega) = s(t) * I_R(t,\omega)$$

$$= r(\omega)\int_0^t s(\tau)e^{r(\omega)(\tau-t)}e^{-j\omega(\tau-t)}d\tau \qquad (4.5)$$

where $I_R(t,\omega) = r(\omega)e^{(-r(\omega)+j\omega)t}, \quad r(\omega) = map(\omega) > 0, \quad t > 0$ (4.6)

In the above equations, I_R denotes the impulse response of the first-order complex resonator filter with oscillation frequency ω, and the factor r(ω) before the integral in the equation (4.5) is used to normalize the gain of the frequency response when the resonator filter's input frequency is the oscillation frequency. The decay factor r is dependent on the frequency ω and determines the exponent window length and the time resolution; at the same time it also determines the bandwidth (i.e. the frequency resolution). More formally, in this thesis, the frequency resolution of time-frequency analysis implemented by the filterbank is defined as the Equivalent Rectangular Bandwidth (ERB) of implementing filter (2.45). The time-frequency resolution distribution can be set efficiently and flexibly through the *map* function between the frequency and the exponential decay factor *r* of the filter impulse response.

Because the RTFI has a complex spectrum, it may be expressed as follows:

$$RTFI(t,\omega) = A(t,\omega)e^{j\varphi(t,\omega)} \quad (4.7)$$

where $A(t, \omega)$ and $\varphi(t,\omega)$ are real functions.

The energy and frequency-difference (FD) spectrum of RTFI can be defined as follows:

$$RTFI_{Energy}(t,\omega) = \left|A(t,\omega)\right|^2 \quad (4.8)$$

$$RTFI_{FD}(t,\omega) = \frac{\partial\varphi(t,\omega)}{\partial t} - \omega \quad (4.9)$$

In the equation (4.9), the first term can be explained the instantaneous frequency of the output of the resonator filter with centre frequency ω, so the $RTFI_{FD}$, in fact, is the difference between the instantaneous frequency and the center frequency of the implementing resonator filter.

The selection of time-frequency resolution distribution is not trivial and has an important effect on the performance of the music analysis system. A time-frequency analysis with an inappropriate time-frequency resolution may cause two disadvantages; one is that it can not provide enough frequency resolution or instead provide a much redundant frequency resolution and increases the unnecessary computation cost in some frequency bands; and another one is that it is not able to provide enough time resolution and catch the necessary transient information. It is application-specific to select an appropriate time-frequency resolution distribution for music signal time-frequency analysis. For example, if one uses the RTFI to perform a timbre analysis for a single monotone note, and the frequency components of the music note are harmonics and evenly spaced in the frequency axis, a constant value of decay factor *r* may be set to make the RTFI have an evenly-spaced time-frequency resolution. It is straightforward and natural to consider the known character of the music signal as the important factors, which determine the time-frequency resolution distribution. In the following it is explained how it may be reasonable to select a nearly constant-Q time-frequency resolution for general-purpose music signal analysis.

In case of the common western music (CWM), the fundamental frequency and corresponding partials of a music note can be described as

$$f_k^0 = 440(2^{\frac{k-69}{12}}) \quad \text{and} \quad f_k^m = m \cdot f_k^0,\ k \geq 1 \qquad (4.10)$$

using the MIDI (Music Instrument Digital Interface) note numbers for note k. Supposing that the energy of every music note mainly distributes over the first 10 partials, and $Energy(f_k^m) \approx 0$ for $m \geq 11$, the frequency ratio between the partials of one note and the fundamental frequency of other notes is as follows:

$$2f_k^0 = f_{k+12}^0,\quad 3f_k^0 / f_{k+19}^0 = 0.9989,\quad 4f_k^0 = f_{k+24}^0$$

$$5f_k^0 / f_{k+28}^0 = 1.0079,\quad 6f_k^0 / f_{k+31}^0 = 0.9989,\quad 7f_k^0 / f_{k+34}^0 = 1.018,$$

$$8f_k^0 = f_{k+32}^0,\quad 9f_k^0 / f_{k+38}^0 = 0.9977,\quad 10f_k^0 / f_{k+40}^0 = 1.0079$$

This means that always the first 10 partials either completely or in part overlap with another fundamental frequency; as the fundamental frequencies follow an exponential law (4.10), so most of the energy is concentrated in frequency bins that are exponentially spaced and then equally spaced according to a logarithmic axis. The frequency bins may be simply expressed according to (4.10) like $\omega_n = AB^n$; the required frequency resolution at frequency area nearly round ω_n may be expressed as follows:

$$resolution(\omega_n) = \omega_n - \omega_{n-1} = AB^n(1 - B^{-1}) = (1 - B^{-1})\omega_n$$

The resolution distribution in the equation above is the constant-Q frequency resolution, which means that the ratio of frequency resolution and frequency is constant. If one wants to implement a constant-Q time-frequency resolution by RTFI, it is only needed to simply select a linear function mapping the frequency to the exponent decay factor as in the following equation:

$r(\omega) = k\omega$, with k being a constant (4.11)

Another approach may be used to define the time-frequency resolution distribution by the known human ear's time-frequency analysis presented in Chapter 2, because the ear performs very well in many music analysis tasks. It is well known that the human ear's frequency analyzer has an almost evenly-spaced time-frequency resolution at low frequencies and a nearly constant-Q time-frequency resolution at high frequencies. One widely-accepted frequency-dependent frequency resolution (in terms of bandwidths) of the auditory filter bank can be approximately described as follows:

$$B = 24.7 + 0.1079 f \quad (4.12) \text{ (Hart97)}$$

Here the bandwidth B is the Equivalent Rectangular Bandwidth (ERB) in Hz. On one hand the human ear frequency analyzer may give us some important enlightenment to determine an appropriate time-frequency resolution for music signal analysis; on the other hand in a practical music analysis system it is not reasonable to apply completely the same time-frequency resolution as human ear's frequency analyzer for the following three reasons. First, it is not completely sure that the current experiments can measure a very exact time-frequency resolution distribution of the human ear's frequency analyzer, and the measured time-frequency resolution is only a rough approximation. Secondly, the time-frequency resolution of the human ear's analyzer is not the absolute optimal for music signal analysis because it may have some physiology limitations. And third, generally speaking time-frequency analysis should be the front-end part of music analysis systems, and it most often needs to be combined with some post-processing phase to usefully complete the music analysis tasks; the two phases should match each other, so if one select a time-frequency analysis front-end part similar to human ear frequency analyzer, then one should also construct some post-processing phase similar to the human auditory system to achieve a performance comparable to the human auditory function; however in current research it is not clear how to construct such post-processing parts simulating a function similar to the human auditory system.

The author's opinion is that it is more reasonable first to define a parameterized set of time-frequency resolution distribution (which is considered as an approximation to the optimal time-frequency resolution distribution of the music signal analysis) based on the inference from the character of music signal itself or on psychoacoustics and physiology research relative to the human auditory system; and then to estimate the parameters of the parameterized resolution and select a more exact time-frequency resolution distribution according to some experiments, which combine the time-frequency analysis front-end phase with the post-processing and determine the resolution parameter values according to the total performance of the music analysis system. Put in another way, when the post-processing phase is fixed, the right time-frequency resolution distribution and corresponding parameters should be selected if they make the system have the best overall performance. For example, if the RTFI is used as time-frequency analysis front-end, we may define a parameterized approximation to the optimal time-frequency resolution by a map function from frequency to the exponent decay factor r as follows:

$r(\omega) = a + b\omega$, with a, b being constants(4.13),

and then combine the post-processing phase into a music analysis system; finally by some experiments the appropriate parameters *a* and *b* can be estimated to make the system perform well in the corresponding music analysis task. In fact, the constant-Q resolution and cochlear resolution (as shown equation (4.12)) can be considered as a special case of (4.13). As shown above, the RTFI can easily and flexibly implement different frequency-dependent time-frequency resolution distributions by simply defining a function mapping frequency to the exponent decay factor of the complex resonator filter bank.

4.2.1 Energy and Frequency-difference Spectrum of RTFI

In this subsection, it is explored how to make best use of the energy and frequency-difference spectrum of the RTFI as efficient time-frequency analysis tool for music signal. A real music signal may be approximately expressed by an additive sinusoidal model as follows:

$$s(t) = \sum_{i=1}^{n} c_i(t) + e(t),$$

$$c_i(t) = a_i(t)e^{j\omega_i t + \phi_0}, \quad a_i(t) \geq 0 \quad (4.14)$$

In this model, the music signal is approximated by the sum of *n* complex sinusoids with time-varying magnitude parameters, whereas *e(t)* denotes the noise component. In the sinusoidal model there is an assumption that the $a_i(t)$ should be a slow varying signal e.g. a low passed signal and $c_i(t)$ locally resembles a pure complex sinusoid. The RTFI is explored as frequency-dependent time-frequency tool that extracts the time-frequency character of the signal that can be approximated by the sinusoid model.

In the simplest case, if the input signal s(t) consists of only one complex sinusoid with the constant magnitude as like,

$$s(t) = e^{j\omega_1 t}\mu(t),\ \mu(t) = \begin{cases} 1 & t \geq 0 \\ 0 & t < 0 \end{cases}$$

then the corresponding RTFI can be written as follows:

$$RTFI(t,\omega) = r(\omega)\int_0^t e^{j\omega_1\tau} e^{r(\omega)(\tau-t)} e^{-j\omega(\tau-t)} d\tau \quad (4.15)$$

$$= r(\omega)e^{j\omega_1 t}\frac{1-e^{(-r(\omega)+j(\omega-\omega_1))t}}{r(\omega)-j(\omega-\omega_1)} \quad (4.16)$$

When considering the steady-state component of RTFI (when t->+∞) in the above equation, then RTFI energy spectrum can be described as follows:

$$RTFI_{Energy}(t,\omega) = \left|RTFI(t,\omega)\right|^2 = \frac{1}{1+(\frac{\omega-\omega_1}{r(\omega)})^2} \quad (4.17)$$

From the equation (4.16), the instantaneous frequency spectrum at frequency $\omega = \omega_1$ can be expressed as follows:

$$RTFI\ (t,\omega_1) = (1-e^{-r(\omega_1)t})e^{j\omega_1 t}$$

$$RTFI_{FD}(t,\omega_1) = 0 \quad (4.18)$$

In summary, if the input signal consists of a single complex sinusoid with constant magnitude and frequency ω_1, the energy spectrum $RTFI_{Energy}$ has the maximum peak at the frequency $\omega = \omega_1$ according to the equation (4.17),and the frequency-difference at the frequency $\omega = \omega_1$ is rightly equal zero, according to the equation (4.18). When the input signal consists of n complex sinusoids with constant magnitudes and the input signal *s(t)* may be expressed as follows:

$$s(t) = \sum_{i=1}^{n} a_i e^{j\omega_i t}, \qquad \text{where } a_i \text{ is constant}$$

And the corresponding RTFI can be expressed as follows:

$$RTFI\ (t,\omega) = r(\omega)\int_0^t \sum_{i=1}^{n} a_i e^{j\omega_1\tau} e^{r(\omega)(\tau-t)} e^{-j\omega(\tau-t)} d\tau$$

$$= \sum_{i=1}^{n} a_i r(\omega) e^{j\omega_i t} \frac{1-e^{(-r(\omega)+j(\omega-\omega_i))t}}{r(\omega)-j(\omega-\omega_i)} \quad (4.19)$$

When considering the steady-state component of RTFI (when t->+∞） in the above equation, then RTFI energy spectrum can be described as follows:

$$RTFI_{Energy}(t,\omega) = \left| \sum_{i=1}^{n} a_i r(\omega) e^{j\omega_i t} \frac{1}{r(\omega)-j(\omega-\omega_i)} \right|^2$$

$$= \sum_{i=1}^{n} c_i^2(\omega) a_i^2 + 2 \sum_{i=1, j=1, i\neq j}^{n} c_i(\omega) c_j(\omega) a_i a_j \cos((\omega_i-\omega_j)t + (\partial_i(\omega)-\partial_j(\omega)))$$

with

$$c_i(\omega) = \frac{1}{\sqrt{1+(\frac{\omega-\omega_i}{r(\omega)})^2}}, \quad \partial_i(\omega) = \arctan(\frac{\omega-\omega_i}{r(\omega)}) \quad (4.20)$$

As shown in the above equations, the RTFI energy spectrum also contains the oscillating cross terms, which are considered as interference because the magnitudes of the input complex sinusoids are constant and the corresponding RTFI energy spectrum should not oscillate. To reduce the oscillation term energy, a low pass filter bank may be used to smooth the RTFI energy spectrum. With the assumption that the smoothed RTFI energy spectrum contains almost no oscillating terms, the smoothed RTFI energy spectrum may be approximated as follows:

$$RTFI_{Energy}^{Smoothed}(t,\omega) \approx \sum_{i=1}^{n} c_i^2(\omega) a_i^2 \quad (4.21)$$

According to equation (4.19), with the ω_k denoting the frequency of the k^{th} input complex sinusoid, then RTFI at the frequency ω_k can be expressed as follows:

$$RTFI(t,\omega_k)=a_k(1-e^{-r(\omega_k)t})e^{j\omega_k t}+\sum_{i=1,i\neq k}^{n}a_i c_i(\omega_k)e^{j\omega_i t+\partial_i}(1-e^{(-r(\omega)+j(\omega-\omega_i))t}) \quad (4.22)$$

Here

$$c_i(\omega_k)=\frac{1}{\sqrt{1+(\frac{\omega_k-\omega_i}{r(\omega_k)})^2}}, \quad i\neq k$$

In the above equations, if the frequency difference between the k^{th} input complex sinusoid and the other n-1 sinusoids is large, so that the term $a_i c_i(\omega_k)$ is omissible compared to the value a_k, then $RTFI(t, \omega_k)$ can be approximated like:

$$RTFI(t,\omega_k)\approx a_k(1-e^{-r(\omega_k)t})e^{j\omega_k t} \quad (4.23)$$

The corresponding instantaneous frequency (IF) spectrum can be expresses as follows:

$$RTFI_{FD}(t,\omega_k)\approx 0 \quad (4.24)$$

In summary, when the input signal consists of *n* complex sinusoids with constant magnitude, if the frequency of the k^{th} sinusoid is ω_k and the frequency difference between the k^{th} sinusoid and the other n-1 sinusoids is large enough, then the sinusoid may have a corresponding peak in the smoothed RTFI energy spectrum along the frequency axis and the peak is nearly around the frequency ω_k, at the same time the k^{th} sinusoid may have the corresponding zero value nearly around the frequency ω_k in the RTFI frequency-difference spectrum

4.3 Discrete Resonator Time-Frequency Image

4.3.1 Definition of Discrete RTFI

For practical applications, it is proposed to use the first order complex resonator digital filter bank to implement a discrete RTFI, which can be described as follows:

$$RTFI\ (n,\omega_m) = s(n) * I_R(n,\omega_m)$$

where $I_R(n,\omega_m) = (1 - e^{\frac{-r(\omega_m)}{f_s}})e^{\frac{-r(\omega_m)+j\omega_m}{f_s}n}, \quad r(\omega_m) = map(\omega_m) > 0, \quad t > 0,$

f_s being the sampling frequency (4.25)

In a discrete RTFI , a corresponding complex resonator filter is used to approximate the frequency response of the continuous one as much as possible; if a continuous resonator filter has the impulse response $h_c(t)$, then we approximate the continuous resonator filter by a digital one, which has a impulse response $h(n)=lh_c(n/f_s)$ and the parameter l normalizes the frequency response of the digital resonator filter when the input is a single complex sinusoid with the oscillation frequency; according to such an approximation, the impulse response I_R ,of the implementing digital filter in a discrete RTFI is achieved and shown in the equation (4.25). As introduced before, the continuous RTFI may be implemented by the first-order complex resonator filter bank at the center frequency ω, which is a continuous variable; that is, countless resonator filters need to be used to implement a continuous RTFI; the discrete RTFI is both time-discrete and frequency-discrete; time-discrete means that the input signal is a discrete sequence and the filter is digital, while frequency-discrete means that center frequency ω of the digital filter bank is a discrete variable and number of the digital filters should be limited.

4.3.2 Implementation of Discrete RTFI

One important issue for implementation of a discrete RTFI is how to determine the number and centre frequencies of the digital filters: it is necessary to consider how to determine the sampling rate in the frequency domain from a continuous RTFI to a discrete RTFI. It is straightforward to place more digital filters in a frequency band that needs better frequency resolution. In the following a way is proposed to determine the centre frequencies of the resonator digital filters for discrete RTFI implementation based on the time-frequency resolution distribution requirement of the RTFI.

To better explain with an example, an ideal rectangle band pass digital filter bank is used to implement a frequency-dependent time- frequency transform (FDTF) with the time-frequency resolution distribution $resolution(\omega) = map(\omega)$, and the filter bank consists of n rectangle band pass filters with centre frequencies ω_k, k=1,2,…N , $\omega_k < \omega_{k+1}$; because the bandwidths of the band pass filters determine the frequency resolution, the bandwidth of the k^{th} band pass filter B_k should meet the constraint

$$B_k = map(\omega_k), \quad k = 1,2,..n \quad (4.26)$$

and if the n rectangle band filters together rightly cover all the analyzed frequency range as shown in Figure 4.2 (b) , then the constraint in equation (4.27) need to be met:

Critical Sampling: $\omega_k - \omega_{k-1} = 0.5(B_k + B_{k-1}), \quad k = 2,3\ldots n$ (4.27)

Under-sampling: $\omega_k - \omega_{k-1} > 0.5(B_k + B_{k-1}), \quad k = 2,3\ldots n$ (4.28)

Over-Sampling: $\omega_k - \omega_{k-1} < 0.5(B_k + B_{k-1}), \quad k = 2,3\ldots n$ (4.29)

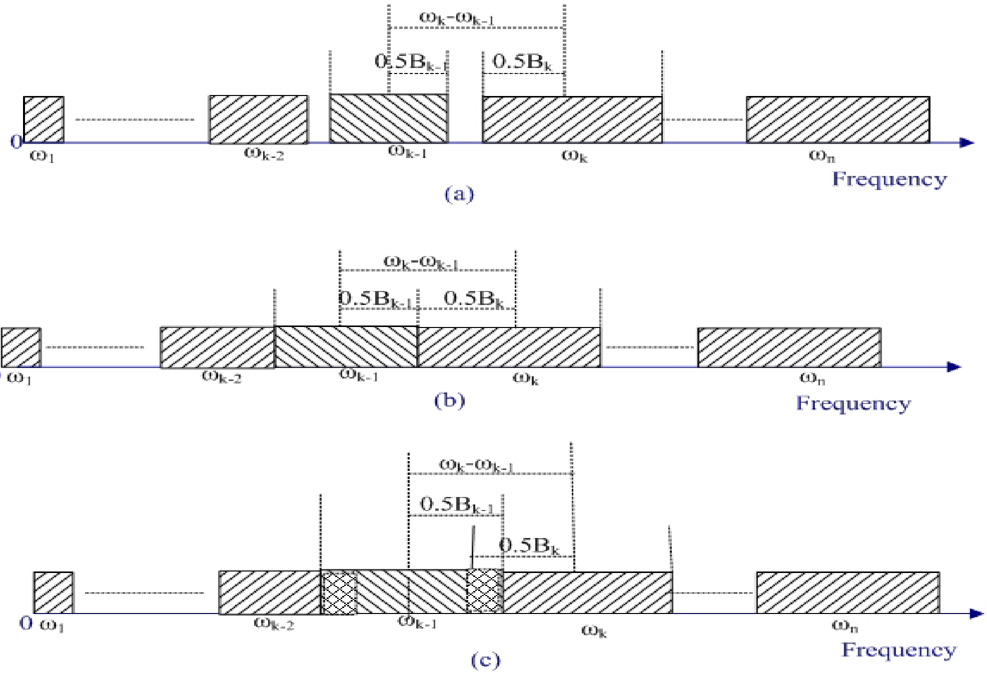

Figure 4.2 Under-sampling, over-sampling and critical-sampling

As mentioned before, the process to determine the center frequencies of filter bank may be considered as frequency sampling from a continuous frequency-dependent time-frequency transform (FDTF) to a discrete FDTF; with the assumption that the selected filter bank can keep the predetermined time-frequency resolution distribution, then the process can be called critical sampling, under-sampling or over-sampling if the center frequencies of the filter bank respectively meet the constraint of equation (4.27), (4.28) or (4.29). As shown in Figure 4.2-(a), in under-sampling some frequency area is not covered by any filter; this means that if there exist some frequency components in that frequency area, the under-sampling discrete FDTF can not detect these frequency components. An over-sampling case is illustrated in Figure 4.2-(c), the neighbor rectangle filter has some overlapped frequency band; compared to critical sampling, the over-sampling increase the number of rectangle filters without improving the frequency resolution and causes redundancy. Here for the sampling process a parameter named sampling factor is defined as follows:

$$SamplingF_k = \frac{\omega_k - \omega_{k-1}}{0.5(B_k + B_{k-1})}, \quad k = 2,3...n \quad (4.30)$$

In a practical implementation, we consider the sampling factor as constant along the frequency axis, so the following equation holds:

$$\omega_k - \omega_{k-1} = SamplingF \cdot 0.5 \cdot (B_k + B_{k-1}), \quad k = 2,3...n \quad (4.31)$$

With the assumption that the frequency resolution is predetermined, according to the equation (4.26), equation (4.31) can be rewritten as follows:

$$\begin{aligned} &\omega_k - SamplingF \cdot 0.5 \cdot (map(\omega_k)) = \omega_{k-1} + SamplingF \cdot 0.5 \cdot (map(\omega_{k-1})) \\ &k = 2,3..n \end{aligned} \quad (4.32)$$

If the sampling factor and the starting analysis frequency ω_0 are determined, one can determine the other filter's centre frequencies ω_k, k=2, 3, …n. according to iterative equation (4.32).

As discussed above a way is proposed to determine the sampling rate for frequency-dependent time-frequency analysis (FDTF), which is implemented by the boxcar filter bank; if FDTF is implemented by a filter of different shape, a similar approach may still be used by replacing the bandwidth of the filter with an Equivalent Rectangular Bandwidth (ERB), and in this case the equations (4.31) and (4.26) can be modified as follows:

$$B_k^{ER} = map(\omega_k), \quad k = 1,2,..n \quad (4.33)$$

$$\omega_k - \omega_{k-1} = SamplingF \cdot 0.5 \cdot (B_k^{ER} + B_{k-1}^{ER}), \quad k = 2,3...n \quad (4.34)$$

with B^{ER} denotes the ERB of the filter.

As mentioned before the commonly-used frequency resolution distribution for music analysis may be expressed like:

$$resolution(\omega) = d + c\omega, \quad d \geq 0 \quad c > 0 \quad (4.35)$$

and the equation (4.33) can be rewritten as like: $B_k^{ER} = d + c\omega_k$, and the following recursive equation can be derived according to equation (4.34)

$$\omega_k = G\omega_{k-1} + H, \quad (4.36)$$

with

$$G = \frac{1 + 0.5c \cdot SamplingF}{1 - 0.5c \cdot SampoingF}, \quad H = \frac{d \cdot SamplingF}{1 - 0.5c \cdot SampoingF}$$

To design a discrete FDTF with frequency resolution according to equation (4.35), one can determine the discrete centered frequencies of the filter bank according to the following formula, which can be derived from equation (4.36):

$$\omega_k = G^k \omega_0 + \frac{1 - G^k}{1 - G} H \quad (4.37)$$

As discussed above, this is a proposed general way to determine the centre frequencies of the filter bank, which is used to implement a discrete FDTF. The RTFI is a special case of the FDTF, and the RTFI is a FDTF that can be implemented by first-order complex resonator filter bank; of course a discrete RTFI also can use the proposed method to determine the centre frequencies of the complex resonator bank.

As shown in the discrete RTFI definition in equation (4.25), to implement a discrete RTFI, two steps are requested: one is to resolve the frequency sampling issue, i.e to determine the centre frequencies ω_m, which can be resolved by the above proposed method. Another issue is to implement the frequency resolution distribution, i.e. to determine the bandwidth of each filter in the filter bank. The bandwidth of the first-order complex resonator filter can be set by the value of exponent decay factor r in its impulse response. As mentioned before the bandwidth is the ERB width, it is necessary to know how the exponent decay factor determines the ERB bandwidth of the complex resonator filter. The ERB bandwidth is defined for the continuous filter in (2.45).

The ERB bandwidth is generalized for a digital filter. The ERB bandwidth of a digital filter is defined. If a continuous filter has the impulse response h(t), and a corresponding digital filter's impulse response is the discrete sampling of h(t), then we approximate the digital filter's ERB width by the continuous filter.

According to the RTFI definition (4.5 and 4.6), the frequency response of the filter to be implemented is centered at frequency ω_k and can be described as follows:

$$|H(f)|^2 = \frac{1}{1 + 4\pi^2 (\frac{f - f_k}{r(\omega_k)})^2} \quad (4.38)$$

The filter ERB can be calculated according to the equation (2.45) and the ERB value can be expressed according angle frequency as follows:

$$B_k^{ER} = r(\omega_k)(0.5\pi + \arctan(\frac{\omega_k}{r(\omega_k)})) \quad (4.39)$$

In practical cases, the resonator filter exponent factor is nearly zero, so *arctan(* $\omega_k/r(\omega_k)$*)* can be approximated to 0.5 π , and equation (4.39) can be approximated as follows:

$$B_k^{ER} = r(\omega_k)\pi \quad (4.40)$$

If the RTFI resolution distribution is according to the equation (4.35), the formula to determine the exponent decay factor for the filter in RTFI filterbank-based implementation can be derived from the equation (4.40) as follows:

$$r(\omega_k)=(d+c\omega_k)/\pi \quad (4.41)$$

In practical application, one issue is that sometime we wish the center frequencies of the implementing filters can be predetermined, for example, we wish the center frequencies always follows a exponent law and make the analysis result can be more conveniently to connect with western music, in this case, the sampling factor can not be predetermined any more, but we can calculate the sampling factor from the known frequency resolution parameters and the centre frequencies according to the relationship equation (4.30), and the calculated sampling factors at different frequency can provide the frequency sampling rate information . When the centre frequencies and exponent decay factors of the impulse response of the implementing digital resonator filters are determined, the z transfer function of the digital resonator filters can be expressed as the following equation:

$$H_m(z)=\frac{1-e^{-r_m/f_s}}{1-e^{(-r_m+j\omega_m)/f_s}z^{-1}} \quad (4.42)$$

As analyzed in the continuous RTFI, the RTFI energy spectrum includes the oscillation terms and need be smoothed by the low-pass filter. We propose a way to get the smoothed discrete RTFI energy spectrum by a special low pass filter, and for the *m*th implementing digital resonator filter, it’s energy spectrum is smoothed by the corresponding low pass filter with the impulse response as like

$$I_L(n,\omega_m)=(1-e^{\frac{-r(\omega_m)}{f_s}})e^{\frac{-r(\omega_m)}{f_s}n} \quad , (4.43)$$

and the low pass filter’ s z transfer function can be expressed as follows:

$$H_m^L(z)=\frac{1-e^{-r_m/f_s}}{1-e^{-r_m/f_s}z^{-1}} \quad (4.44)$$

There exist two reasons to select such a special low pass filter for smoothing the energy spectrum of the discrete RTRI. First, a important advantage of the RTFI is it's computation-efficiency, so we need keep the advantage and the low pass filter's order need be also small as possible. Secondly, the impulse responses of the *m*th resonator filter and the corresponding *m*th low pass filter for smoothing the energy spectrum have the equal exponent decay factor, and this makes the energy spectrum smoothing process still keep a similar time-frequency resolution distribution as defined in the discrete RTFI. The smoothed energy spectrum of a discrete RTFI at the frequency ω_m can be expressed as follows according to the responses of the implementing resonator filter and it's corresponding low pass filter.

$$RTFI_{Energy}^{Smoothed}(n,\omega_m) = \left|s(n) * I_R(n,\omega_m)\right|^2 * I_L(n,\omega_m) \quad (4.45)$$

Where the I_R and I_L is respectively defined in the equation (4.25) and (4.43)

We calculate the frequency-difference spectrum of a discrete RTFI at the frequency ω_m and time point n by the following formula:

Given the values : $RTFI(n,\omega_m) = a_n + jb_n, \quad RTFI(n-1,\omega_m) = a_{n-1} + jb_{n-1},$

$$RTFI_{IF}(n,\omega_m) = \begin{cases} f_s \arccos\left(\dfrac{a_n a_{n-1} + b_n b_{n-1}}{\sqrt{\left(a_n^2 + b_n^2\right)\left(a_{n-1}^2 + b_{n-1}^2\right)}}\right) - \omega_m & if: b_n a_{n-1} - a_n b_{n-1} > 0 \\ -f_s \arccos\left(\dfrac{a_n a_{n-1} + b_n b_{n-1}}{\sqrt{\left(a_n^2 + b_n^2\right)\left(a_{n-1}^2 + b_{n-1}^2\right)}}\right) - \omega_m & if: b_n a_{n-1} - a_n b_{n-1} < 0 \end{cases} \quad (4.46)$$

In the practical application of the discrete RTFI, we need consider not only computation but also the memory issue , generally speaking it is impossible and also not necessary to keep all the RTFI energy spectrum and frequency-difference spectrum at every time sampling point; to reduce the requirement of the memory to store the RTFI values, we separate the RTFI into different time frames and calculate the average RTFI values in each time frame, finally the average smoothed RTFI energy spectrum and frequency-difference spectrum are used to track a time-frequency character of the music signal. The average RTFI energy spectrum and frequency–difference spectrum may be expressed as follows:

$$ARTFI_{Energy}(k,\omega_m) = db(\frac{1}{M}\sum_{i=(k-1)M+1}^{kM}\left|RTFI(n,\omega_m)\right|^2 \quad (4.47)$$

$$ARTFI_{FD}(k,\omega_m) = \frac{1}{M}\sum_{i=(k-1)M+1}^{kM} RTFI_{FD}(i,\omega_m) \quad (4.48)$$

Where the M is an integer and M/fs is the duration time of the frame in the average process.

As analyzed in the continuous RTFI, if there exist several sinusoid components in the input signal, then the corresponding smoothed RTFI energy spectrum may exist a peak along the frequency axis nearly around the frequency of each sinusoid component. A discrete RTFI can be considered as an approximated implementation of continuous RTFI, so it is reasonable to consider the discrete RTFI still almost keeps some basic characters of the continuous RTFI, this also has been testified by a lot of experiments in our research of performing the time-frequency analysis for music signal by the discrete RTIFI. In the discrete RTFI, we do not directly find the peak in the smoothed RTFI energy spectrum, but in the average smoothed RTFI energy spectrum to reduce the memory requirement as mentioned before, and the process to find the peak value in the average smoothed RTFI energy spectrum may be expressed as follows:

$$\begin{array}{l} if : (ARTFI_E^S(k,\omega_m) > (ARTFI_E^S(k+L,\omega_m)+\delta))and(ARTFI_E^S(k,\omega_m) > (ARTFI_E^S(k-L,\omega_m)+\delta)) \\ then : Peak = ARTFI_E^S(k,\omega_m); \\ else : Peak = a; \end{array}$$

In the above expressions, the *L* and δ are the two parameters to define the peak. In the general case, we set L=1, and the δ can be considers as a threshold that is useful to remove the noise peak. In the average smoothed RTFI energy spectrum, if the point is not a peak in the frequency axis, its value is set to the constant *a*, which is usually set to the minimum of the smoothed RTFI energy spectrum.

Similar to the case in the continuous RTFI frequency-difference spectrum, in the discrete RTFI average frequency-difference spectrum, if the average frequency-difference $ARTFI_{FD}(k, \omega_m)$ is nearly to zero , this means that it is probable that, in the input signal, there exists a sinusoid component with the frequency ω_m at the *k*th time frame.

4.3.3 An Example of Discrete RTFI

In the previous sections, an original time-frequency analysis tool called RTFI has been formulated. In the following paragraphs, an example of the discrete RTFI is introduced to explain the implementation of a discrete RTFI and to demonstrate the RTFI performance in the music signal analysis. As discussed above, there exist two cases in the design process of the discrete RTFI. One case is that first the sampling factor is determined and then the center frequencies are calculated, in this case , the frequency sampling rate can be assured equal in all the frequency range, but the center frequencies can not be predetermined. A second case is that the center frequencies are determined first, but the frequency sampling rate can not be assured equal in different bands, and the sampling factor in a different band can be calculated to provide the frequency sampling rate information. In the proposed example, the method belongs to the second case, and the centre frequencies are set like

$$\omega_m = P^m \omega_0 , \quad (4.49)$$

$$P = 2^{\frac{1}{12q}} \text{ and } \omega_0 = 2\pi \cdot 440 \cdot 2^{\frac{StartNoteN - 69}{12}} \quad (4.50)$$

where q and StartNoteN is two integer parameters.

According to the equation (4.49, 4.50), the center frequencies of the implementing filter bank can be rewritten as follows:

$$\omega_m = 2\pi \cdot 440 \cdot 2^{\frac{StartNoteN + m/q - 69}{12}} \quad (4.51)$$

In equation (4.57), *StartNoteN* is an integer parameter indicating the lowest note number (MIDI note numbers are used) in the considered range, and *q* is another integer parameter used to denote how many filters are used to cover the frequency band of one semitone. Because the fundamental note frequencies in CWM follow an exponential law, if the center frequencies of the filters are determined by equation (4.58) and also according to the exponential law, it will become more convenient to map the analysis results of the discrete RTFI to CWM notation.

As already said, there exist four parameters that completely determine a discrete RTFI implementation, the parameters are the frequency resolution distribution parameters *c* and *d*, sampling factor *SamplingF* , starting analysis frequency ω_0; in this example, *SamplingF* and ω_0, are indirectly set by the two integer parameters *q* and *StartNoteN* , so that the centre frequencies always can meet the definition in equation (4.51). And the relationship between the parameter *SamplingF*, the integer parameter *q* and resolution distribution parameters can be derived. For convenience of computation, in this example RTFI, the approximated sampling factor *A_SamplingF* is derived, which is the sampling factor when the center frequency equals the fundamental frequency of a CWM note A_0 :

$$A\_SamplingF = \frac{\pi \cdot 440\,(1 - 2^{-\frac{1}{12q}})}{d + \pi c \cdot 440\,(1 + 2^{-\frac{1}{12q}})} \qquad (4.52)$$

After the center frequencies and exponent decay factors of the digital resonator filters are determined, the example of the discrete RTFI can be implemented according to the method introduced in the previous section.

The real music application examples in music signal analysis can be found in Chapter 5- 9.

4.3.4 Multiresolution Fast Implementation of Discrete RTFI

4.3.4.1 Proposed Multiresolution Fast Implementation

For practical applications, a multiresolution fast implementation for the discrete RTFI has been developed. The basic idea is to reduce the redundancy in computation: in some cases it is not necessary to keep the same sampling frequency of the input for every filter in the filter bank. For the filters with lower center frequencies, the sampling rate can be decreased. At the same time, because the main partials of music notes exist according to the exponential law, the high frequency regions need a lower frequency resolution. This means that a shorter duration signal frame is enough for the frequency analysis.

The block diagram of the proposed implementation is shown in Figure 4.3

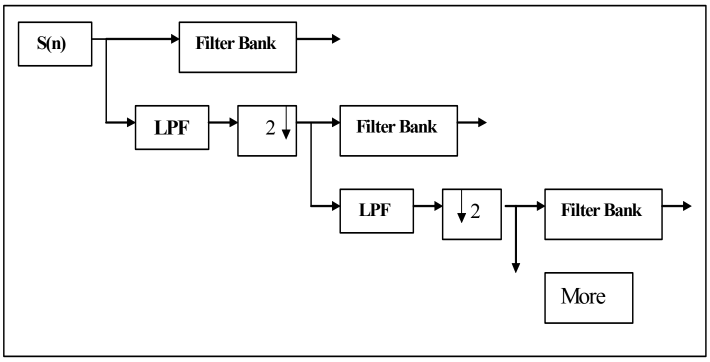

Figure 4.3: Block diagram for the proposed multi-resolution fast implementation

Considering a filter bank without fast implementation, the center frequencies are selected according to the expression

$$\omega_m = \frac{2\pi f_0 2^{\frac{m}{K}}}{f_s} \quad , (m = 1,2,....M; \text{ N=M/K integer}) \quad (4.53)$$

The filter bank is separated into N frequency bands, every frequency band has K filters, and the center frequencies of the filters in n^{th} frequency band are:

$$\omega_{((n-1)*K+i)}, \quad (i = 0,1,2,...K\text{-}1) \qquad (4.54)$$

Using the fast implementation, the signal is recursively low pass filtered and down sampled by a factor 2 from the highest to the lowest frequency band according to the scheme in Figure 4.3. The signal sampling rate ratio between the n^{th} frequency band and the original sampling rate is

$$f_{sn} = 2^{n-N} f_s$$

and according to equation (4.53), the center frequencies of the filters in n^{th} frequency band are changed as

$$\omega'_{((n-1)*K+i)} = 2^{N-n}\omega_{((n-1)*K+i)} = \omega_{((N-1)*K+i)} \, (i = 0,1,...K\text{-}1)$$

Consequently, all the other *n*-1 frequency bands use the same filters as the filters in the highest frequency band.

If the computation cost of one frequency band is ***C***, for N frequency bands the total computation cost of the filter bank without fast implementation is

$$C_{original} = C \cdot N$$

whereas the computation cost of fast implementation is

$$C_{fast} = C + \frac{1}{2}C + \frac{1}{4}C + \ldots + \frac{1}{2^{N-1}}C < 2C$$

The computation cost of the low pass filter is negligible. The fast implementation is about N/2 times faster than a normal implementation.

The proposed algorithm is especially conceived for multi pitch tracking based on short signal frames, which in a large majority of frames corresponds to a monotone or polyphonic stationary situation. In the spectrum extraction algorithm, first the signal is separated into 8 different frequency bands according to the fast implementation introduced above. At the same time, since the required frequency resolution at higher frequencies is lower, shorter time frames are used to compute the power spectrum in order to reduce the computation cost further. Detailed information is shown in Table 4.1. As shown in the table, the downsampling begins from the sixth frequency band; this is reasonable choice to make the ratio between sampling rate and analysis frequency about 20 or more according to an experimental rule of thumb. Finally the spectrum peaks are extracted independently in different frequency bands; a small overlap between neighbor frequency bands is used to find the spectrum peaks for the frequency bin at the edge of the frequency band. . Every frequency band includes 60 frequency bins (the overlap frequency bins are not considered here). The above algorithm has been used in our polyphonic transcription system, which is introduced in the Chapter 5.

Table 4.1 Fast Implementation of RTFI

Band Number	Sampling Rate (Hz)	Frequency Range (Hz)	Used samples	Duration time (Sec)
1	689.06	25.96--55.00	680	0.9861
2	1378.12	51.91--110.0	680	0.4934
3	2756.25	103.8--220.0	1360	0.4934
4	5512.5	207.7--440.0	1360	0.2467
5	11025	415.3--880.0	2720	0.2467
6	22050	830.6--1760	2720	0.1234
7	44100	1661--3520	2720	0.0617
8	44100	3322--7040	2720	0.0617

4.3.4.2 Comparison with other Multiresolution Fast Implementations

With the muliresolution analysis and computing efficiency, different mulitrate filter bank has been explored to resolve music problems [Keren98, Levine98, Jang05]. Wavelet is another constant-Q filter bank and much preferred for audio compressing and music synthesis because wavelet often has the orthonormal or biorthornormal characteristics; but it has little been used for music analysis because the commonly used dyadic sampling fast Discrete Wavelet Transform (DWT) only provide the very coarse frequency resolution, which is far from the requirement of the music analysis, on the other hand the orthonormalization or biorthonormalization not necessary for music analysis, thirdly most of the wavelet is implemented by FIR that need much more computation then IIR. In [Levine98] and [Jang05] the multirate filter bank is used to separate the signal into several octave spaced subband and then the sinusoids analysis has been done in every subband. In [Keren98], similar to the way in [Levine98] and [Jang05], signal is also first separated into several octave subband by multrate filter bank and then the detail frequency analysis is performed by FFT filter. On the one hand, the multirate complex resonator filter bank in the discrete RTFI use similar way to first separate the signal into the several octave spaced subband; on the other hand, different from the existing ways, still keep the constant-Q frequency resolution for further detail frequency analysis in every subband. But for example in [Keren98], when performing the detail frequency analysis in every subband, the FFT filter has equally-spaced frequency resolution.

Chapter 5

MUSIC ONSET DETECTION

5.1 Introduction

The audio signal is often considered to be a succession of the discrete acoustic events. The term *onset detection* refers to detection of the instant when a discrete event begins in an acoustic signal. The human perception of the onset is commonly related to the salient change in the sound's pitch, intensity or timbre. Onset detection plays an important role in music analysis and has very broad-range music applications. The information from onset detection is usually used for the music's temporal analysis, such as tempo identification and meter identification. As a more typical example, automatic transcription of polyphonic music commonly needs to segment the analyzed signal into different notes by onset detection. It is also able to facilitate the edit operations of audio recordings and the synchronization: synchronization of music with video and the synchronization of music with lighting effects.

Many onset detection systems have been developed. They have different advantages and disadvantages. Most of them consist of three stages. Firstly, the analyzed music signal is transformed into a more efficient time-frequency representation, such as a spectrogram. Then, the representation data is further processed to derive the detection function. Finally, the onset is achieved by a certain peak-picking algorithm from the detection function. The first phase is especially important because an inappropriate transform may lose some useful information. This can greatly affect the overall detection performance. In the existing onset detection systems, three commonly-used transform analysis tools are multi-band filtering, STFT, and constant-Q transform. Energy change and pitch change are the two main clues for onset detection. Here are two typical cases: (a) given two successive music notes and wanting to detect onset of the second one, if both notes have the same pitch, the energy change is the only clue. Time-frequency decomposition is almost useless as a means to improve onset detection; (b) in most cases, the two successive notes have different pitches. At the onset time the harmonic frequency components of the second note begin to increase in energy, at the same time, the first note probably enters into the offset time and decreases in energy. The overall energy may only undergo a minor change. Accordingly, an appropriate time-frequency decomposition should be used so that the frequency components of the two successive notes can be decomposed into different frequency channels and the energy-increasing information can be detected in independent frequency channels that correspond to the frequency components of the second note. The note onsets may be classified as “soft” or “hard” onsets to denote slow or fast transitions between the two successive notes. The hard onset is accompanied by a sudden change in energy, whereas the note transition with soft onset shows a gradual change. For example, piano and guitar music often have a number of hard onsets. On the other hand, violin music and singing have many soft onsets. With the appropriate time-frequency representation, the hard onsets can be easily detected by the energy-based detection algorithms. However, the detection of soft onset has been proved to be a very difficult task because real-life music signals often contain noise and vibrations associated with frequency and amplitude modulation. The energy-change in the vibration probably surpasses the energy-change of soft onset and this makes it very difficult to distinguish true onsets from vibration based only on the energy-change clue.

In principle, the time-frequency resolution of the time-frequency representation for the energy-based onset detection algorithm must be one of the most critical factors to affect the detection performance. However, there is no thorough investigation of how time-frequency resolution affects the performance of onset detection system. As indicated in the previous chapters, I propose a new computation-efficient time-frequency representation called Resonator Time-Frequency Image (RTFI). The RTFI is a more general time-frequency representation and can perform a time-frequency analysis with different time-frequency resolutions. Based on the RTFI, I have developed an energy-based onset detection algorithm that is simple and performs very well in the detection of hard onsets. For the detection of the soft onsets, I propose a new pitch-based detection algorithm. It has achieved an excellent performance compared to existing onset detection systems. Both of the energy-based and pitch-based detection algorithms have been tested on a dataset that includes 30 real-life musical excerpts, a total of more than 15 minutes in duration and 2543 onsets.

5.2 Reviews of Related Work

There are many different onset detection systems. Most of them can be described as processing chains, which include three different phases: time-frequency processing, a detection function production, and peak-picking. The processing chain is illustrated in Figure 5.1.

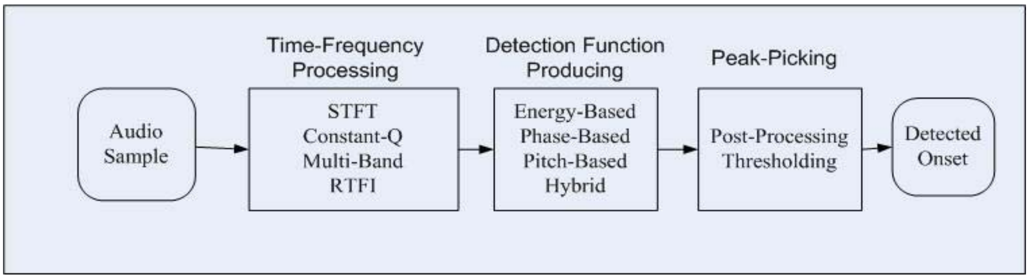

Figure 5.1: A General Onset Detection System

5.2.1 Time-Frequency Processing

In the past, the whole envelope of waveform was used to detect the note onset. This approach has been proved to be inefficient for onset detection in real music signals. For example, consider two successive music notes in the duration of the note transition. The first note probably enters into the offset time and decreases in energy, while the second note enters into the onset time at the same time and increases the energy. So, no change in total energy is noticeable. Some researchers have found it useful to separate the music signal into several frequency bands and then detect the onsets across the different frequency channels. This is so-called multi-band processing. For example, Goto utilized the rapid energy change to detect onset in 7 different frequency ranges and used these onsets to track the music beats by a multi-agent architecture [Goto03]. Klapuri divided the signal into 21 frequency bands by the nearly critical-band filter bank [Klapuri99]. Based on the psychoacoustic knowledge, he used the amplitude envelope to detect the onsets across the different frequency bands. Most of the existing onset detection systems have selected STFT as the time-frequency representation, although the constant-Q transform is another popular alternative. Some researchers combine different time-frequency processing methods. For example, Duxbury first utilized the constant-Q conjugate quadrature filter to implement a multi-band processing and then used the different ways to detect onsets in the different frequency subbands [Duxb02]. In the high frequency subbands, he used the energy change information. In the low frequency subbands, he included the STFT analysis to better detect the change of frequency content.

5.2.2 Detection Function Producing

In the second phase, the output of time-frequency processing can be further used to derive the detection function, which reflects the time-varying character of the analyzed signal in a simplified form. The onset detection systems can derive the detection function by several clues, such as energy-change, phase-change and pitch-change. These clues are often used to classify the detection systems into different types, such as energy-based, phase-based and pitch-based systems.

5.2.2.1 Energy-Based Detection

In early methods, the amplitude envelop of music signal was used to derive the detection function. The amplitude envelope can be constructed by rectifying and smoothing the signal:

$$A(n) = \sum_{m=-N/2}^{N/2-1} |s(n+m)| w(m)$$

where w(m) is N-point window. A variation on this is to derive the detection function from local energy, instead of amplitude.

$$E(n) = \sum_{m=-N/2}^{N/2-1} s^2(n+m) w(m)$$

In a number of practical onset detection systems, the first order of difference function of energy or amplitude is selected as the detection function. However, the first order of difference function is usually not able to precisely mark the onset time. As a refinement, Klapuri introduced relative difference as the detection function, using psychoacoustics knowledge [Klapuri99]. According to the principle of psychoacoustics, the increase in the perceived loudness of the sound signal is relative to its level. The same increase in energy can be perceived more easily in a quiet signal. For a continuous time signal E(t), the relative difference is calculated by the *d(log(E(t))/dt,* instead of *d((E(t))/dt.*

Let us consider the STFT of the signal s(n):

$$X_k(n) = \sum_{m=-N/2}^{N/2-1} s(nh+m) w(m) e^{-2j\pi mk}$$

where w(m) is N-point window and h is the hop size.

For a more general case, when the STFT is selected as the time-frequency processing tool, the spectrum of the different frequency bins in the same time frame may be considered as a N-dimension vector. The detection function can be constructed by the "distance" between the successive STFT spectra. For example, Duxbury uses a standard Euclidean Distance Measure (EDM) [Duxb02] in his system:

$$EDM = \begin{cases} \sum_{k=0}^{N/2-1} \left\{ |X_k(n)| - |X_k(n-1)| \right\}^2, (|X_k(n)| - |X_k(n-1)|) > 0 \\ 0, (|X_k(n)| - |X_k(n-1)|) \leq 0 \end{cases}$$

The distance has a non-zero value only when $|X_k(n)| - |X_k(n-1)|$>0. This limitation is used to select the energy-increase information because the energy should increase at the onset time.

5.2.2.2 Phase-Based Detection

Different than the standard energy-based detection, the phase-based detection makes use of the spectral phase information as its source of information. The STFT can also be considered as complex band-bass filter banks with equal bandwidth, and the STFT coefficient $X_k(n)$ denoting the output of the k_{th} filter. In cases in which there is only one sinusoid component passing the k_{th} band-pass filter and at the same time this sinusoid component is stable, the output of the k_{th} filter must have a nearly constant frequency. Therefore, the difference between two consecutive unwrapped phase values of the X(n) must remains nearly constant:

$$\varphi_k(n) - \varphi_k(n-1) \approx \varphi_k(n-1) - \varphi_k(n-2)$$

where the $\varphi_k(n)$ is defined as the 2π-upwrapped of the STFT coefficient $X_k(n)$. The phase deviation $\triangle\varphi_k(n)$ can also be defined as:

$$\Delta\varphi_k(n) = \varphi_k(n) - 2\varphi_k(n-1) + \varphi_k(n-2) \approx 0$$

During the stable-state part of the signal, the $\triangle\varphi_k(n)$ is nearly equal to zero. During the transient part, the frequency of $X_k(n)$ is not constant, and the $\triangle\varphi_k(n)$ tends to be large. Bello extended this analysis to the distribution of phase deviations of all frequency bins of the STFT [Bello03A]. During the steady-state part of the signal, the values of phase deviations are expected to be close to zero, and the distribution is pointed. In the transient part, the corresponding distribution is flat and wide. Bello quantified these observations by calculating the inter quartile range and the kurtosis coefficient of distribution. Phase-based onset detection has demonstrated a better performance in the detection of the soft onset than have standard energy-based methods. However, it is susceptible to phase distortion and to phase noise introduced in the phases of low energy components. In another approach, Bello proposed to use both the energy and phase information for onset detection [Bello04]. And the complex coefficients of STFT are used to calculate Euclidean distance between the $X_k(n)$ and that predicted by the previous frame, $\hat{X}_k(n)$. For a local stable-state part in the analyzed signal, the frequency and amplitude is assumed to be constant. Then the complex coefficient in the k_{th} frequency bin of STFT can be predicted as:

$$\hat{X}_k(n) = \hat{R}_k(n) e^{j\hat{\Phi}_k(n)}$$

where the predicted magnitude $\hat{R}_k(n)$ is the magnitude of the complex coefficient $X_k(n-1)$ of the previous frame, and the angle $\hat{\varphi}_k(n)$ can be calculated as the sum of the previous phase and phase difference between previous frames:

$$\hat{\varphi}_k(n) = princ \arg[2\varphi_k(m-1) - \varphi_k(m-2)]$$

and the stationary character of the signal in frame n can be quantified by the Euclidean distance measure $\Gamma_k(n)$between the $X_k(n)$ and the predicted $\hat{X}_k(n)$:

$$\Gamma_k(n) = \left\{ (real(X_k(n)) - real(\hat{X}_k(n)))^2 + (imag(X_k(n)) + imag(\hat{X}_k(n)))^2 \right\}^2$$

and the sum of all Euclidean distance measure $\Gamma_k(n)$ across all the frequency bins is used to generate the detection function.

5.2.2.3 Pitch-Based Detection

Pitch changes are the most salient clues for note onset detection of the music signal with soft onset. On the one hand, there are many onset detection systems that use energy change and/or phase change as the source of information. On the other hand, there are only a few pitch-based onset detection systems. One important reason for this is that pitch-tracking itself is a challenging task. Collins proposed a pitch-based onset detection system [Collins05A], in which a constant-Q pitch detector is used to track pitch and then the tracked pitch information is used to find a possible transition between notes. The system is designed to only detect onset of monophonic music signal with soft onset, but its actual use is very limited because the real-life music signal is usually polyphonic.

5.2.2.4 Onset Detection Using Neural Network

There are several studies that utilize machine learning for onset detection [Maro01, Lacoste05]. Marolt utilized the neural network to construct an onset detection system for piano music. He first separated the input signal into several frequency bands by an IIR auditory filter bank, and then used the output envelope of the filter bank to detect the onset by the combination of a integrate and fire neurons and multi-layer perceptron neural network. The system performs well for synthesized recording, but poorly for real music recordings. Lacoste proposed another onset detection system using the neural network. In this system, he first performed a time-frequency analysis, such as STFT and constant-Q analysis for the music signal. Then, corresponding energy and phase information is used to classify every frame as being onset or non-onset by a neural network. It is reported that the detection algorithm achieved the best overall performance in the MIREX 2005 audio onset detection contest.

5.3 Onset Detection System

5.3.1 System Overview

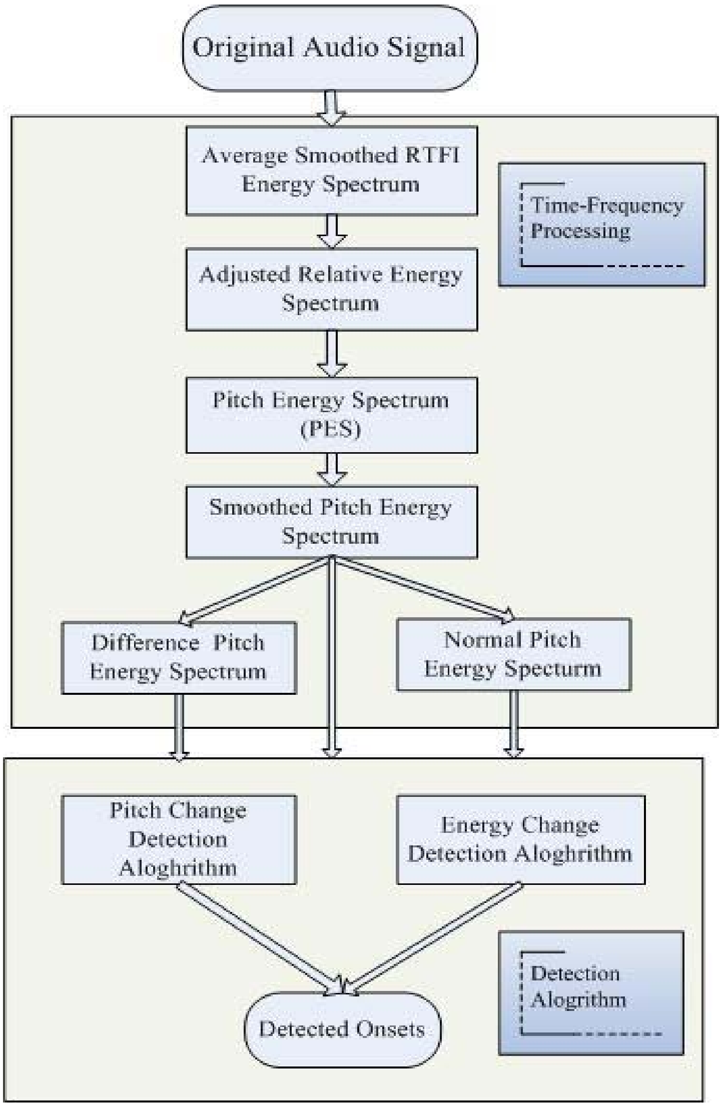
Original Audio Signal
Average Smoothed RTFI Energy Spectrum
Adjusted Relative Energy Spectrum
Pitch Energy Spectrum (PES)
Smoothed Pitch Energy Spectrum
Difference Pitch Energy Spectrum
Normal Pitch Energy Specturm
Time-Frequency Processing
Pitch Change Detection Aloghrithm
Energy Change Detection Aloghrithm
Detected Onsets
Detection Alogrithm

Figure 5.2: Proposed Onset Detection System

I propose an onset detection system that uses a combination of pitch-based and energy-based detection algorithms based on the RTFI analysis. As shown in Figure 5.2, the system consists of two main parts - time-frequency processing and detection algorithms.

5.3.2 Time-Frequency Processing

The monaural music signal is used as the input signal at a sampling rate of 44.1Hz. The system utilized RTFI as the basic tool for time-frequency processing. The center frequencies of discrete RTFI are according to logarithmic scale; 10 filters are used to cover the frequency band of one semitone and there is a total of 960 filters in the analyzed frequency range, which extends from 46 Hz to 6.6 kHz .

It is well known that the human auditory system has different sensitivities to the different frequency bands. This is often described by equal-loudness contours. The human auditory system has a maximum of sensitivity at about 3-4 kHz, while it is less sensitive to the low-frequency bands. This psychoacoustics knowledge is useful in resolving some difficult issues in real-life music analysis. For example, in the detection system, we want to remove the noise in the energy spectrum and must select a threshold value of the energy spectrum below which it will be considered as a noise spectrum. The selection of the threshold will be very difficult without considering psychoacoustics knowledge. In the real-life music signal, the values of the low frequencies of the noise's energy spectrum are even higher than the values of the energy spectrum of the harmonic components at high frequencies. In this case, if one wants to both remove the low-frequency noise spectrum and keep the energy spectrum of the harmonic components at the high-frequencies, he must select different thresholds for the different frequency channels. However, the question of how to select different thresholds for the different frequency channels is still difficult. To resolve this issue, the RTFI energy spectrum is transformed into the Adjusted Energy Spectrum (AES) according to the Robinson and Dadson equal-loudness contours, which have been standardized in the international standard ISO-226. In order to simplify the transformation, only an equal-loudness contour corresponding 70db is used to adjust the RTFI energy spectrum. The standard provides equal-loudness contour limited to 29 frequency bins. Then, this contour is used to obtain the equal-loudness contour of 960 frequency bins by cubic spline interpolation in the logarithmic frequency scale. Let us define this equal-loudness contour as Eq (ω_m). Then, the Adjusted Energy Spectrum (AES) can be expressed as follows:

$$AES(k,\omega_m) = ARTFI(k,\omega_m) - \mathrm{Eq}(\omega_m)$$

where k denotes the k_{th} time-frame, and ω_m denotes the angel frequency of the m_{th} frequency bin.

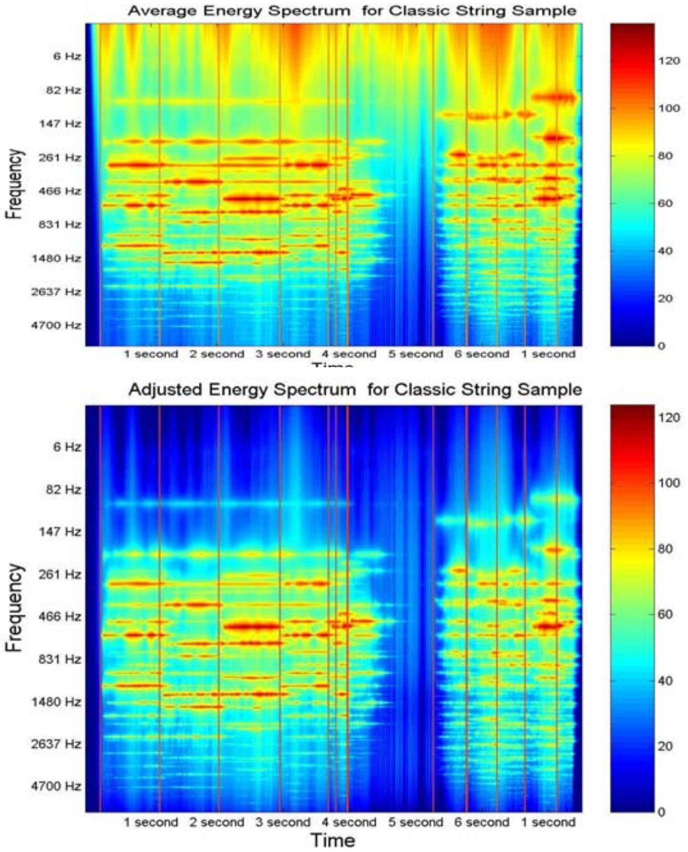

Figure 5.3: Comparing the Average Energy Spectrum with Adjusted Energy Spectrum

Experiments have proved that this method is a good solution for removing the low-frequency noise. In the Adjusted Energy Spectrum, one can select the same threshold for all frequency channels to remove the low-frequency noise very well. Figure 5.3 illustrates the change from the Average Energy Spectrum to the Adjusted Energy Spectrum of classical string music. In comparing the Adjusted Energy Spectrum (AES) (Figure 5.3, top sub-image) to the Average Energy Spectrum (Figure 5.3, down sub-image), one can see that the low-frequency noise has been removed and the low-frequency intensity has obviously been reduced. This is useful because the human auditory system is less sensitive to low frequency sound. The vertical line in each image denotes the correct position of true note onset. Then the Adjusted Energy Spectrum is further recombined into the Pitch Energy Spectrum (PES) according to the following equation:

$$PES(k, \omega_m) = \frac{1}{5} \sum_{i=1}^{5} AES(k, i \cdot \omega_m)$$

The music signal is organized according to "note". It is more interesting than if an energy spectrum is organized according to pitch instead of a single frequency component. In order to further reduce noise, the pitch energy spectrum is then smoothed in both time and frequency as follows,

$$SPES(k, \omega_m) = \frac{1}{25} \sum_{i=k-2}^{k+2} \sum_{m-2}^{m+2} PES(k, \omega_m)$$

The smoothed pitch energy spectrum is used to produce the difference pitch energy spectrum (DPES) and the normal pitch energy spectrum (NPES):

$$DPES(k, \omega_m) = SPES(k, \omega_m) - SPES(k-3, \omega_m)$$

$$NPES(k, \omega_m) = SPES(k, \omega_m) - \max((SPES(k, \omega_m))_{m=1:N})$$

where N is the total number of frequency bins in the Smoothed Pitch Energy Spectrum . The Normal Pitch Energy Spectrum is a relative measure of the maximum value of Smoothed Pitch Energy Spectrum in a certain time-frame. The most silent pitch has the maximum value 0db.

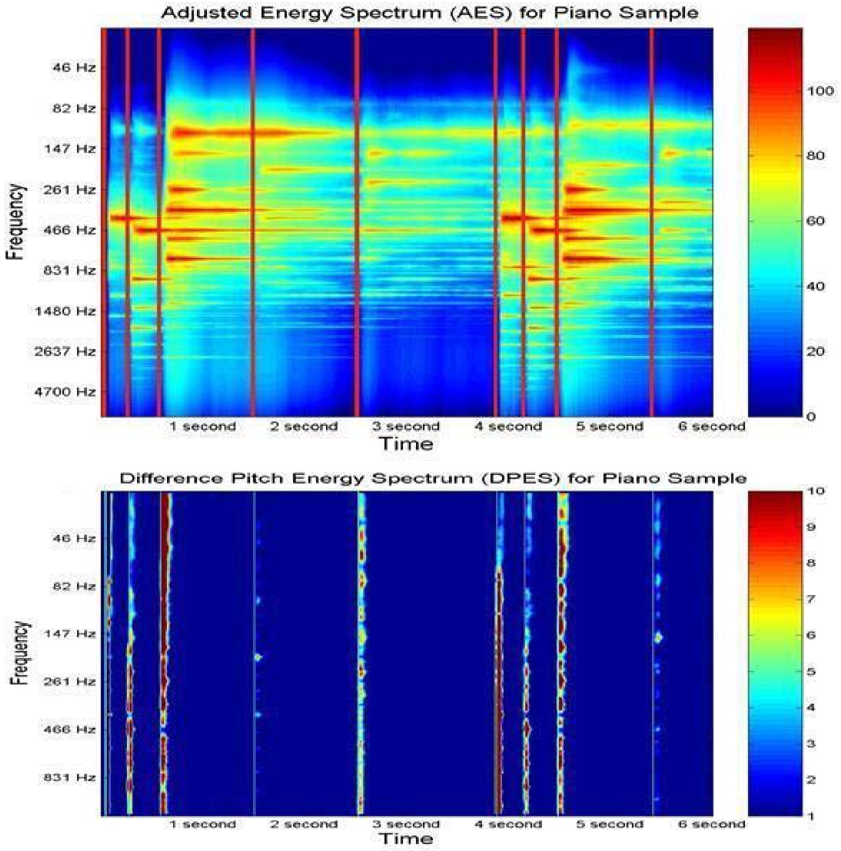

Figure 5.4: Difference Pitch Energy Spectrum

The Difference Pitch Energy Spectrum makes the energy change more obvious. Figure 5.4 shows the Adjusted Energy Spectrum and Difference Pitch Energy Spectrum of an example of piano music. The Difference Pitch Energy Spectrum clearly demonstrates that the main energy-increasing change only exists in the onset time of the piano example.

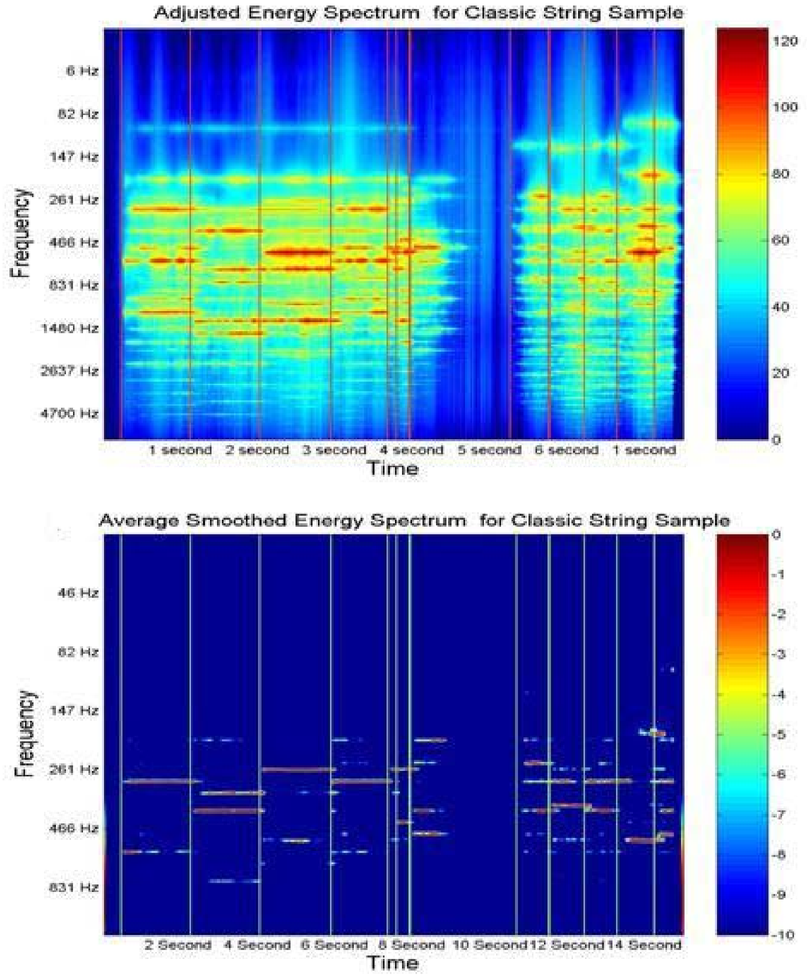

Figure 5.5: Normal Pitch Energy Spectrum

In Figure 5.5 the Normal Pitch Energy Spectrum of the classic string music sample is displayed for values between 0 db and -10 db, and it clearly illustrates the main pitch-change. Finally the Difference Pitch Energy Spectrum, Normal Pitch Energy Spectrum, and Smoothed Pitch Energy Spectrum together are considered as the input for the second stage of the onset detection algorithm.

5.3.3 Detection Algorithms and Experiments

5.3.3.1 Performance Evaluation, Tuning Database and Test Database

In this thesis, three measurements for detection performance: - **precision, recall**, and **F-measure -** are used as an evaluation rule. They are also used for measurements in the Music Information Retrieval Evaluation Exchange (MIREX) 2005. The detected onsets must be compared to the reference onset labels. For a given reference onset label, if there is a detection within a tolerance window of -50ms to 50ms, it is considered to be a correct detection (CD). If not, there is a false negative (FN), and all detections outside of the tolerance window are considered to be false positives (FP). The three measurements for onset detection performance, **precision, recall**, and **F-measure** can be expressed as follows:

Precision=Ncd/(Ncd+Nfp),

Recall = Ncd/(Ncd+Nfn),

F-measure=2*P*R/(P+R)

where the Ncd, Nfp, and Nfn denote the total number of correct detections, false positives and false negatives.

Given a test database, one may get a better result by setting more appropriate parameters for the evaluated algorithm. Consequently, the performance may be overestimated because the parameters may over fit the test examples. In order to prevent such an overestimate, two databases have been constructed. One is a tuning database, which is utilized to tune the parameters of detection algorithms. Another is the test database. there is no duplication between tuning and test database. The parameters can be tuned on the tuning database and good ones may be selected according to some evaluation rules. However, when the algorithms are tested on the test database, the parameters of algorithms are fixed, so that the test results of algorithms on the test database are comparable and not overestimated.

Table 5.1: Tuning Database

#	Content	Reference	Duration	Onset Num
1	Solo Piano (piano fast)	RWC-M06TR1, 2:28-2:48	20s	110
2	Folk music (Folk1)	RWC-M07TR5, 0:00-0:11	11s	36
3	Solo Guitar, Classics	RWC-M06TR4, 0:00-0:30	15s	64
4	Female Singing (accompanied by piano)	RWC-M07TR11, 0:00-0:15	15s	35
5	Country music	RWC-M07TR10, 0:00-0:15	16s	37
6	Piano,Classical Baroque	RWC-M06TR2, 0:00-0:15	15s	76
7	String Quartet	RWC-M06TR2, 3:04-3:28	20s	40
8	Solo Trumpet	Commercial CD	21s	43
9	Solo Clarinet	Commercial CD	30s	31
10	Solo Violin Bow	Commercial CD	46s	43
Total			3 Min 29s	515

The tuning dataset selects 10 different examples of music of different genres and instruments. The respective details are listed in Table 5.1. There are 7 examples in the dataset that have been excerpted from the RWC music database [Goto03], and the positions of these examples in the RWC database are shown in the Reference column of the Table. The other 3 examples are excerpted from commercial CDs. For the tuning database and test database, the true onsets are all first labelled by hand. The detailed information of test database will be introduced in the later sections.

5.3.3.2 Proposed Energy-based Detection Algorithm

The music signal usually includes two parts - a transient part and a stable part. The Difference Pitch Energy Spectrum from the RTFI analysis as introduced previously can be used to track the transient information, such as the onset of the music note. I propose a method to track the transient information based on the Difference Pitch Energy Spectrum. The method can be simply described as follows:

$$LDPES(k,\omega_m) = Limit(DPES(k,\omega_m),\theta_1) - \theta_1 \quad (5.1)$$

where $Limit(Array(m,n),\theta_1) = \begin{cases} Array(m,n) & if : Array(m,n) > \theta_1 \\ \theta_1 & if : Array(m,n) \le \theta_1 \end{cases}$

$$Mean\_LDPES(k) = \frac{1}{N}\sum_{m=1}^{N} LDPES(k,\omega_m) \quad (5.2)$$

where N is the total number of frequency bins in the Difference Pitch Energy Spectrum .

In this method, firstly the Difference Pitch Energy Spectrum is limited by a threshold θ1 so that only the values that exceed threshold θ1 are considered to be possible transient clues; and then the Limited Difference Pitch Energy Spectrum are averaged across all pitch channels to generate the detection function. The detection function is further smoothed by a moving-average filter and a simple peak-picking is used to find the note onsets. In the peak-picking, another threshold θ2 needs to be set and only the peaks having values greater than threshold θ2 are considered as the possible onset candidates. In the final step, if there are two onset candidates and the position difference between them is smaller than or equal to 50ms, then only the onset candidate with the greater value will be kept. The algorithm is illustrated in Figure 5.6.

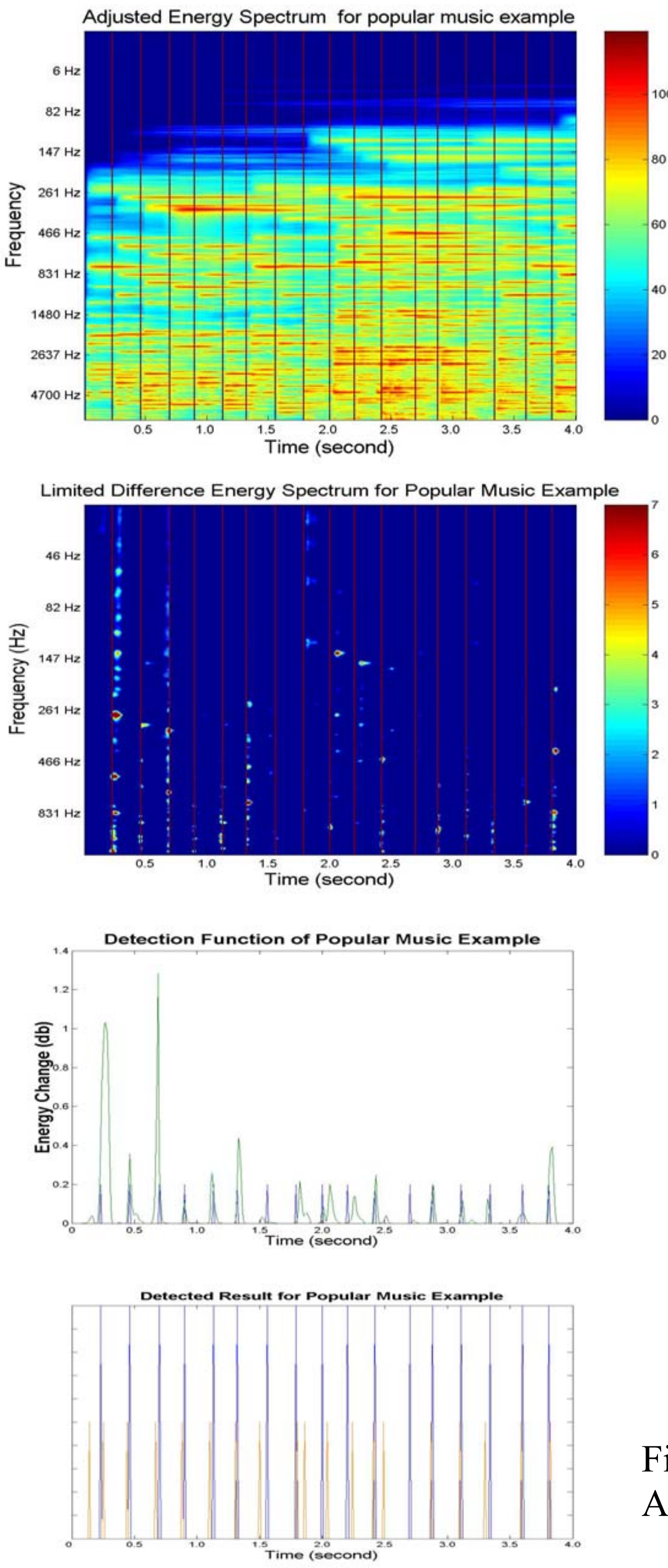

The left image illustrates the Energy-based detection algorithms for a popular music example with duration time 4 seconds. The vertical line in the image denotes the label of the true onsets. The first image is the Adjusted Pitch Energy Spectrum. And the second image is the Limited Difference Energy Spectrum with a threshold θ1=3 db according to the equation (5.1). In this example, it is obvious that most of the main energy-changes only exist in the onset time. The Limited Difference Energy Spectrum is averaged across all the frequency channels to generate the detection function. The detection function is further smoothed to detect onset by a simple peak-picking. The smoothed detection function is shown in the third sub-image, and the blue line in this image denotes the position of the true note onsets. Finally a simple peak-picking is used with the second threshold θ2=0.02 db; additionally, if there exist two successive onset candidates and the position difference between them is smaller or equal 50ms, only the onset candidate with bigger value will be kept. The detecting result is shown the last sub-image, the blue line in this image denotes the position of the true note onsets and the red line denotes the position of detected onsets.

Figure 5.6: Energy-Based Detection Algorithm

In the energy-based detection algorithm, two threshold parameters need to be selected. Some experimental results in Table 5.2 demonstrate that different parameters need to be set for the algorithm in order to achieve the best performance for the different types of music signals of the tuning database.

Table 5.2: Result of Energy Detection Algorithm
With Best Fitting Parameter for Each Example

#	Content	FMeasure	Best Fitting Parameter
1	Solo Piano	98.2%	Threshold: θ_1=1; θ_2=0.01
2	Folk music	98.5%	Threshold: θ_1=1; θ_2=0.02
3	Solo Guitar, Classics	97.7%	Threshold: θ_1=1; θ_2=0.03
4	Female Singing	65.0%	Threshold: θ_1=2; θ_2=0.19
5	Country music	80.9%	Threshold: θ_1=0; θ_2=0.06
6	Piano, Classical Baroque	97.3%	Threshold: θ_1=3; θ_2=0.01
7	String Quartet	48.2%	Threshold: θ_1=3; θ_2=0.01
8	Solo Trumpet	92.6%	Threshold: θ_1=3; θ_2=0.14
9	Solo Clarinet	93.1%	Threshold: θ_1=3; θ_2=0.01
10	Solo Violin Bow	80.0%	Threshold: θ_1=7; θ_2=0.01

In practical applications, it is difficult to select appropriate parameters for music examples to test. It is proposed to use a tuning database to select the best parameters. The parameters will be considered to be the best global parameters if they make the detection algorithm have best overall performance on the all types of examples in a tuning database. The average F-measure across all examples is selected as the evaluation rule for the global performance. The best global performance of this energy-based detection algorithm in the tuning dataset is illustrated in Table 5.3.

Table 5.3: Result of Energy-Based Detection Algorithm
with Global Best Fitting Parameter (achieving the best average-FMeasure)
Threshold: $\theta_1=3$; $\theta_2=0.02$, average-FMeasure=77.8%

#	Content	F-Measure	Recall	Precision
1	Solo Piano	93.4%	89.2%	99.0%
2	Folk music	93.9%	88.6%	100%
3	Solo Guitar	97.7%	96.9%	98.4%
4	Female Singing	62.0%	86.1%	48.4%
5	Country music	75.0%	64.8%	88.9%
6	Piano, Baroque	97.3%	96.1%	98.7%
7	String Quartet	48.2%	48.8%	47.6%
8	Solo Trumpet	84.9%	95.5%	76.3%
9	Solo Clarinet	75.4%	74.2%	76.7%
10	Solo Violin, Bow	51.0%	89.6%	36.1%
Average		77.8%	82.9%	77.0%

The results in this table clearly demonstrate that the energy-based detection algorithm performs very well on the examples (such as Solo Piano, Solo Guitar, Classical Baroque) with strong, hard onsets. However, it did not perform as well on the examples (such as String Quartet, Solo Bow Violin) with soft onsets. Figure 5.7 illustrates an example of energy-based detection for bow violin. Many notes in this example have very strong vibrations. As shown in the second sub-image in Figure 5.7, the Difference Pitch Energy Spectrum demonstrates that the salient energy-change exists not only in the onset time, but also in the note duration time. In the detection function (sub-image 3), it is seen that there are many spurious peaks that are, in fact, not relate to the true note onsets. Consequently, the energy-based detection algorithm shows very low performance in this example (the F-Measure is 51.0% as shown in the Table 5.3)..

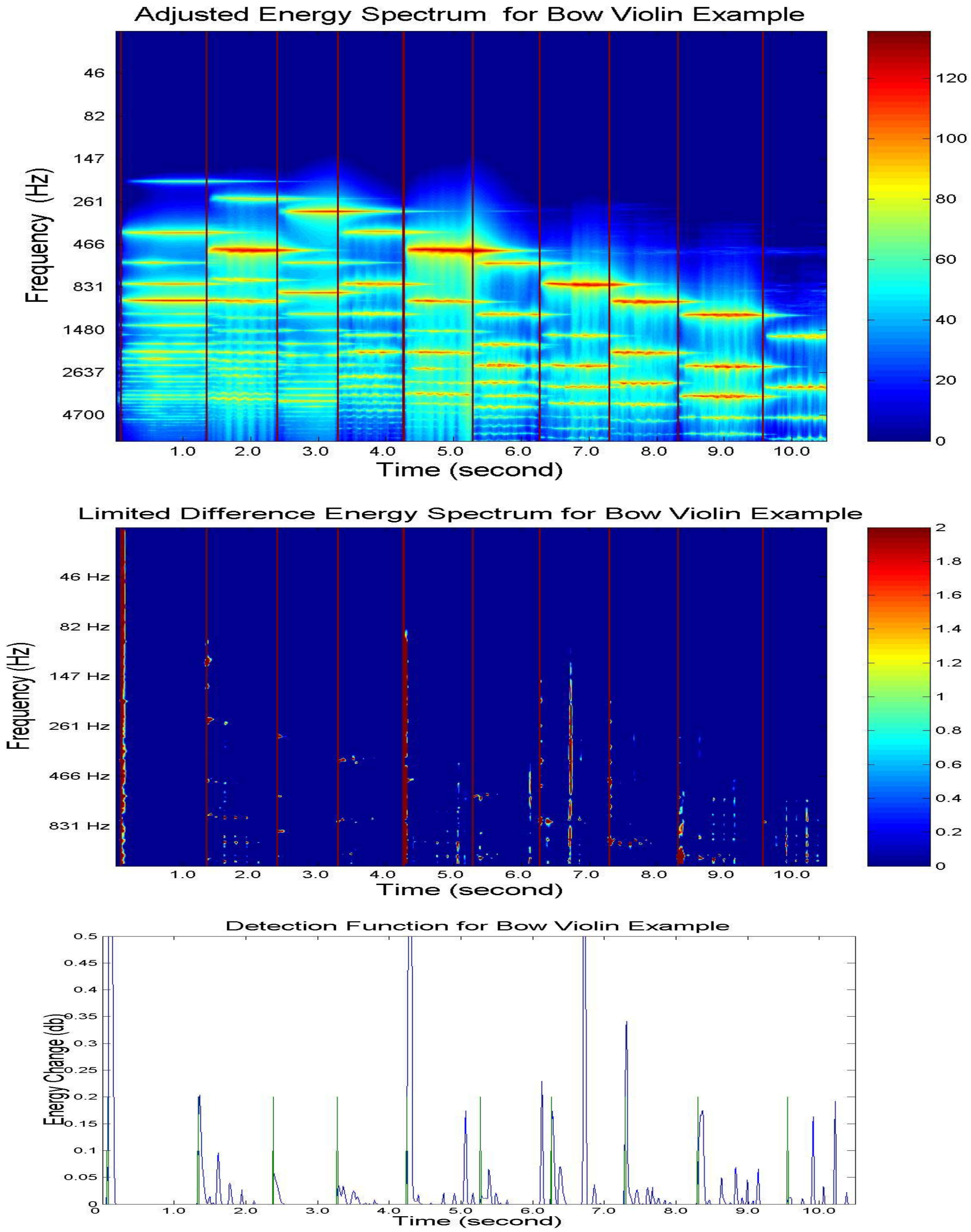

Figure 5.7: Energy-Based Detection of Bow Violin with soft onsets

5.3.3.3 Proposed Pitch-based Detection Algorithm

As mentioned before, the energy-based detection algorithm is not good at detecting soft onsets. Consequently, I propose a pitch-based detection algorithm, which performs well on both hard and soft onsets. In particular, it has greatly improved the detection performance for the detections of soft onsets. Generally speaking, the music note consists of two different parts, a transient part and a stable part. In the stable part, the pitch change is small. The pitch is almost stable. In the proposed pitch-based detection algorithm, the music signal is first divided into transient and stable parts by the pitch-change clue, and then the onset is located in the transient part by energy-change. As the output of RTFI time-frequency processing, the Smoothed Pitch Energy Spectrum, Different Pitch Energy Spectrum and Normal Pitch Energy Spectrum are used together as the input for this detection algorithm. The algorithm can be separated into two steps:

1) Searching the possible note onsets with the approximate fundamental frequency ω_m.

2) Combining the detected onset candidates across all of the frequency channels and generating the final result for onset detection.

1) Search of the Onset Candidates

The algorithm searches possible pitch onsets in every frequency channel. It is emphasized that, when searching in a certain frequency channel with frequency ω_m, the detection algorithm tries to find only the onset where the new occurred pitch rightly has an approximate fundamental frequency ω_m. If a pitch with a fundamental ω_m occurs in a certain time segment, then probably there is a peak line in this time segment around the frequency ω_m in the Smoothed Pitch Energy Spectrum and the intensity of the Normal Pitch Energy Spectrum should be stronger than a threshold.

The proposed detection strategy consists of searching for the pitch onset based on the two following assumptions, which are reasonable in most cases. Under the first assumption, when searching for the pitch onset in a certain frequency channel with frequency ω_m, the detection algorithm first tries to find the time segment T , where the intensity of the Normal Pitch Energy Spectrum is strong enough. Then, check that the average Smoothed Pitch Energy Spectrum across the corresponding time segment has a spectrum peak in the frequency axis near the frequency ω_m. If the two conditions are met within the time segment T, then it is considered possible that a new pitch with fundamental frequency ω_m occurs in that time segment T. Two thresholds are used to evaluate whether the pitch in the segment T is noticeable: i) all of the Normal Pitch Energy Spectrum in segment T exceeds threshold α_1; ii) the maximum value of the Normal Pitch Energy Spectrum in segment T exceeds threshold α_2. For a better explanation of the detection algorithm, the classic music excerpt is selected as an example. The two thresholds are selected as follows: α_1=-10, α_2=-5; The Normal Pitch Energy Spectrum of this sample is shown in Figure 5.8. Its duration time is 8 seconds and only the values that are more than -10 db are displayed.

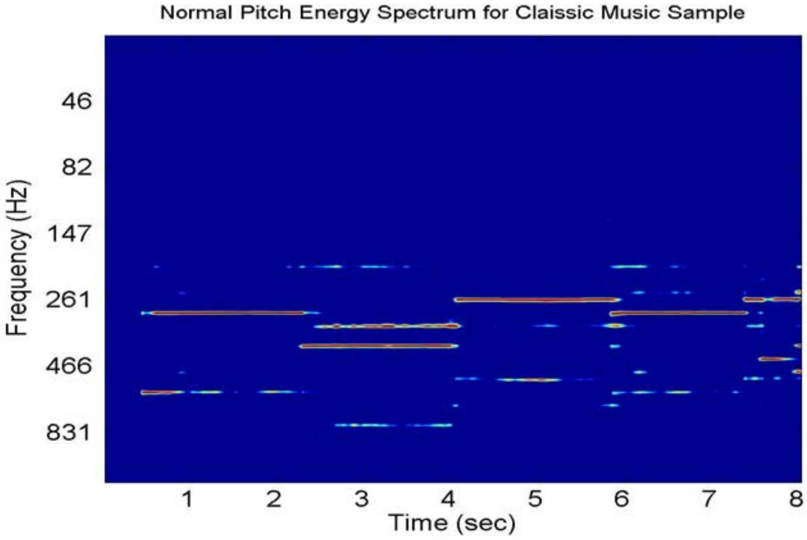

Figure 5.8: Normal Pitch Energy Spectrum for a classic string music sample

For example, when searching for the pitch onset in the 293Hz frequency channel for the classic music sample, the corresponding Normal Pitch Energy Spectrum, Difference Pitch Energy Spectrum and Smoothed Pitch Energy Spectrum are as shown in Figure 5.9. The detection algorithm first searches the Normal Pitch Energy Spectrum and finds that two time segments T1 [0.3sec, 2.3sec], and T2 [5.8sec, 7.6sec] have values higher than, or equal to, -10 db. Additionally, their maximum is more than threshold α_2=-6. This implies that, in the duration time of the two segments, the Pitch Energy Spectrum intensity of this frequency channel is strong enough compared to the other frequency channel. Then, the sum of Smoothed Pitch Energy Spectrum (SPES) in the two time segments has to be computed respectively as follows,

$$Sum\_SPES^{T1}(\omega) = \sum_{i=30}^{230} SPES(k,\omega)$$

$$Sum\_SPES^{T2}(\omega) = \sum_{i=580}^{760} SPES(k,\omega)$$

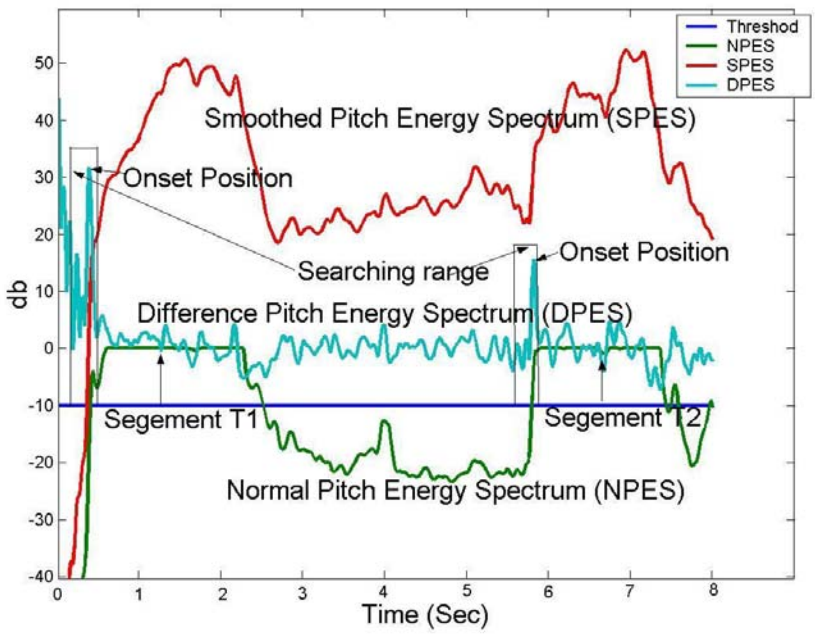

Figure 5.9: Searching of the pitch onsets in one frequency channel

And if there is a peak at the 293 Hz frequency in the Sum_SPES^{T2}, it is considered probable that there is a new note with a fundamental frequency of 293 Hz occurring in the time segment T2. Then the detection algorithm locates the onset position of this new note by searching for a noticeable energy-change peak greater than the threshold α_3 (in this example, α_3=2) in the Difference Pitch Energy Spectrum. The searching is backward from the beginning of the time segment T2, and the searching range is limited in the 0.3 second window before the time segment T2. As shown in the Difference Pitch Energy Spectrum of the Figure 5.9, there exists a peak with the value more than the threshold α_3 nearly at the 5.8th second; the time position of this energy-change peak of the Difference Pitch Energy Spectrum is considered as a candidate pitch onset. In summary, in the frequency channel with frequency ω_m, the algorithm first tries to find the time segment T where a new note with fundamental frequency ω_m probably occurs, and then locates the onset position of this new note backward from the time segment T by the noticeable energy-change from the Difference Pitch Energy Spectrum. The basic algorithm has been explained by the simple example. An additional constraint needs to be added to improve the detection performance in practical cases. If a new note is considered to occur in the time segment T, then the duration time of segment T must be more than 0.01 second.

After all frequency channels have been searched, the pitch onset candidates can be found and expressed as follows:

$$Onset\_C(k,\omega_m) \geq 0 \text{, m=1, 2, 3, …N,}$$

where k denotes the time frame and N denotes the total num of the pitch channels. If $Onset\_C(k, \omega_m)=0$, no onset exists in the k_{th} time-frame and m_{th} frequency channel. If the $Onset\_C(k, \omega_m)>0$, there is an onset candidate in the k_{th} time-frame and m_{th} frequency channel, and the value of $Onset\_C(k, \omega_m)$ is equal to the value of DPES$((k, \omega_m)$ (Difference Energy Spectrum in the k_{th} time-frame and m_{th} frequency channel) .

2) Combination of onset candidates

Finally the detection algorithm combines the pitch onset candidates across all the frequency channels to get the final onset. The combining procedure can be separated into two phases - canceling and merging. In the first phase, if two onset candidates are neighbors in a 0.05 second time window, then only the onset candidate with the greater value will be kept. The onset candidate with smaller value will be cancelled. The task in the second phase is to determine if the two neighbor onset candidates should be merged into a single onset. In the time segment between the two neighbor onset candidates if the first pitch is still in the transient part, then the two onset candidates will be merged into a single note onset, whose time position is the mean of the time positions of the two merged onset candidates. Figure 5.10 illustrates the processing steps in pitch-based onset detection.

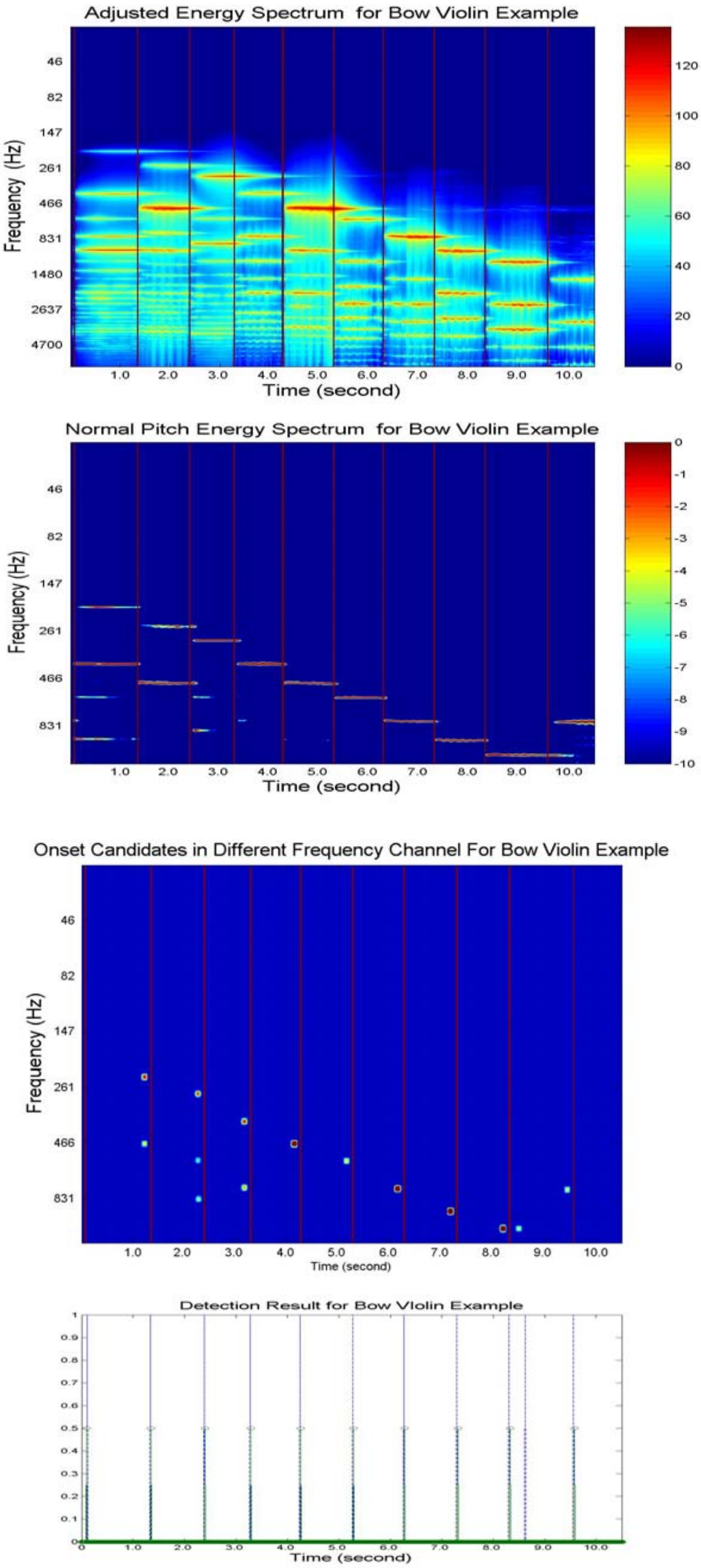

The left image illustrates the pitch-based detection algorithm for a bow violin example with duration time 10 second. The red vertical lines in all the sub-images denote the time position of the true onsets. Very strong vibration can be obviously viewed from it's Energy Spectrum shown in the first sub-image. As introduced before, the energy-based detection algorithm shows very low performance on this example (referring to the Figure 7) because the vibration causes that the noticeable energy-change also exists in the note's stable parts. As shown in the second sub-image, the Normal Pitch Energy Spectrum clearly demonstrates it's pitch-change. Here the pitch-based detection algorithm makes best use of the pitch-change clues to separate the signal into transient and stable parts, and then searches the onset candidates only in the transient part of the signal according to different frequency channels. The dots in the third image denote the detected onset candidates in the different frequency channel by the algorithm. Finally the detection algorithm combines the pitch onset candidates across all the frequency channels to get the final result, which is shown in the last sum-image. In the last sub-image, the blue line denotes the time position of the true onset, and the green line with circle on the top denotes the time-position of the detected onsets.

Figure 5.10: Pitch-Based Detection Algorithm

Tuning the Parameters of the Algorithm

As indicated earlier, there are 3 parameters that need to be set in the proposed pitch-based detection algorithm. The two thresholds, α_1 and α_2, are used to determine if any pitch energy is noticeable in a time segment T. The third threshold, α_3, is used to locate the onset position of a detected pitch by the energy-change in its transient part. As in the parameter tuning of the proposed energy-based detection algorithm, the idea here is to tune the parameters of the pitch-based detection algorithm. The tuning database is used to tune the parameters. The more appropriate values of the parameters should cause the detection algorithm to have better global performance in the tuning databases. The different parameter values are tried by the heuristic method. Those that cause the algorithm to have the best average F-Measure in all the examples of the tuning database are selected. The detection results for the tuning database are shown in Table 5.4.

Table 5.4: Results of Pitch-Based Detection Algorithm
with Global Fitting Parameter, Threshold: α_1=-10; α_2=-3; α_2=2;
average-FMeasure=92.0%

#	Content	FMeasure	Recall	Precision
1	Solo Piano	91.6%	84.5%	100%
2	Folk music	95.5%	91.4%	100%
3	Solo Guitar, Classics	98.4%	96.7%	100%
4	Female Singing	81.8%	85.1%	77.0%
5	Country music	80.6%	69.4%	96.2%
6	Classical Baroque	98.0%	96.5%	100%
7	String Quartet	90.0%	85.7%	94.7%
8	Solo Trumpet	94.0%	90.7%	97.5%
9	Solo Clarinet	96.8%	100%	93.8%
10	Solo Violin, Bow	93.3%	97.7%	89.4%
Average		92.0%	89.7%	94.9%

5.4 Results of Database

5.4.1 Results

The performance evaluation and comparison of different automatic onset detection algorithms in the publications is a difficult task because there is no common test collection and evaluation rule. I propose two onset detection algorithms (energy-based and pitch-based detection). Their detection performances have been compared with the same test dataset to find their advantages and disadvantages on the different types of music signal. At the same time, the detection results of the proposed detection systems will be compared with the best results in MIREX 2005 [Mirex05]. Music Information Retrieval Evaluation Exchange (MIREX) proposes a common test environment for the contest. In MIREX 2005, some algorithms have been tested and compared on the same test collection. Unfortunately, the test database of MIREX contest is not public distributed. So, it must be emphasized that the comparison is only approximate because the test databases are different.

As mentioned before, two different databases (tuning database and test database) are constructed in my experiments.. The parameters of algorithms are tuned and selected by the tuning database. When the algorithms are tested on the test database, no changes to the corresponding parameters are permitted. This method prevents the parameters of the evaluated algorithm form over fitting the test examples and ensures that the test results on the test database are more comparable and not overestimated.

The test database contains different types of excepts from the broad range of real-life music, which are played by different music instruments, such as piano, guitar, violin, cello, clarinet, flute, oboe, trumpet and horn. It also includes different genres of music, such as Jazz, Rock, Popular, Dance, Latin and Country. In the test database, some examples have been selected from the Real World Computing (RWC) music generic database, which is often selected as a common foundation for research.. Some are selected from a Public distributed database, which contains 17 short music sequences in different music instruments and genres, and the validated onset labels for more than 700 corresponding onsets are also freely distributed. The other examples are selected from commercial music CDs. In total, the test database includes 30 music excerpts, more than 15-minutes in duration time and 2543 onsets. Similar to the MIREX 2005, the test examples in the test database are classified into classes: Plucked String, Sustained String, Brass, Winds, Complex Mixes.

The piano is considered as a single class because most of the piano music contains many hard onsets. In the MIREX 2005, the class Plucked String and Sustained String only contains the monophonic. However, in this test dataset, both the Plucked String class and the Sustained String class contain real-life polyphonic music. The complete test results of the proposed energy-based and pitch-based detection algorithms of all class examples are listed in Table 5.5-5.10. At the same time, the tables contain detailed information for every example, such as duration time, source reference, instrument or generic, and total number of labelled onsets.

Table 5.5: Test Results for Plucked String

(5 Files ,Total 2 minutes 15 second duration, 421 Onsets)

				Result of Pitch-Based Detection Algorithm				**Result of Energy-Based Detection Algorithm**			
#	**Content**	**Ref**	**Duration**	**CO**	**FP**	**FN**	**F-Measure**	**F-Measure**	**CO**	**FP**	**FN**
1	**Guitar I**	**Commercial CD**	**60s**	**102**	**3**	**11**	**93.6%**	**88.6%**	**109**	**24**	**4**
2	**Guitar II**	**Public**	**15s**	**53**	**1**	**4**	**95.5%**	**99.1%**	**57**	**1**	**0**
3	**Violin I**	**Public**	**15s**	**50**	**4**	**22**	**79.4%**	**81.8%**	**54**	**6**	**18**
4	**Violin II**	**Commercial CD**	**30s**	**116**	**7**	**9**	**93.6%**	**88.4%**	**122**	**29**	**3**
5	**Cello I**	**Public**	**15s**	**36**	**5**	**18**	**75.8%**	**60.0%**	**24**	**2**	**30**
				Average F-Measure: 87.6%				**Average F-Measure: 83.6%**			

Table 5.6: Test Results for Solo Winds

(5 Files, Total 2 minutes 32 second duration, 375 Onsets)

				Result of Pitch-Based Detection Algorithm				Result of Energy-Based Detection Algorithm			
#	**Content**	**Ref**	**Duration**	**CO**	**FP**	**FN**	**F-Measure**	**F-Measure**	**CO**	**FP**	**FN**
1	**Clarinet I**	**Commercial CD**	**30s**	**23**	**5**	**1**	**88.5%**	**68.9%**	**21**	**16**	**3**
2	**Clarinet II**	**Commercial CD**	**30s**	**28**	**4**	**1**	**91.8%**	**79.3%**	**23**	**6**	**6**
3	**Flute I**	**Commercial CD**	**45s**	**68**	**0**	**19**	**87.7%**	**75.0%**	**67**	**23**	**20**
4	**Flute II**	**Commercial CD**	**30s**	**92**	**1**	**37**	**82.3%**	**85.1%**	**106**	**14**	**23**
5	**Oboe**	**Commercial CD**	**17s**	**90**	**0**	**16**	**91.8%**	**92.1%**	**99**	**10**	**7**
				Average F-Measure: **88.4%**				**Average F-Measure:** **80.8%**			

Table 5.7: Test Results for Piano

(2 Files, Total 2 minutes duration, 449 Onsets)

				Result of Pitch-Based Detection Algorithm				Result of Energy-Based Detection Algorithm			
#	**Content**	**Ref**	**Duration**	**CO**	**FP**	**FN**	**F-Measure**	**F-Measure**	**CO**	**FP**	**FN**
1	**Piano I**	**Commercial CD**	**60s**	**152**	**1**	**19**	**93.8%**	**99.1%**	**169**	**1**	**2**
2	**Piano II**	**Commercial CD**	**60s**	**248**	**6**	**40**	**91.5%**	**96.2%**	**268**	**1**	**20**
				Average F-Measure: **92.7%**				**Average F-Measure:** **97.7%**			

Table 5.8: Test Results for Solo Brass

(3 Files , Total 1 minutes 17 second duration, 230 Onsets)

				Result of Pitch-Based Detection Algorithm				Result of Energy-Based Detection Algorithm			
#	**Content**	**Ref**	**Duration**	**CO**	**FP**	**FN**	**F-Measure**	**F-Measure**	**CO**	**FP**	**FN**
1	**Trumpet I**	**Public**	**15s**	**51**	**0**	**7**	**93.6%**	**90.6%**	**53**	**6**	**5**
2	**Trumpet II**	**Commercial CD**	**30s**	**74**	**0**	**7**	**95.5%**	**85.4%**	**79**	**25**	**2**
3	**Horn**	**Commercial CD**	**32s**	**76**	**1**	**15**	**90.5%**	**87.3%**	**86**	**20**	**5**
				Average F-Measure: 93.2%				**Average F-Measure: 87.8%**			

Table 5.9: Test Results for Sustained String

(6 Files with polyphonic sound, Total 4 minutes 12 second duration, 378 Onsets)

				Result of Pitch-Based Detection Algorithm				Result of Energy-Based Detection Algorithm			
#	**Content**	**Ref**	**Duration**	**CO**	**FP**	**FN**	**F-Measure**	**F-Measure**	**CO**	**FP**	**FN**
1	**Violin**	**Commercial CD**	**50s**	**86**	**7**	**4**	**93.9%**	**56.0%**	**84**	**126**	**6**
2	**String Quartet I**	**Commercial CD**	**50s**	**65**	**14**	**9**	**85.0%**	**43.2%**	**46**	**93**	**28**
3	**String Quartet II**	**Commercial CD**	**36s**	**36**	**10**	**5**	**82.8%**	**29.2%**	**19**	**70**	**22**
4	**String Quartet III**	**RWC**	**30s**	**42**	**9**	**3**	**87.5%**	**38.5%**	**21**	**43**	**24**
5	**Violin/ Viola I**	**Commercial CD**	**50s**	**67**	**13**	**13**	**83.8%**	**50.9%**	**69**	**122**	**11**
6	**Violin/ Viola II**	**Commercial CD**	**36s**	**40**	**2**	**8**	**88.9%**	**46.5%**	**33**	**61**	**15**
				Average F-Measure: 87.0%				**Average F-Measure: 44.1%**			

Table 5.10: Test Results for Complex Music

(9 Files , Total 3 minutes 28 second duration, 690 Onsets)

				Result of Pitch-Based Detection Algorithm				**Result of Energy-Based Detection Algorithm**			
#	**Content**	**Ref**	**Duration**	**CO**	**FP**	**FN**	**F-Measure**	**F-Measure**	**CO**	**FP**	**FN**
1	**Jazz I**	**Public**	**15s**	27	5	9	79.4%	88.6%	35	8	1
2	**Jazz II**	**RWC**	**20s**	71	3	22	85.0%	94.9%	92	9	1
3	**Rock I**	**RWC**	**30s**	100	6	27	85.8%	96.9%	126	7	1
4	**Rock II**	**Public**	**15s**	40	2	19	79.2%	82.7%	43	2	16
5	**Popular I**	**Public**	**15s**	27	5	10	78.3%	87.5%	35	8	2
6	**Popular II**	**RWC**	**42s**	75	8	20	84.3%	84.2%	93	33	2
7	**Latin**	**RWC**	**30s**	84	5	16	88.9%	97.5%	98	3	2
8	**Dance**	**RWC**	**30s**	66	2	18	86.8%	97.6%	82	2	2
9	**Country**	**RWC**	**11s**	46	4	25	76.0%	89.8%	66	10	5
				Average F-Measure: 82.6%				**Average F-Measure:** 91.0%			

5.4.2 Discussion

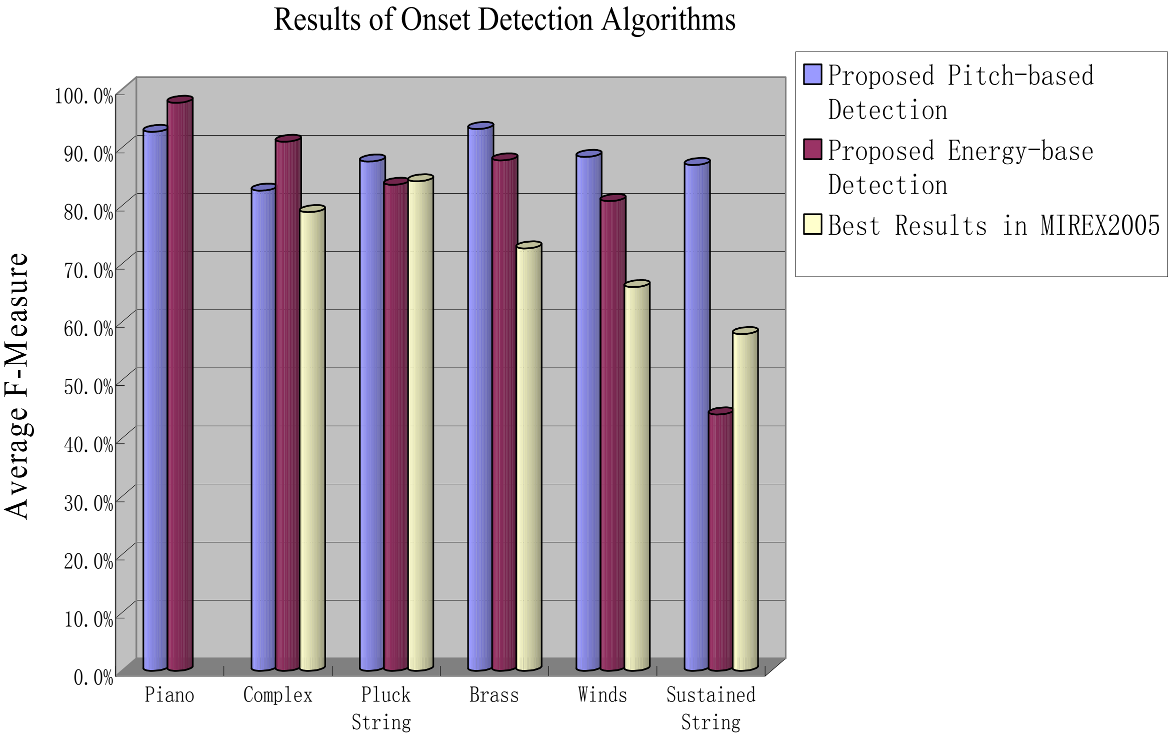

Figure 5.11: Comparison of Results among the Different Detection Algorithms

The total results of the proposed Energy-based and Pitch-based detection algorithms appear in Figure 5.11. The best results in the MIREX 2005 are also shown in this diagram for an approximate comparison.

Overall, the proposed Pitch-based detection performs best. In this evaluation, the Average F-Measure is used to evaluate detection performance. On the one hand, the proposed Energy-based detection algorithm performs better than does the Pitch-based detection algorithm on the Piano and Complex music, which contains a lot of hard onsets. The Energy-based detection wins 5.0% for Piano music and 8.4 % for the Complex music. On the other hand, the Pitch-based detection algorithm performs better in the Pluck String, Brass, Winds and Sustained String where note onsets are softer. Especially, for the Sustained String, the Pitch-based detection algorithm wins 42.9% and greatly improves the performance from 44.1% to 87.0%. The Pitch-based detection algorithm wins 5.4%, 7.6%, 4.0% respectively for Brass, Winds, and Pluck String than the Energy-based detection algorithm.

Compared with the best results in the MIREX 2005, the performance of the proposed Pitch-based detection algorithm has been a great improvement for the Brass, Winds and Sustained String. The proposed Pitch-based detection algorithm wins 20.5% on the Brass, 22.4% on the Winds, and 29.1% on the Sustained String. Most of the existing onset detection algorithms are based on the energy-change or phase-change clues. However, in some real-life music signals with soft onsets, the energy-change in the note transition may be not noticeable. At the same time, for some music signals, the noticeable energy-change does not necessarily only exists the note onset time. A typical example is the music of sustained string, such as bow violin; where, because of the vibration caused by the frequency modulation, the music note probably has a very noticeable energy change in the stable part of the note. In this case, an energy-based detection algorithm probably is misdirected by such a noticeable energy change and will cause a lot of false positives in the detection results. This is an important reason why the proposed Energy-based detection algorithm shows very low performance on the Sustained String. In the same case, in the MIREX 2005, all of the detection algorithms exhibit very low performance on the Sustained String (the best result is 57.9%). The reason is that most of the detection algorithms in the MIREX 2005 are based on energy-change clue s[Bross05, Collins05, Lacoste05, West05, Pert05]. One of them also combines the phase information with energy information. However, the phase information is very sensitive to noise and exhibits very low performance on the onset detection of real-life music.

The proposed Pitch-based detection algorithm first makes best use of pitch change clues to separate the music signal into a transient and a stable part, and then searches for the possible note onsets only in the transient part. This method greatly reduced the false positives that are caused by the salient energy-change in the stable part of the music note, and greatly improved the detection performance of the music signal with many soft onsets or vibrations. Because of the reduction of false positives, the proposed Pitch-based detection algorithm has not only greatly improved the overall detection performance, but also endowed the detection result with very high precision. A comparison between the precision of the detection results of the proposed Pitch-based and Energy-based detection algorithm is illustrated in Figure 5.12. The better precision is very meaningful for practical applications in which high confidence in the detected onsets may be required, even at the expense of under-detection.

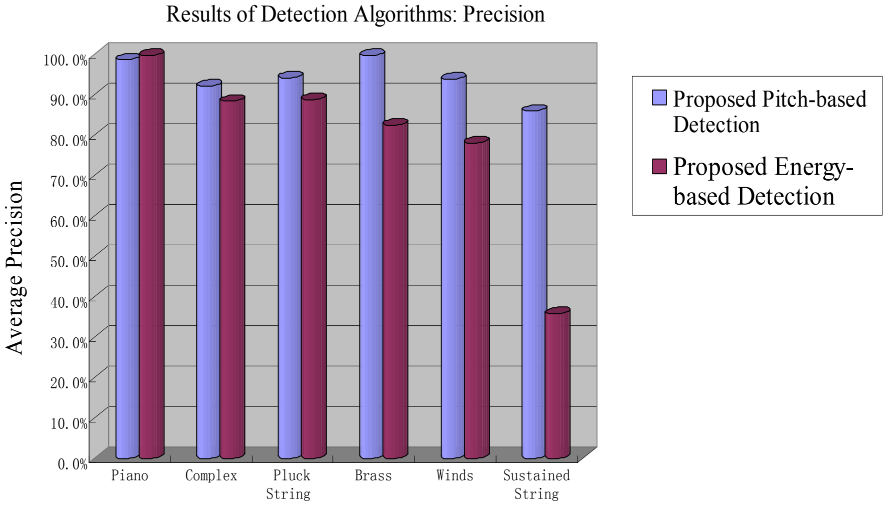

Figure 5.12: Comparison of the Precision of Proposed Pitch-based and Energy-based Detection Algorithms

Chapter 6

INTRODUCTION TO POLYPHONIC PITCH ESTIMATION

6.1 Introduction

Pitch is a perceptual and subjective attribute of sound and plays an important role in the human understanding of sound. Although the pitch estimation of monophonic sound is well resolved, the polyphonic pitch estimation has been proved to be a very difficult task. Polyphonic pitch estimation requires the resolution of some difficult problems that do not exist in the estimation of monophonic pitch. For example, one polyphonic music note consists of two music notes with fundamental frequencies of F_0 and F_1, and a ratio between F_0 and F_1 of approximately 2:3。Then, this probably causes the non-exist pitch with fundamental frequency $F_0/2$ to be detected. In most polyphonic pitch estimation systems, the analyzed music signal must be first decomposed into different time-frequency components, which can be further organized into different sound sources according to some measurable cues, such as harmonic frequency relation and synchronous change. In this chapter, some related works in this field are reviewed, and the problems in polyphonic pitch estimation are discussed.

6.2 Reviews of Related Work

Most approaches to polyphonic pitch estimation are very complex. The approaches often consist of different phases, utilize different knowledge and combine different processing principles. Consequently, it is very difficult to classify theses approaches according to a single taxonomy. The following reviews are focused on some typical polyphonic pitch estimation methods. There are a number of polyphonic music transcription systems, which more or less utilize the human auditory model. Therefore, the reviews begin with the human auditory model.

6.2.1 Auditory Model of Pitch Perception

It is a long research history to understand how the human ear achieves a pitch perception of sound. An important goal of modern psychoacoustics research is to construct a human pitch perception model based on some known physiological and psychoacoustic knowledge. There are two different main theories of human pitch perception: the spectral theory and the temporal theory.

The spectral theory considers pitch perception to be pattern recognition processing of an acoustical signal. In the human auditory system, the cochlear is an important component that performs spectrum analysis as a frequency analyzer [Plomp64, Plomp68]. Sinusoid frequency components can be tracked by the spectral peaks in the sound spectrum. The human auditory system can use the position pattern of the relative spectral peaks to form a pitch perception by pattern recognition processing. Goldstein proposed an optimum processor theory [Gold73]. In this theory, a central processor is considered to be the recognizer of the spectral pattern provided by the auditory peripheral frequency analyser. A maximum likelihood statistical estimator determines which pitch best matches the spectral pattern of the analyzed acoustical signal. The theory can explain a wide range of auditory phenomena, such as the pitch of sounds that are missing a fundamental frequency, the percept of dichotic pitch.

Unlike the spectral theory, the temporal theory uses temporal processing to detect the periodicity in different cochlear channels. In the temporal theory, acoustical signal is first processed by the cochlear frequency analyzer; and then the periodicity is detected by the time-domain envelope of the output signal of every cochlear channel, instead of extracting the spectral peaks. There are several temporal theories that explain human pitch perception.

In [Meddis97], Meddis and O'Mard summarized a more general model: unitary model, which consists of four successive stages: 1) peripheral (mechanical) band-pass filtering, 2) half-wave rectification and low-pass filtering, 3) within-channel periodicity extraction, 4) across-channel aggregation of periodicity estimates. The final pitch estimation utilizes only the results of across-channel aggregation in stage 4. Figure 6.1 illustrates the system structure of the general model. Stages 1 and 2 model the function of the middle and inner ear, and stages 3 and 4 model the function of brain activity. The four stages can be described as follows:

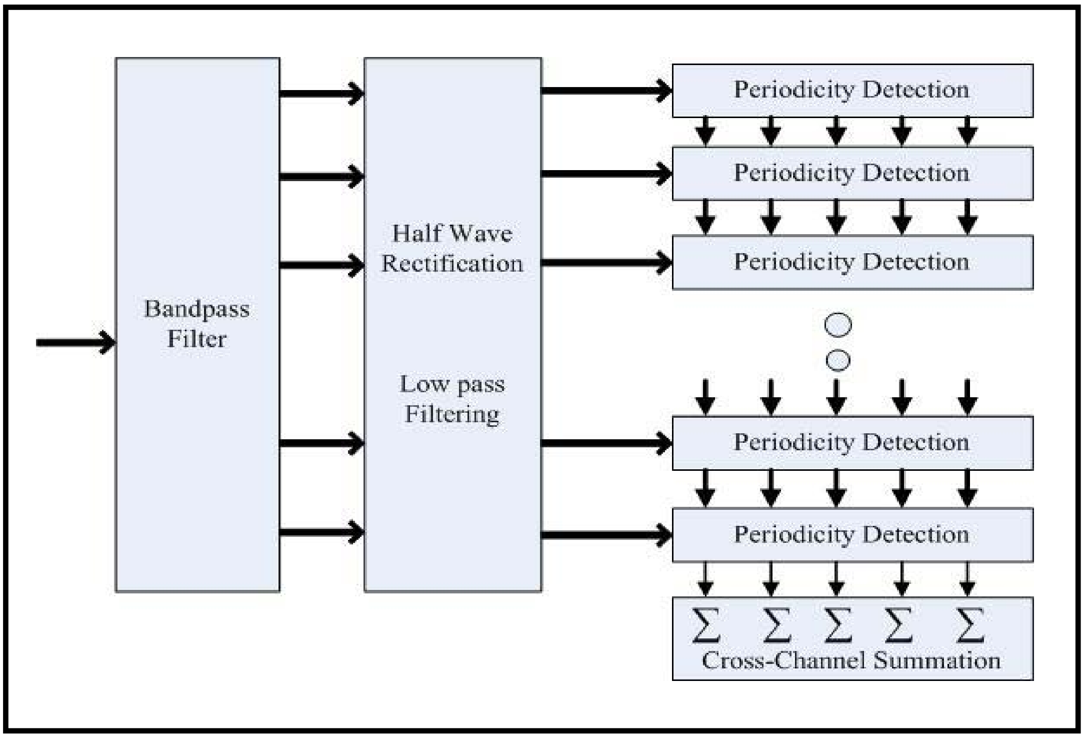

Figure 6.1: General Four-Stages Pitch Perception Model

1. A band-pass auditory filter bank is used to simulate the cochlear function and separates the input acoustical signal into tens of different frequency bands (or channels). The bands (or channels) are distributed approximately uniformly on a logarithmic frequency scale. The commonly-used band-pass filter is the gammatone filter, which was proposed by the Patterson [Patterson92, Slaney93].

2. The output signal at each cochlear channel is passed to the Meddis' model of hair cell transduction. In each cochlear channel, the hair cell model transforms the output signal into the firing probability of auditory nerve activity. The model is often implemented by compressing, half-wave rectification and low-pass filtering.

3. Within every cochlear channel, the short-time autocorrelation function (ACF) is used to detect the periodicity.

4. The ACFs across all cochlea channels are summed linearly to create a *summary autocorrelation function* (SACF). The maximum value of the SACF is typically used to determine the time delay (lag) that corresponds to the pitch period.

The model can explain a wide range of pitch perception phenomena. However the model computation cost is very expensive. Modified versions of this model are used in a number of practical music analysis systems.

6.2.2 Blackboard System

The blackboard system is a problem solving model, which is able to flexibly integrate knowledge from different sources. It was first introduced in the field of artificial intelligence. The first known blackboard system was developed to resolve problems of speech comprehension. A blackboard system frequently consists of three components: a blackboard, a set of knowledge sources (KSs), and a control mechanism. The blackboard is a global database in which data and hypothesis are stored. The global database is shared by all of the knowledge sources and is organized into different abstract levels. The knowledge sources are independent of each other. Their inner interaction is by means of the global database. The control mechanism decides when each knowledge sources is activated.

Martin proposed a polyphonic music transcription system to transcribe the four-voice piano music of Bach chorales. The system is based on the blackboard architecture and combines top-down and bottom-up processing. The STFT is used as the time-frequency processing front-end. The short-time running energy of the input signal is measured by the squaring and low-pass filtering of the signal. The salient rising energy-increasing information is used to track the onset and to segment the signal. In every segment, the magnitude output of the STFT is averaged over the segment and produces an average spectrum. The partials are tracked by peak-picking on the average spectrum. The list of the track from the time-frequency analysis is used as the input of blackboard system. Each track is associated with an onset time, frequency and magnitude. The blackboard workspace is organized into a hierarchy of five levels: Tracks, Partials, Notes, Intervals and Chords. The blackboard system includes thirteen knowledge sources, which can be categorized into three broad areas: garbage collection, knowledge from physics, and knowledge from the music practice. It is reported that the system can transcribe synthesized piano performances with some limitations. More detailed reviews of the blackboard system in music applications can be found in the reference [Bello03].

6.2.3 Machine-learning Methods

Recognizing a note in note-mixtures is a typical pattern recognition problem. This, it is rather intuitive and reasonable to transform the polyphonic pitch estimation to pattern recognition problem, which can be resolved by machine learning methods.

Marolt used neural networks to construct a polyphonic music transcription system for piano music [Marolt04]. The system is based on the combination of adaptive oscillators and neutral networks. The auditory model is considered to be the main part of time-frequency processing. In the system, the input signal is first separated into 200 different frequency channels by a gammatone auditory filter bank with logarithmically-spaced centre frequencies. Then the outputs of gammatone filter bank are further processed by Meddis's hair cell model. The human ear time-model assumes that the pitch perception comes from the periodicity detection of every frequency channel. The most common way to detect the periodicity is to use the autocorrelation. In the system, Marolt used the adaptive oscillators to track the partial in every frequency channel. Further, the network of the adaptive oscillators is used to track a group of harmonically relative partials. Finally, the neural network is used to recognize music notes. A combination of oscillators' network output and amplitude envelopes in every frequency channels are used as the input for the neural network. He compared the performance of the Different types of neural networks: multi-layer perceptrons (MLPs), radial basis function (RBF) networks, time-delay neural networks (TDNN), Elman's partially recurrent networks. It is reported that TDNN performs better than the other three types of neural networks. The system performance is evaluated by testing with synthetic and real piano music. It is reported that the system achieves a good performance on synthetic piano music, but a low performance on real piano music.

Pertusa and his colleagues proposed another polyphonic transcription system using the time-delay neural network [Pert03]. Their purpose was to determine if neural network fed only with a spectrogram can work well for the polyphonic transcription problem. In contrast to Marolt's system, Pertusa selected STFT as the basic time-frequency processing tool instead of the auditory filter bank. In Pertusa's system, the spectrum of 1024-point STFT is combined into the 94 frequency band in the logarithm scale. Then the 94-dimension spectrum is used as the input vector of a time-delay neural network, which is used to recognize music notes. The system is limited to recognizing musical notes only in mono-timbre polyphonic music. The training samples are selected from the different synthetic mono-timbre polyphonic notes, which are generated from MIDI files using a physical virtual synthesizer. It is reported that the system trained by a mono-timbre polyphonic music will perform better on the same timbre test examples than on the other timbre test examples. The system performance on real-music is not reported.

6.2.4 Iterative Methods

Klapuri proposed a polyphonic pitch estimation algorithm based on the iterative method [Klapuri03]. In this algorithm, first the predominant pitch of concurrent musical sound is estimated, and then the detected sound corresponding to the predominant pitch is removed from the mixture. The process is repeated iteratively on the residual signal. Figure 6.2 presents an overview of this polyphonic pitch estimation algorithm.

The acoustical input signal is first preprocessed to suppress the noise by a magnitude warping technology. In the predominant pitch estimation stage, the fundamental frequency of the most prominent sound is estimated in the mixture, where there is also some other harmonic sounds and noise. To find the predominant pitch, the preprocessed spectrum is first separated into 18 different frequency bands that are logarithmically spaced between 50Hz-6kHz. In every frequency band, a corresponding weight vector is calculated to represent the likelihood of a different pitch. The calculation of the weight vector is based mainly on the harmonic group principle that simultaneous harmonic-relative spectral components are grouped into a single sound source. The calculation also considers the inharmonic sounds, those in which the frequencies of the overtone partials *do* not occur in exact integer ratios.

Then, the bandwise likelihood vectors are combined to globally estimate the predominant pitch across the different frequency bands. In the next stage, the spectrum of the sound with the predominant pitch is estimated and subtracted from the mixture according to the spectral smoothness principle. The estimation and subtraction is repeated iteratively on the residual signal until there is evidence that all of the harmonic sounds have been detected. The algorithm has been tested on polyphonic mixtures with multiple timbres under different acoustic conditions, and performs very well.

Wan and his colleagues proposed another iterative method of polyphonic pitch estimation. In this method, the predominant pitch is first detected and, then, in the original analyzed signal, the detected sound is weakened, according its corresponding harmonic structure. The processing is repeated for the weakened residual signal. Figure 6.3 illustrates the main procedures of this algorithm. In this algorithm, only the half wave rectification is utilized to enhance the harmonic structures, instead of the complete auditory model processing. The input signal first is transformed into frequency spectrum by FFT, and then the spectrum is band pass filtered in the 50Hz-6000Hz range.

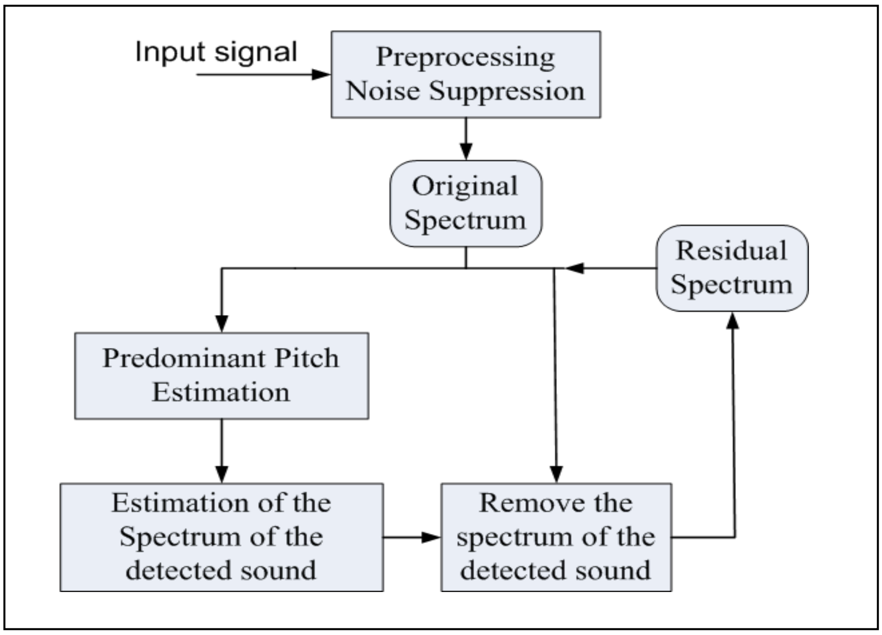

Figure 6.2: Overview of Klapuri's Iterative Method

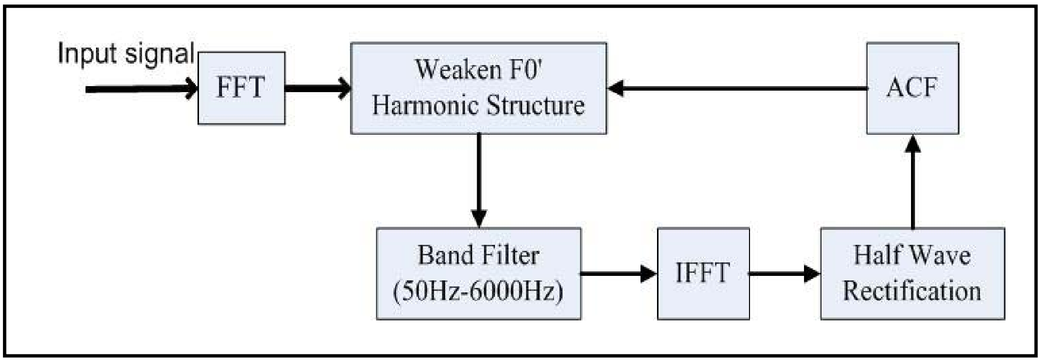

Figure 6.3: A Harmonic Enhancement Based Pitch Estimation Algorithm

By means of the IFFT, the band-limited signal is transformed into a time-domain signal, which is processed by half-wave rectification to enhance harmonic structures. This harmony-enhanced time-domain signal is used to extract the predominant pitch by an autocorrelation operation. To detect the multiple pitches, the corresponding harmonic structures of the predominant pitch will be weakened in the spectrum of the original signal and produce the residual signal. The residual signal is used to find the next possible predominant pitch by the same iterative processing. The number of iterations is controlled by various stop criteria, such as prior knowledge and psychoacoustic knowledge. Some results are reported with monophonic and polyphonic music samples.

6.2.5 Estimation Using Instrument Model

Yin and his colleagues proposed a polyphonic pitch estimation algorithm based on the instrument model [Yin05]. They used the instrument model to characterize the harmonic structure of different instruments to assist a stronger polyphonic pitch estimation. In their algorithm, the FFT is used to generate the amplitude spectrum of the instrument sample, and then the amplitude spectrum is separated into 88 semitone frequency bands. The middle frequency of each band consists of the fundamental frequencies of a western music note, and the bandwidth is a semitone. The amplitude spectrum bins in every frequency band are combined to generate the band energy spectrum Z[i], i=1,2,…88, (A0..C8) where the frequency band index i corresponds to the MIDI note number of a western music note. For music note i, Z[i] denotes the energy of the fundamental, and the energy of the lowest 16 harmonics partials lie in the Z[i], Z[i+12], Z[i+19],...Z[i+48]. The band energy spectrum 49 number vector Z[i…i+48] is considered to be the instrument model of a music note with pitch i (according to the MIDI note number). In the instrument model, it is assumed that the harmonic structure of the music note is the same, regardless of pitch. Based on this assumption, for a certain music instrument, only one 49 number vector I[0…48] can completely signify the harmonic structure of music notes with different pitches. For a music note with volume *a* and MIDI number *p*, the note's spectrum can be generated as:

$$F(I,a,p)=\begin{cases} a\cdot I[i-p] & i\in[p...p+48] \\ 0 & otherwise \end{cases}$$

Then, for a polyphonic music note with band energy spectrum Z_M, which is played by the instrument with instrument model I, the polyphonic pitch estimation is converted to resolve the following minimization problem:

$$Minimizing\ \left| Z_M-\sum_{i=1}^{n}F(I,a_i,p_i)y_i \right|^2$$

where n is the total number of the estimated notes, and ($a_{i,}$ p_i) denotes the volume and pitch .

The algorithm has been evaluated by only very limited several MIDI files, and they claim that music transcription performance can be improved by using the instrument model if the musical sounds have stable harmonic structures.

6.3 Problems in Polyphonic Pitch Estimation

Polyphonic pitch estimation of music signals is very challenging because of the wide pitch range and great variety of the spectral structures of different instruments' sounds. The sounds of most of musical instruments are more or less harmonic relative. For the ideal harmonic sound, the ratios of the frequencies of the harmonic components (partials) and fundamental frequency should be integers. The frequency ratios of harmonic components to fundamental often are not strictly integers, although nearly so. For example, the partial frequencies of a monophonic piano note can be expressed as follows:

$$f_n = nF\sqrt{1+\beta(n^2-1)} \quad (6.1)$$

where n denotes the index of partials, F is the fundamental, and β is the inharmonic factor, . As shown in the equation 6.1, the frequencies of the higher order partial exhibit a greater difference from the ideal harmonic position. Figure 6.4 illustrates the inharmonic spectral structure of a piano example.

The most difficult problem in the polyphonic pitch estimation is caused by coinciding harmonic components. In the most severe case, given two music notes with fundamental frequencies f_1=nf_2 and n is an integer, the harmonic components of the music note that has the higher fundamental frequency can be completely overlapped by another music note. Then, the frequency of the k^{th} harmonic component of the music note with fundamental frequency f_1 is equal to the frequency of the $(nk)^{th}$ harmonic component of another music note with fundamental frequency f_2. For a more general case, if two music notes with a fundamental frequency relation of:

$$f_2 = f_1\frac{n}{m}$$

where the m and n is integer, then the frequency of the p^{th} (p=nk) partial of the music note that has the fundamental frequency f_1 is equal to the frequency of the q^{th} (q=mk) harmonic component of the music note with fundamental frequency f_2.

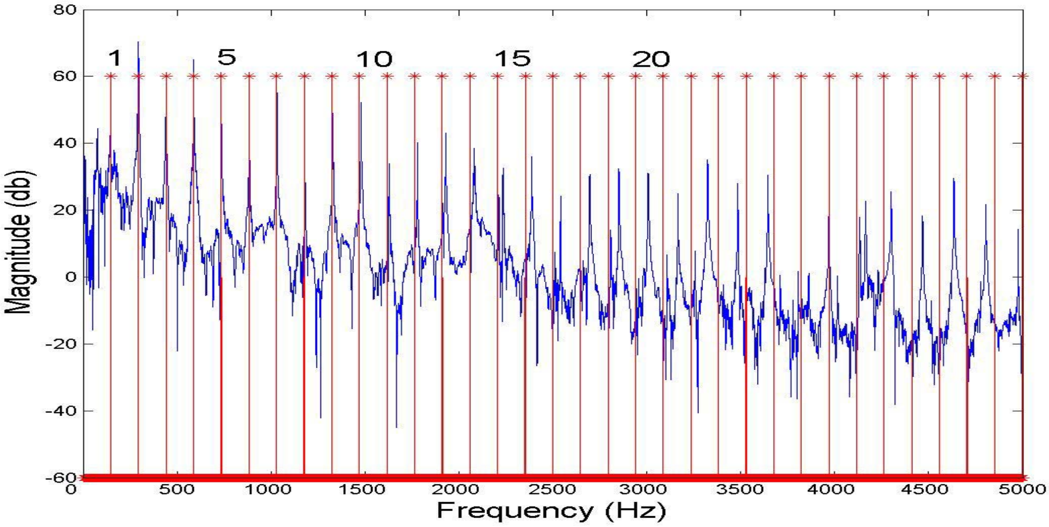

Figure 6.4 Inharmonic Spectral Structure of a Piano Note

This Figure shows the inharmonic Spectral Structure of a Piano Note Example with the fundamental frequency of 148 Hz. The red line denotes the ideal harmonic position. It can be viewed that the real frequencies of the 15th or higher order harmonic components are obviously deviate from the ideal harmonic position.

In common western music, the fundamental frequencies of the musical notes can be expressed as follows:

$$f_L = 440 \cdot 2^{\frac{L-69}{12}} \quad (6.2)$$

where L denotes the MIDI number according to the MIDI notation. The interval between the L^{th} and $(L+1)^{th}$ music note is equal to a semitone.

The fundamental frequency ratio of two musical notes is determined by their music interval. Table 6.1 illustrates the note intervals that can make the fundamental frequency ratio nearly equal to m/n and m and n are small integers.

Table 6.1 Small Integer Ratio and Note Interval

Note Interval	Small Integer Ratio	Deviation
3	6:5	-0.92%
4	5:4	+0.79%
5	4:3	+0.11%
7	3:2	-0.11%
12	2:1	0.00%
16	5:2	+0.79
19	3:1	-0.11%
28	5:1	+0.79%
31	6:1	-0.11%

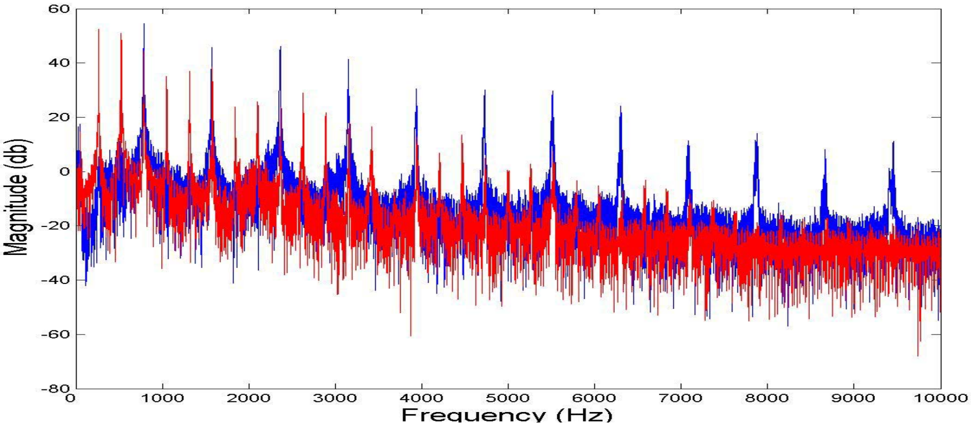

Figure 6.5 Coinciding Harmonic Components in Two Violin Notes

This Figure illustrates the spectral magnitude of the two violin music notes with fundamental frequencies 261.6 Hz and 784.0Hz. The blue line denotes the spectrum of the note with lower pitch and the red line denotes the other note. It is obviously viewed that harmonic components of the high pitch note are completely overlapped by the every third harmonic component of the low pitch note.

Figure 6.5 illustrates the magnitude spectrum of two violin music notes, in which the partials of the high pitch note are completely overlapped by the harmonic components of the other music note.

Chapter 7

A NEW POLYPHONIC PITCH ESTIMATION METHOD: METHOD I

Two new polyphonic pitch estimation methods have been proposed in this thesis. This chapter introduces the polyphonic pitch estimation method no. I. Method no. I performs a polyphonic pitch estimation based on the harmonic relation and spectral smoothing principle.

7.1 System Overview

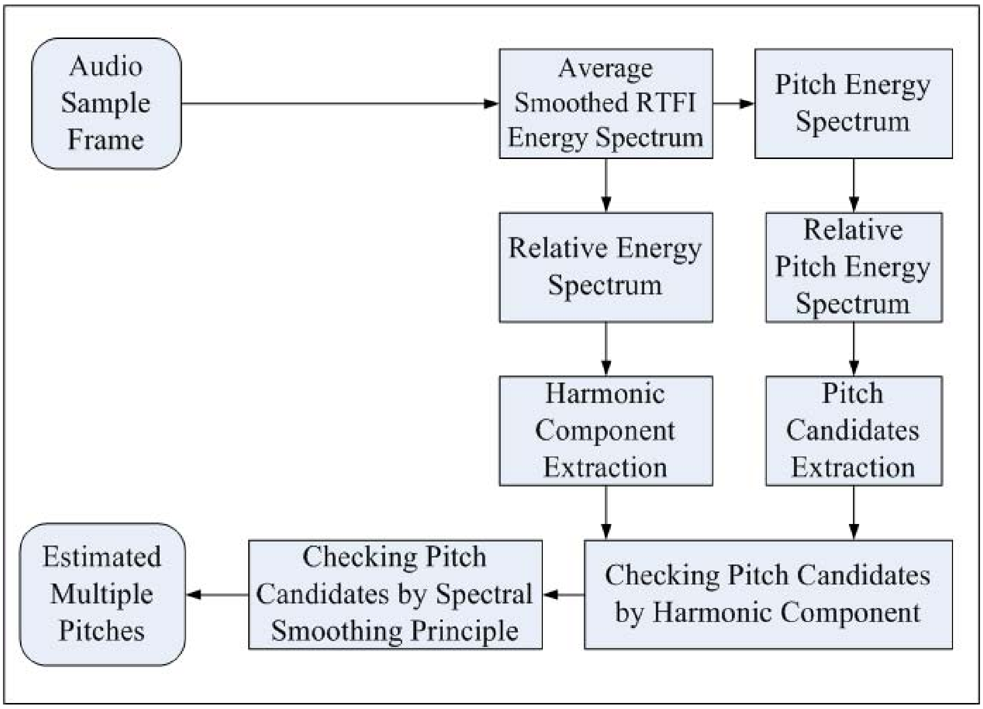
Audio Sample Frame
Average Smoothed RTFI Energy Spectrum
Pitch Energy Spectrum
Relative Energy Spectrum
Relative Pitch Energy Spectrum
Harmonic Component Extraction
Pitch Candidates Extraction
Estimated Multiple Pitches
Checking Pitch Candidates by Spectral Smoothing Principle
Checking Pitch Candidates by Harmonic Component

Figure 7.1 Overview of Proposed Polyphonic Pitch Estimation Algorithm I

Figure 7.1 illustrates the system overview of the proposed polyphonic pitch estimation method no. I. The method can be separated into five different steps:

1) Time-frequency processing based on the RTFI analysis

2) Transforming the input RTFI Energy Spectrum into the Relative Energy Spectrum, and extracting the harmonic components

3) Transforming the RTFI Energy Spectrum into the Relative Pitch Energy Spectrum and making a preliminary estimate of the possible multiple pitches.

4) Cancelling pitch candidates without enough confidence from the extracted harmonic components.

5) Judging the existence of the pitch candidate by the spectral smoothing principle.

7.2 Time-frequency Processing Based on the RTFI Analysis

In the first step of this method, RTFI is used to analyze the input music signal and produce a time-frequency energy spectrum. The input sample is a monaural music signal frame at a sampling rate of 44.1Hz. The frame length is not necessarily fixed. This is designed for a real polyphonic music transcription task, in which the frame length varies for different music notes. Discrete RTFI with constant-Q resolution is selected for the time-frequency analysis to produce the time-frequency energy spectrum. All 1250 filters are used. The middle frequencies are set in logarithm scale,. The centre frequency difference between two neighbouring filters is equal to 0.1 semitone and the analyzed frequency range is from 8Hz to 6.6 kHz. Then, the time-frequency energy spectrum is further averaged across the time domain in the input frame to obtain an average energy spectrum. This RTFI average energy spectrum is used as the only input vector for later processing in this polyphonic pitch estimation method. In the description of this method, the integer k is used to denote the frequency index in the logarithm scale, whereas f_k denotes the corresponding frequency value in Hz as follows:

$$f_k = 440 \cdot 2^{(k-690)/120} \quad (7.1)$$

One example for the input RTFI energy spectrum of a piano note is provided in the upper image in Figure 7.2.

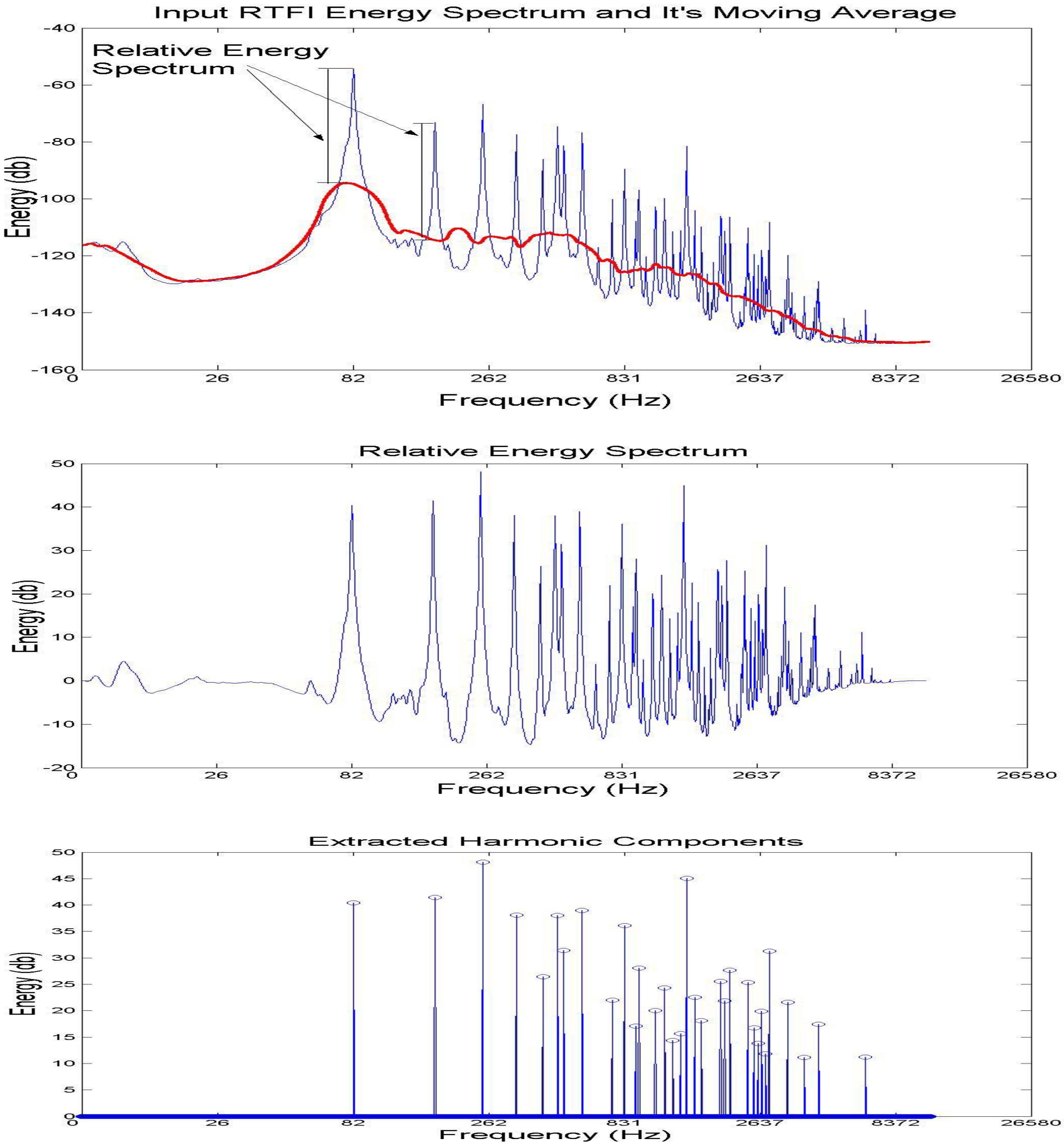

Figure 7.2 The Input RTFI Energy Spectrum, Relative Energy Spectrum and Extracted Harmonic Components of a piano polyphonic note consisting of two concurrent notes with fundamental frequencies 82 Hz and 466 Hz

7.3 Extracting Harmonic Components

In the second step, the input RTFI energy spectrum is first transformed to the relative energy spectrum (RES) according to the following expression:

$$RES(f_k) = RTFI(f_k) - \sum_{i=k-N/2}^{k+N/2} RTFI(f_i)\,, \quad \text{k=1,2,3,\ldots (7.2)}$$

where k denotes the frequency index in the logarithm scale, the second term in the right hand part of the equation denotes the moving average of the input RTFI energy spectrum, and N is the length of the window for calculating the moving average.. In the heuristic way, N is set to 30. As shown in the upper image in Figure 7.2, the red line denotes the moving average of the RTFI energy spectrum, and the relative energy spectrum RES(k) in fact is a relative measure of the energy spectrum for a frequency bin of k. This contrasts with the energy spectrum of a frequency range that is around the frequency bin of k. The middle image in Figure 7.2 illustrates the relative energy spectrum of a piano example.

The transformation from the original energy spectrum to a relative energy spectrum has been proven by experiments to be very useful for improving the method's performance. If there is a peak in the relative energy spectrum at the frequency index equal to k and the value RES(f_k) is more than a threshold *A1*, it is likely that there is a harmonic component at the frequency index k. The corresponding value RES(f_k) is assumed to be a measure of confidence of existence of the harmonic component. The third image in the Figure 7.2 shows the extracted harmonic components of the piano example.

7.4 Making Preliminary Estimation of Possible Multiple Pitches

In the third step, based on the harmonic grouping principle, the input RTFI energy spectrum is first transformed into the pitch energy spectrum (PES) and the relative pitch energy spectrum (RPES) as follows:

$$PES(f_k) = \sum_{i=1}^{L} RTFI(i \cdot f_k)\,, \quad \text{k=1,2,3,\ldots (7.3)}$$

$$RPES(f_k) = PES(f_k) - \sum_{i=k-N/2}^{k+N/2} PES(f_i) \text{ ,k=1,2,3,...}$$

Where the L is a parameter that denotes how many low harmonic components are together considered as important evidence for judging the existence of a possible pitch. The ideal parameter L and N value need to be set by the experiments on the tuning database. In the following reported test experiments, L and N are fixed at 4 and 50 respectively.

In practical implementations, instead of using the equation (7.3), the pitch energy spectrum can be easily approximated in the logarithm scale by the following calculation (here L is less than 10):

$$PES(f_k) = \sum_{i=1}^{L} RTFI(f_{k+A[i]}) \text{ ,}$$

$$A[10] = [1,120,190,240,279,310,337,360,380,399]$$

Table 7.1 Deviation between approximation and ideal values										
i	1	2	3	4	5	6	7	8	9	10
$f_{k+A[i]} / i \cdot f_k$	0%	0%	-0.11%	0%	0.21%	-0.11%	0.07%	0%	-0.23%	0.21%

As shown in Table 7.1, the deviation between the approximate and ideal values is negligible.

There are two assumptions made when making a preliminary estimate of the possible pitches from the relative pitch energy spectrum. If there is a pitch with fundamental frequency f_k, in the input sample, 1) there should be a peak around the frequency f_k in the relative pitch energy spectrum; 2) the peak value should be large enough and surpass a threshold *A2*. Both assumptions fit well for real music examples if a suitable threshold *A2* is selected.

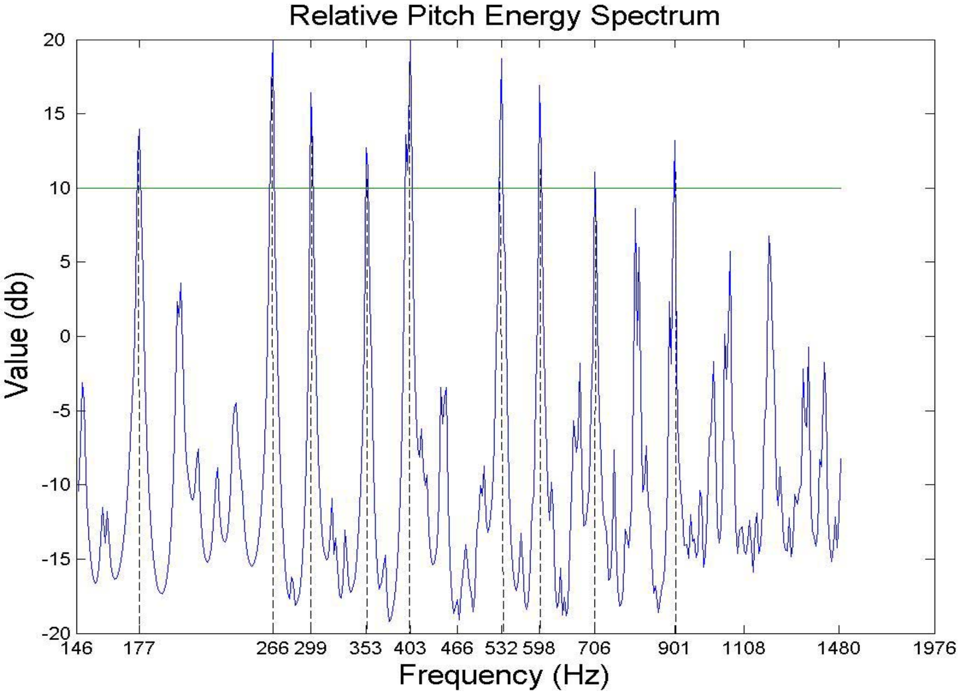

Figure 7.3 Relative Pitch Energy Spectrum of a violin example consisting of four concurrent notes with the fundamental frequencies 266Hz, 299Hz, 353Hz and 403Hz.

Figure 7.3 illustrates the relative pitch energy spectrum of a violin example, which consists of four concurrent notes with fundamental frequencies of 266Hz, 299Hz, 353Hz and 403Hz respectively. As shown in Figure 7.3, there are 9 pitch candidates that can be preliminarily estimated. when selecting the threshold *A2*= 10db, The fundamental frequencies of the 9 pitch candidates are 177 Hz, 266Hz, 299Hz, 353Hz, 403Hz, 532Hz, 598Hz, 796Hz and 901Hz. In this preliminary estimate, all 4 true pitches in the example have been correctly estimated. On the other hand, 5 extra pitches have been incorrectly estimated. The estimated extra pitches usually share many harmonic components with the true pitches. In this example, the estimated extra pitch of 177Hz is nearly half of the true pitch of 353 Hz. The extra pitches 532Hz, pitch 598Hz are nearly twice of the true pitch 266Hz, pitch 299Hz respectively; and the extra pitch 796Hz is nearly triple of the true pitch 266Hz. The extra pitch estimations are considered to be cancelled in the next two steps.

7.5 Cancelling Extra Pitches by Checking Harmonic Components

Throughout a great number of experiments, it has been noted that, in most real music instruments, the several lowest harmonic components of the music notes are strong and can be extracted reliably through the second step of this method. Only a very low music note may have a very faint first harmonic component that cannot be extracted reliably. Based on these observations, some assumptions can be made for judging whether there is a pitch using the extracted harmonic components. For example, in this method, there is the following assumption:

If there is a pitch with a fundamental frequency of more than 82 Hz, either the lowest three harmonic components, or the lowest three odd harmonic components of this pitch, should all be present in the extracted harmonic components. If there is a pitch with a fundamental frequency that is lower than 82 Hz, four of the lowest six harmonic components should be present in the extracted harmonic components.

In two typical cases, the extra estimated pitches can be cancelled based on the above assumption. In the first case, the extra pitch estimation is caused by the noise peak in the preliminary pitch estimation. In the second case, the harmonic components of an extra estimated pitch are partly overlapped by the harmonic components of the true pitches. In this case, the non-overlapped harmonic components become important clues to check the existence of the extra estimated pitch. For example, if a polyphonic note contains two concurrent music notes C5 and G5, the fundamental frequency ratio of the two notes is nearly 2:3. Then, it is probable that there is extra pitch estimation on the C4, because the C4's second, fourth, sixth,…harmonic components are overlapped by the C5' first, second, third,… harmonic components, and the C4's third, sixth, ninth,… harmonic components are nearly overlapped by the G5's first, second, third,…harmonic components. However the C4's first, fifth, seventh harmonic components are not overlapped, so the extra C4 estimation can be easily cancelled by checking the existence of the first harmonic component based on the above assumption.

7.6 Judging the Existence of the Pitch Candidate by the Spectral Smoothing Principle

Through the last several steps, the extra incorrect estimation focused on the pitches whose note intervals are 12, 19, and 24 semitones higher than the true pitches. In this case, the fundamental frequencies of these extra estimated pitches are 2, 3 or 4 times those of a true pitch and the harmonic components of each extra pitch are completely overlapped by a true pitch. For example, two of the estimated pitch candidates are the notes with fundamental frequencies f_l and $3f_{l.}$ Here the difficulty is to determine if the note with the fundamental frequency $3f_l$ really occurs or, in fact, is an incorrect extra estimation caused by the overlapped frequency components of the lower music note. This is the most difficult case in the polyphonic pitch estimation, and the problem can be well resolved by the spectral smoothing principle.

Here, the spectral smoothing principle refers to the fact that the corresponding harmonic spectral envelop of a real monophonic music note often gradually changes. In other words, the spectral value difference between two neighbouring harmonic components is small and random in most cases. However, when a music note with the fundamental frequency f_l is mixed with another note with the higher integer ratio fundamental frequency nf_1, then the corresponding harmonic spectral envelope often will not be smooth again and the spectral value of every nth harmonic component become obviously larger than the neighbouring harmonic components. Figure 7.4 illustrates the RTFI energy spectrum of the first 30 harmonic components of two piano music samples. The upper image presents the analysis results for the piano sample that contains only one music note with a fundamental frequency of 147 Hz. The lower image shows the result of analysis for the other piano sample that has two concurrent music notes with a fundamental frequency of 147 Hz and 440Hz ($\approx$3*147Hz). It is apparent that, in comparison to the upper image, the 3rd, 6th, 9th, …, harmonic components are strengthened and their spectral values are almost larger than the neighbouring harmonic components.

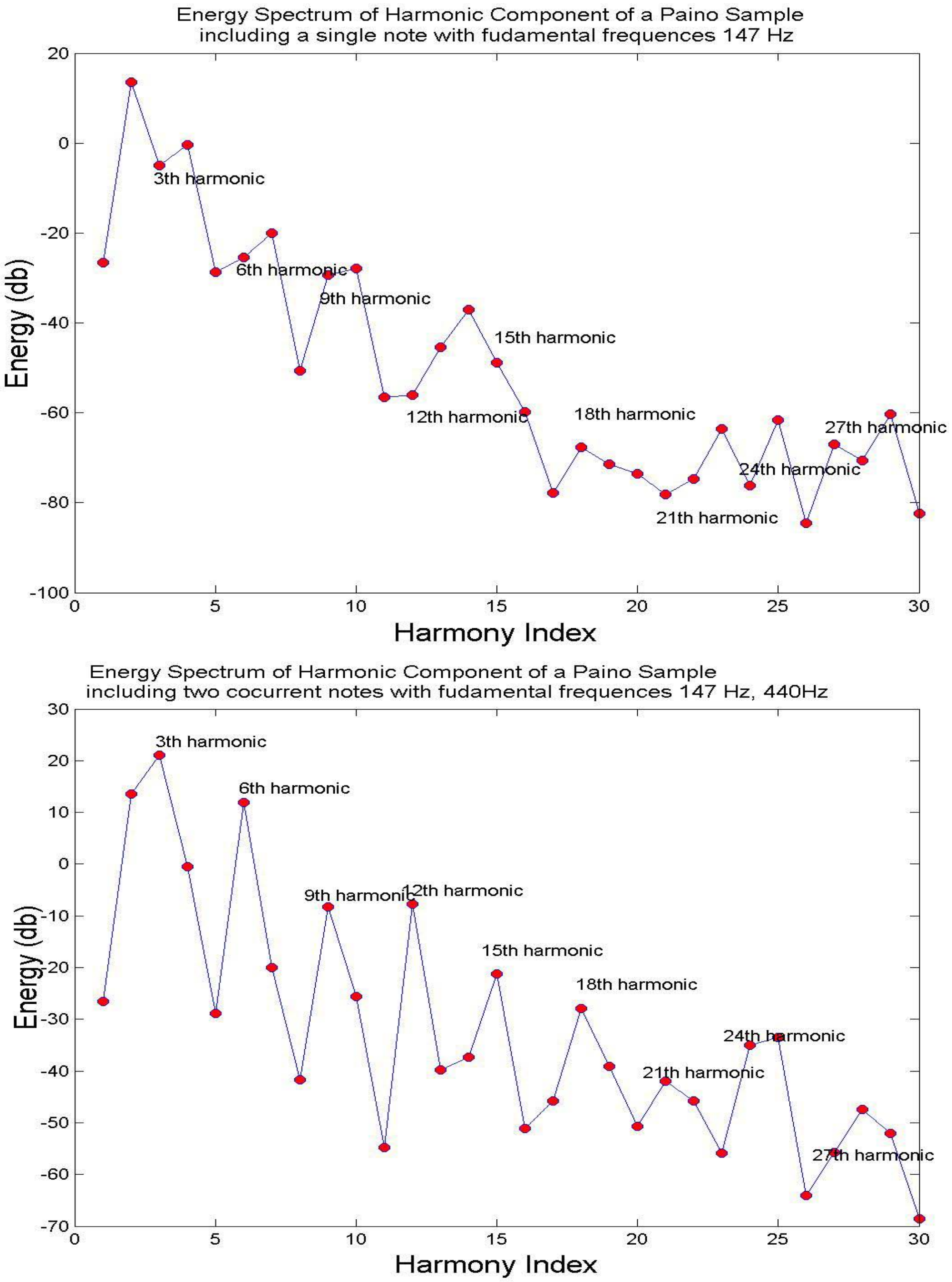

Figure 7.4: Harmonic Component Energy Spectrum of Two Piano Samples.

If there are two estimated pitch candidates that have fundamental frequencies of f_l and f_2 ($f_2 \approx nf_l$), and a frequency ratio that is approximately an integer n, then the proposed method has the following two steps to judge if the higher pitch with the fundamental f_2 occurs. Firstly, the energy spectrum of the first 10n corresponding harmonic components with the fundamental frequency f_l is calculated by an RTFI analysis with constant-band resolution.

As mentioned before, for the overall polyphonic estimation, the spectral analysis in the logarithm scale is reasonable and the constant-Q frequency resolution is better. However, for the corresponding harmonic spectral analysis of a certain known fundamental frequency, the constant-band frequency resolution is necessary because the harmonic components are equally spaced on the frequency axis. And the centre frequencies of the constant-band resolution RTFI analysis filter is set at f_l, $2f_l$, $3f_l$, ..., $(10n)f_l$.. The corresponding harmonic RTFI energy spectrum can be expressed as $RTFI_H(k)$, k=1, 2, 3,…,(10n), where k denotes the harmonic component index

Secondly, the Spectral Irregularity (SI) is calculated as follows:

$$SI(n) = \sum_{i=1}^{9} (RTFI_H(i \cdot n) - (\frac{RTFI_H(i \cdot n - 1) + RTFI_H(i \cdot n + 1)}{2}))$$

As indicated before, if two of the estimated pitch candidates have the fundamental frequencies, f_l and f_2 ($f_2 \approx nf_l$) and if the higher pitch does not occur, then the SI(n) is often smaller, according to the spectral smoothing principle. On the other hand, if the higher pitch does occur, then the overlapped harmonic components are often strengthened so that the SI(n) has the larger value. So, in the proposed method, when the SI(n) is smaller than a threshold, the overlapped higher pitch candidate is cancelled. The threshold is determined by experiments. In practical examples, most incorrect extra estimations caused by overlapping harmonic components are 2, 3, or 4 times the true pitches. Consequently, the proposed method only consider cases in which two pitch candidates have fundamental ratio at the 2,3 and 4.

Chapter 8

A NEW POLYPHONIC PITCH ESTIMATION METHOD COMBINING SVM AND SIGNAL PROCESSING: METHOD II

The second proposed polyphonic pitch estimation method is based on machine learning. The basic idea is to consider the polyphonic pitch estimation as a pattern recognition problem.

8.1 System Overview

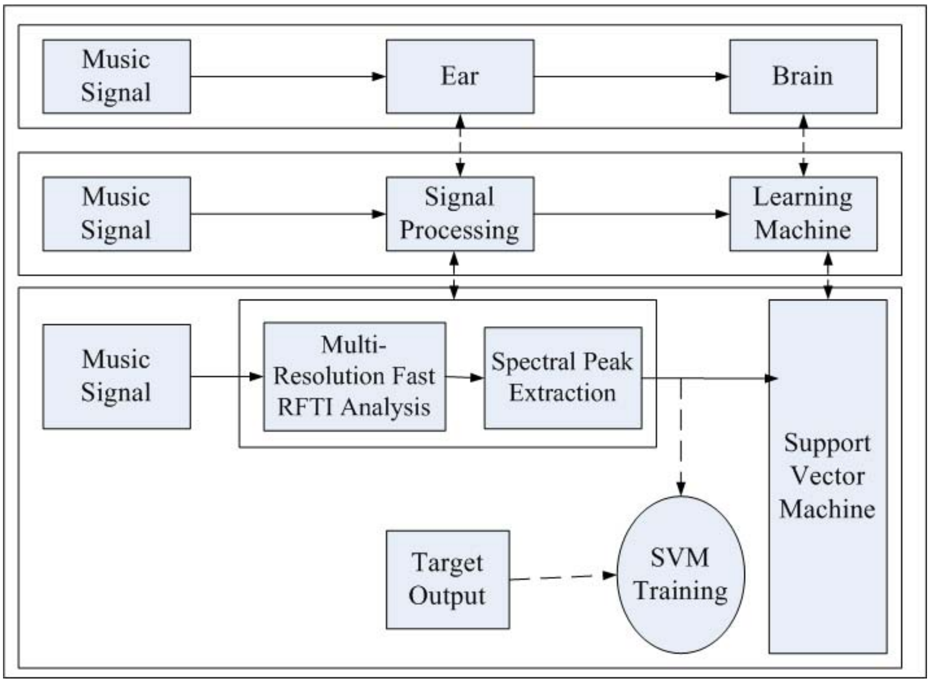

Figure 8.1 System Architecture of Proposed Polyphonic Pitch Estimation II

The proposed estimation method is composed mainly by a signal processing block followed by a learning machine. Compared to the human listening system, the signal processing stage is a time-frequency signal analysis tool that is similar to a cochlear filter, whereas the learning machine plays a role similar to one of the human brains. A multi-resolution, fast RTFI is used as signal processing component, and a support vector machine (SVM) is selected as an intelligent agent. Figure 8.1 shows the main system block diagram. Firstly, the music signal is processed to produce the average energy spectrum by a multi-resolution fast RTFI analysis (as introduced in Chapter 4, Section 3) on the logarithm scale. Finally, the peaks are picked from the average energy spectrum to produce the input vector to the SVM. In the training phase, the extracted peaks are used with the target output to produce the SVM polyphonic estimator. In the application phase, the SVM polyphonic estimator uses the peaks vector to perform multiple pitch tracking. The SVM polyphonic estimator consists of 88 two-class classifiers for 88 notes (piano extension from A0 to C8). Each two-class SVM classifier recognizes whether an input sample includes the corresponding note or not; and can also output the probability that every music note can occur in the input sample.

8.2 Motivation for Selecting SVM Instead of Neural Network

For the uses for which the machine type, SVM has been chosen, as it provides several important advantages. Firstly, SVM is based on Structural Risk Minimization (SRM) and provides the theoretical support and related tools to control the ability of generalization, whereas a neural network design often depends on heuristics and easily leads to an overfitting problem. Secondly, SVM can achieve a global solution, whereas the neural network can only converge on a local solution. Finally the input vector is composed by the extracted spectrum peaks that only exist in some frequency bins with the result that the input vector is sparse and high dimensional, SVM can process such sparse input vector very efficiently. In our experiments, the input vector size was up to 960 and the SVM still worked well. This property is very useful. On the contrary, neural networks with hidden layers training are very time consuming for high dimensional input vectors.

In practice, the LIBSVM [Chang01] software has been used as a major tool for SVM training. To train a SVM classifier, it is first necessary to select a kernel function. The library provides linear kernel, RBF kernel, sigmoid kernel and polynomial kernel. Indeed the linear kernel is a special case of RBF kernel [Hsu], sigmoid kernel is not test under some conditions [Cortes95], and polynomial kernel classifier needs too long a training time for such a high-dimension classification problem; RBF has therefore been chosen as the kernel function.

8.3 Input Vectors and SVM Training

Every input sample is pre-processed to a normal amplitude. The normal input sample is first processed by the multi-resolution fast RTFI analysis, and then the peaks are extracted from the outputted RTFI energy spectrum. Every peak value is added by a 200 db, and the spectrum values at the frequency bins without peak are set to zeros. Because the spectral peak only exists in limited frequency positions, the spectral peak vectors are sparse vectors. The vector size is 960 frequency bins and the analyzed frequency range is from 27 Hz to 6.6 KHz. Figure 8.2 illustrates the input spectral peak vector that is extracted from the RTFI energy spectrum of a polyphonic violin example with four concurrent notes.

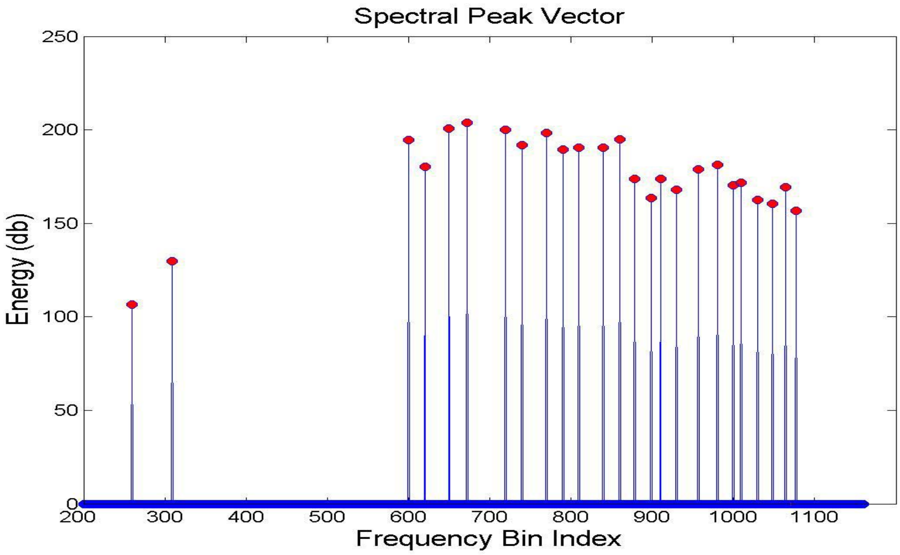

Figure 8.2 illustrates a SVM input spectral peak vector. The input vector is extracted peaks from a polyphonic violin sample, comprising of four concurrent notes with the note number 60,62,65,67 in MIDI notation. The frequency is in the logarithm scale. And the frequency distance between two neighbour frequency bins is 0.1 semitone. The analysis frequency range is from 27 Hz(20th semitone) to 6.6 kHz (116th semitone). According to the frequency bin index, the first several corresponding harmonic components of Note 60 is at the 600th, 720th, 790th, … frequency bin; as shown in the image, the spectral peaks do exist in these frequency bins. The spectral peaks at the first several harmonic components of the other 3 notes also can be viewed in the image. It also can be viewed that values on the most of the frequency bins are zeros, so it is a sparse vector.

Figure 8.3 illustrates the detailed structure of the SVM polyphonic estimator, and its input vector and output. As shown in Figure 8.3, the SVM polyphonic estimator consists of 88 two-classifiers, each of which is responsible for recognizing a certain single note. All note recognizers uses the same input vector, but the output of each note recognizer is determined by the input sample. For example, if the input sample contains four concurrent music notes - A3, B3, C3, G3 - the ideal outputs of these note recognizers would be that the outputs of the A3, B3,C3,and G3 note are ‘Yes’ and the outputs of all other note recognizers are ‘No.’ Every note recognizer should also be able to output the probability that the corresponding note occurs.

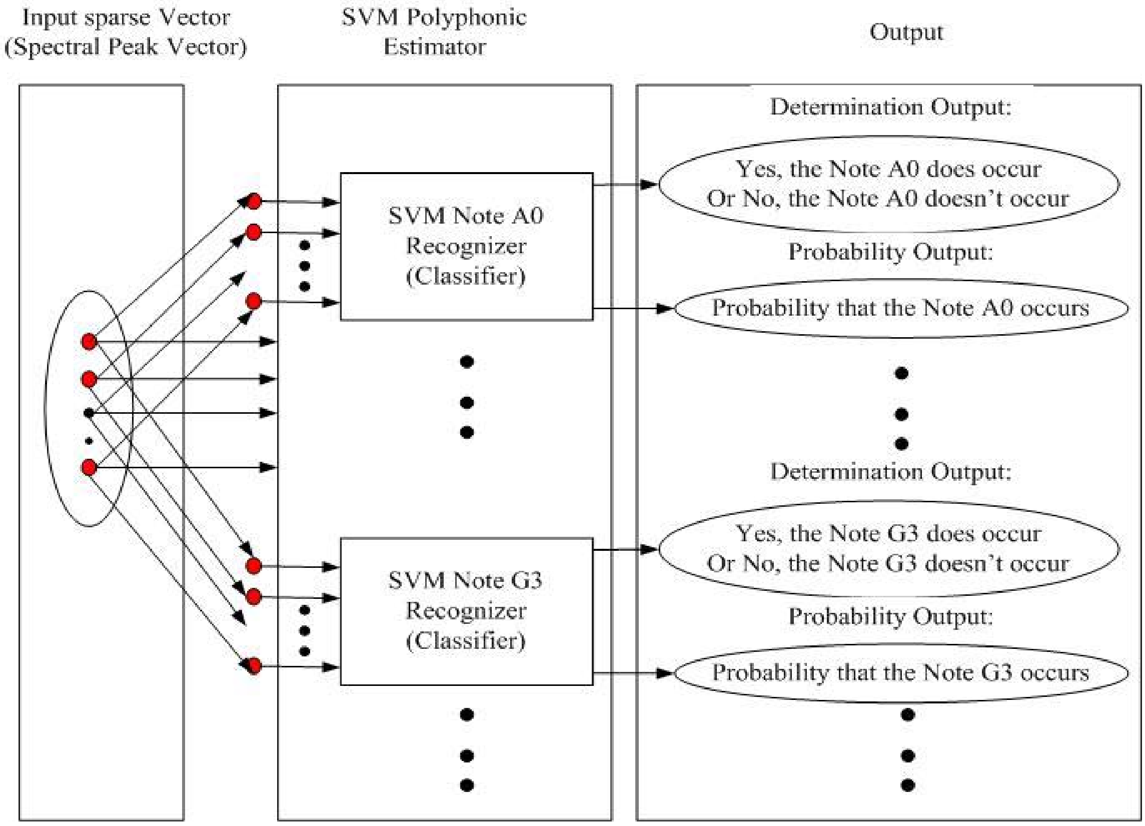

Figure 8.3 SVM Polyphonic Estimator

In the training phase, every note recognizer is trained independently, but the input spectral vectors can be re-used by all of the note recognizers. This also reduces the difficulty in preparing a great number of training samples. Figure 8.4 illustrates several training examples of two note recognizers. For details about the training database, refer to section 9.2 of Chapter 9.

```
9 training examples for Note Recognizer C4 and E4:
Training Examples for Note Recognizer C4:
1, -1  199:175   248:159   287:148   319:166   346:159   390:143  408:143  ...
2, -1  208:182   258:162   297:155   328:154   355:152  379:136  418:138 ...
3, -1  269:157   340:146   389:171   427:148   459:165   486:159   509:170 ...
4, -1  110:98  230:105  327:125   440:181   540:172   560:176   631:172 ...
5, -1  69:130   189:175   259:165   309:154   348:165   380:164   405:149 ...
6, -1  103:108   199:156   299:149   357:155   370:156   389:179   418:165 ...
7, -1  334:119   508:134  635:141  681:151   712:150   751:187   800:186   ...
8, -1  279:179   349:177   399:155   497:148  520:154   541:148   583:171  ...
9, 1  109:111    490:172    519:175   589:163  610:167  680:147   692:142 ...

Training Examples for Note Recognizer E4:
1, -1  199:175   248:159   287:148   319:166   346:159   390:143  408:143  ...
2, -1  208:182   258:162   297:155   328:154   355:152  379:136  418:138 ...
3, -1  269:157   340:146   389:171   427:148   459:165   486:159   509:170 ...
4, 1  110:98  230:105  327:125   440:181   540:172   560:176   631:172 ...
5, -1  69:130   189:175   259:165   309:154   348:165   380:164   405:149 ...
6, -1  103:108   199:156   299:149   357:155   370:156   389:179   418:165 ...
7, -1  334:119   508:134  635:141  681:151   712:150   751:187   800:186   ...
8, -1  279:179   349:177   399:155   497:148  520:154   541:148   583:171  ...
9, -1  109:111    490:172    519:175   589:163  610:167  680:147   692:142 ...
```

* The every row denotes an input sparse vector, only the first several peak values are displayed because of the limited space. The red digit denotes the target output, 1 denotes the certain note occurs in the input sample. The green digit denotes the vector index of the input peak vector. And black digit following the vector index denotes the spectral peak value in the vector index. The value of vector index not listed in the row is zero.

* It can be viewed in fact that the input peak vectors of the training examples are same for all the note recognizer. The difference is that the target values are different for different note recognizer.

Figure 8.4, Training Examples of Two Note Recognizers

When using the RBF kernel, two parameters, *C* and γ, specify the function. *C* is the penalty parameter of the error term and γ is the RBF kernel parameter([Cortes95]). An optimal *(c, γ)* is needed to make the classifier perform well on unknown new samples. This is achieved by grid-search using crossing validation. First, I try several *(c, γ)* pairs and pick the pair, with which the trained classifier has the best crossing-validation accuracy. Hundreds of classifiers have to be trained and every classifier has more than 100,000 training samples. So, it is impossible to run an extensive grid-search to find *(c, γ)*. A subset is selected from the training samples, and this subset is used to find the good *(c, γ)* by grid-search and crossing-validation. Then, the parameter pair *(c, γ) that* is selected will be used to train the classifier on the complete training set.

Chapter 9

EXPERIMENTAL RESULTS OF POLYPHONIC PITCH ESTIMATION METHODS

9.1 Performance Evaluation Criteria

Four criteria are used to evaluate the performance of the proposed polyphonic pitch estimation methods. These criteria are note precision (NP), note recall (NR), note f-measure (NM), and chord error rate (CER). The estimated fundamental frequencies must be compared to the reference fundamental frequency labels. A given reference fundamental frequency is considered to be a correct estimation (CE), if the estimation has an error of no more than 3% (0.5 semitone) from the reference fundamental frequency. If not, it is a false negative (FN) and any estimation that deviates by more than 3% from the reference fundamental frequency is considered to be a false positive (FP). The performance measurements for the polyphonic pitch estimation method, note precision, note recall, and note F-measure can be defined as follows:

Precision=Nce/(Nce+Nfp),

Recall= Nce/(Nce+Nfn),

F-measure= 2*P*R/(P+R)

where the Nce, Nfp, and Nfn denote the total number of correct estimations, false positive and false negative. Chord precision (CP) is defined as the percentage of the sound mixture where no pitch class identification error occurs.

Additionally, another performance measure, Note Error Rate (NER), is also used for the comparison with the Klapuri’s estimation methods. The NER is defined as the sum of the fundamental frequency estimation errors divided by the number of the fundamental frequencies in the reference estimation. The errors can be classified as three different types: substitution errors, deletion errors and insertion errors. If the number of estimated fundamental frequencies is smaller than the number of fundamental frequencies in the reference, then the difference is considered to be the number of the delete errors. If the number of estimated fundamental frequencies is greater than the number of the fundamental frequencies in the reference, the difference is considered to be the number of insertion errors. The substitution errors are defined as the errors in which a given F0 is detected, but the estimated value differs by more than 3% from the reference.

9.2 Training/Tuning Database and Test Database

The proposed method II is to perform the polyphonic pitch estimation by machine learning, which requires a lot of training samples. However, it is difficult to record thousands and thousands of polyphonic samples from different musical instruments and label their polyphony content. The music synthesizer can conveniently provide training samples with known polyphonic content, but is not ideal because the timbre of the synthetic and real music samples differ greatly. A good way is to produce the polyphonic samples by mixing real recorded monophonic samples of different music instruments. In these experiments, two different monophonic sample sets are used to create the training and test sample database. As shown in Figure 9.1, the monophonic sample set I consists of a total of 755 monophonic samples from 19 different instruments, such as piano, guitar, winds, strings, and brass, etc. Every monophonic sample is pre-processed to normal amplitude and fades into a one second duration time. The high number of polyphonic samples can be generated by randomly mixing these different monophonic samples. For example, the number of possible different 3-note polyphonic samples is more than 7 million by mixing these monophonic samples. The number of possible generated 4-note polyphonic samples is more than 610 million. Based on the monophonic sample set I, a total of 150,000 polyphonic samples with the polyphony from two to six note mixtures are generated for training database. The training database is used to train the SVM polyphonic estimator. The monophonic sample set I is also used to generate the polyphonic samples which are used to tune the parameters in the proposed polyphonic estimation method I.

In practical applications, tested polyphonic samples can be considered to be mixtures of monophonic samples, which are probably played by different performers and instruments from different instrument manufacturers. As shown in Figure 9.1, in order to obtain fairer evaluation results of practical cases, another monophonic sample set II is used to generate the Test Database I (Polyphonic Mixtures) in the same way in which the training database has been produced from the monophonic sample set I. The monophonic samples in set I and set II are different. Compared to set I, the set II has some samples for instrument types that are not present in set I. The monophonic samples for the same type of instrument in set II are played by different performers and instruments from different instrument manufacturers. Set II includes 23 different instrument types, a total of 690 monophonic samples in the five octave pitch range of 48 Hz to 1500 Hz. The Test Database 1 is used for performance evaluation of both proposed estimation methods. All the monophonic samples in sets I and set II are selected from the RWC instrument sound database.

The Test Database 2 consists of six real-life music excerpts, most of which are selected from a RWC generic database. The detailed information about the Test Database 2 is listed in Table 5.1. The sound of the drum has not been considered for transcription, but is permitted to be present in the analyzed music signal.

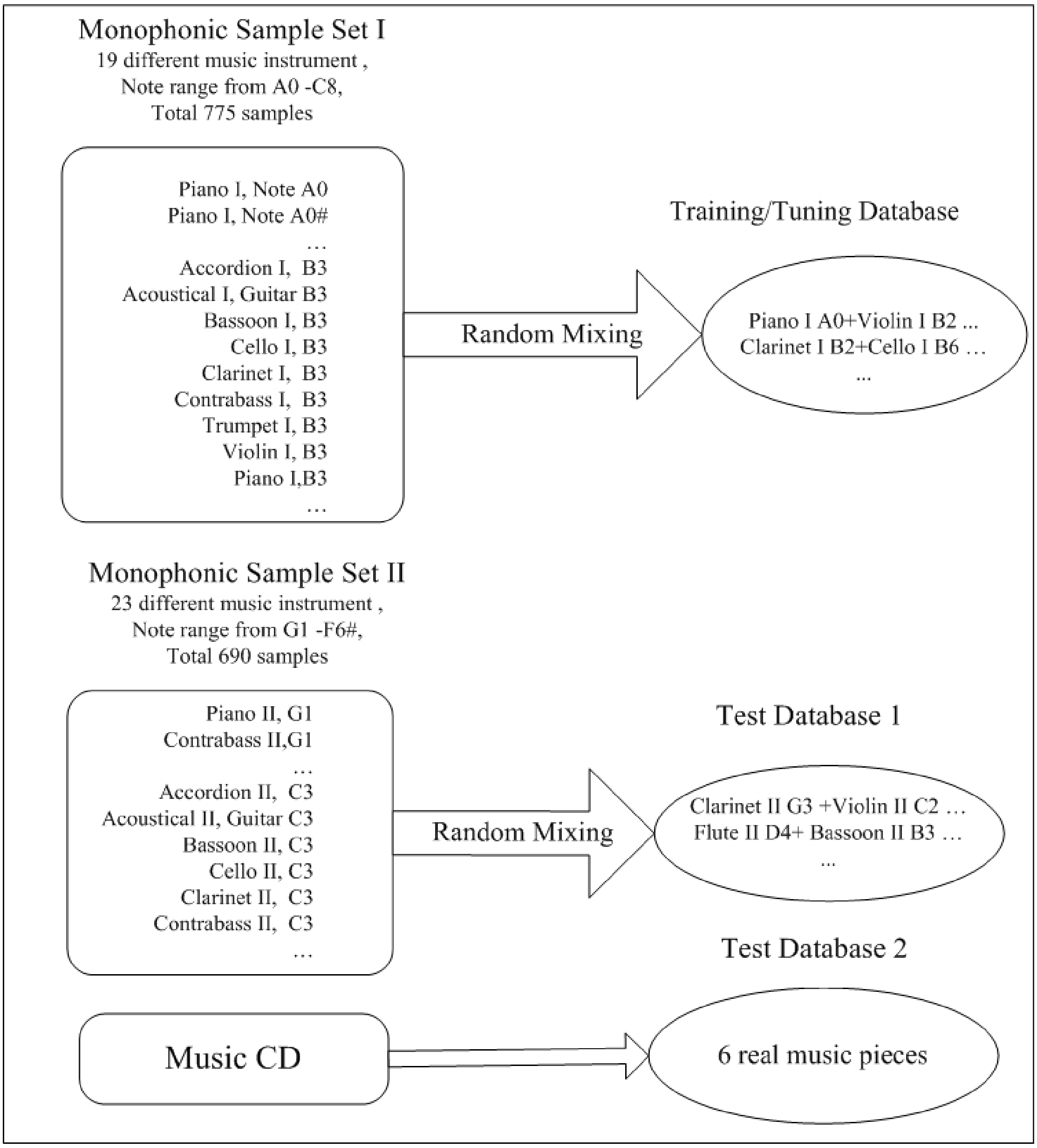

Figure 9.1: Training/Tuning Database and Test Database

Table 9.1 Test Database 2-(Real Music Excerpts from Music CDs)

#	Title	Reference	Instrument	Duration Time
1	Chuggin	RWC-MDB-G2001 No 32	Jazz, Piano, Bass , Drums	20s
2	Beethoven, <Egmont> Overture, op.84	RWC-MDB-G2001 No 50	Orchestral, Violin, Viola, Clarinet, Contrabass, Trombone, oboe, etc	50s
3	Mozart, Rondo in D major, K.485	RWC-MDB-G2001 No 59	Solo, Piano	30s
4	Haydn, String Quartet no.77 in C major	RWC-MDB-G2001 No 60	Chamber, Violin, Viola, Bass	50s
5	Tchaikovsky, String Quartet no.1 in D major	RWC-MDB-G2001 No 61	Chamber, Violin, Viola, Cello	30s
6	Beethoven, Piano Sonata No 26 in E-flat major	Commercial CD	Solo, Piano	50s

9.3 Test Results on the Test Database 1 (Polyphonic Mixtures)

9.3.1 Test Results of Method I on Polyphonic Mixtures

Figure 9.2-9.6 show the estimation performance (F-measure, Recall, Precision, Note Error Rate (NER), Chord Error Rate) of method I in case of different pink noise levels. The pink noise is generated in the frequency range of 50 Hz to 10K Hz. The Signal-to-Noise refers to the ratio between the clean input sample signal and the added pink noise. In general, method I is robust, even in cases of severe noise levels. The tested samples are classified into five different sample subsets according to the polyphony number of the polyphonic samples. For example, in Figure 9.2, the F-measure corresponding to the polyphony number 2 denotes the F-measure value estimated on the sample subset, in which every polyphonic sample consists of a two-note mixture. In this test experiment, 100 test examples are randomly selected from the Test Database 1 for every sample subset. Depending on applications, better Precision (percentage of the transcribed notes that are correct) or better Recall (percentage of all the notes that are found) is preferred for a polyphonic pitch estimation method. For example, in some music transcription systems, the extra notes in the result are very harmful, so better Precision is preferred. However, if the output result will be used for further improvement with the combination of some higher level knowledge, better Recall is preferred. In method I, if the parameter set is tuned for larger values, then the estimation performance will have better Precision. Otherwise, the estimation performance will have better Recall. Figure 9.7 shows the estimation performance (F-measure, Recall, Precision) of method I with two different parameter sets. Comparing the left image (with a smaller parameter value) to the right image (with the larger parameter value) in Figure 9.7, the corresponding estimation Precision shown in the right image becomes better in price of the lower Recall. In general, the total estimation performance, F-measure, is reduced by increasing the polyphony number of the estimated polyphonic sample. It can also be noted in Figure 9.7 that the estimation of Recall is greatly reduced in cases where the polyphony number is increased. On the other hand, the precision is gradually changed. Similarly, Figure 9.8 shows the estimation of Note Error Rate (NER) of method I with two different parameter sets. It is clearly evident that, when the larger parameter value is selected, the insertion errors are reduced for the estimated polyphonic sample with a low polyphony number, in price of the total increased deletion errors

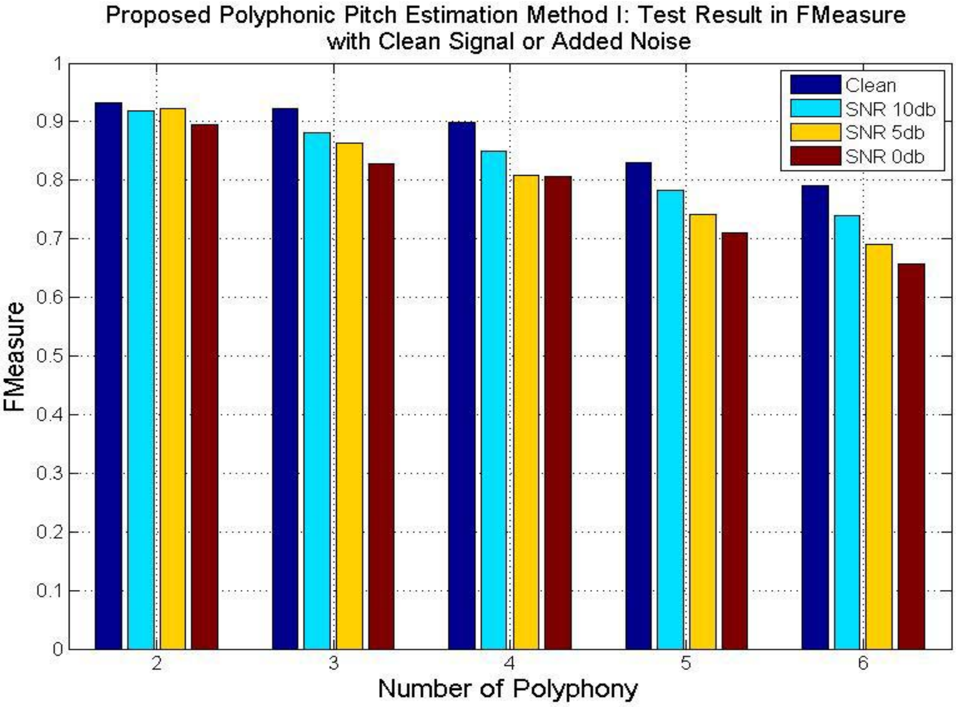

Figure 9.2, FMeasure of Test Results of Method I with Clean signal or Added Noise

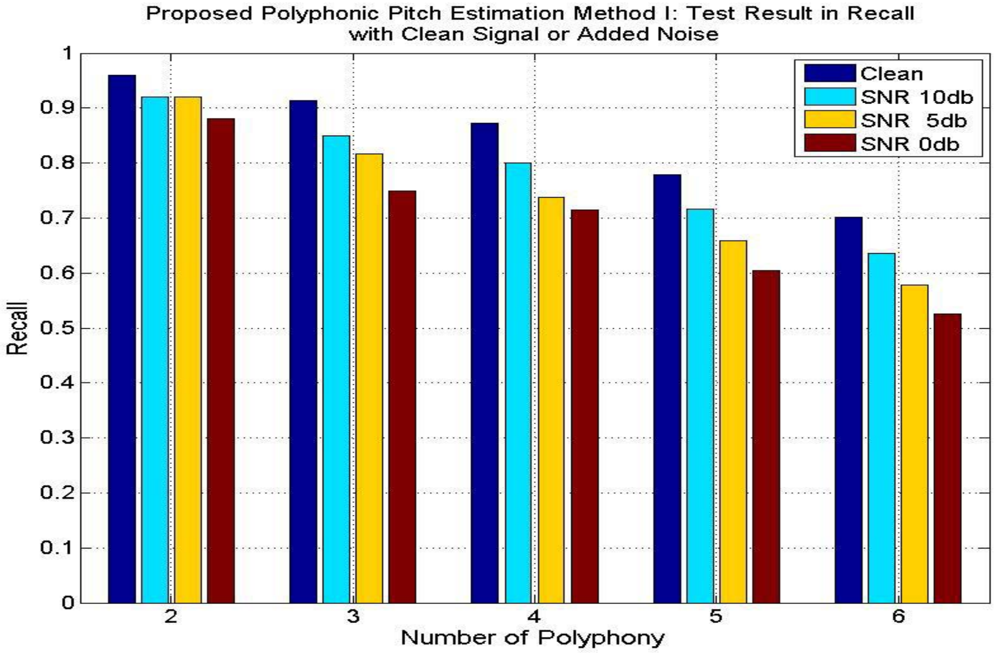

Figure 9.3, Recall of Test Results of Method I with Clean signal or Added Noise

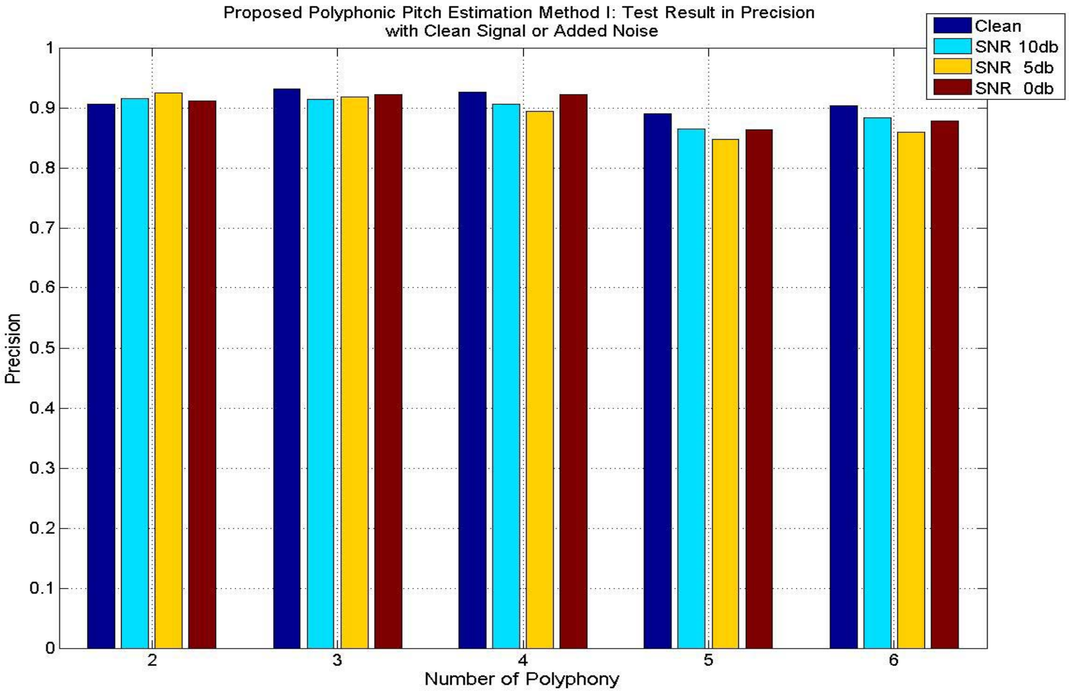

Figure 9.4, Precision of Test Results of Method I with Clean signal or Added Noise

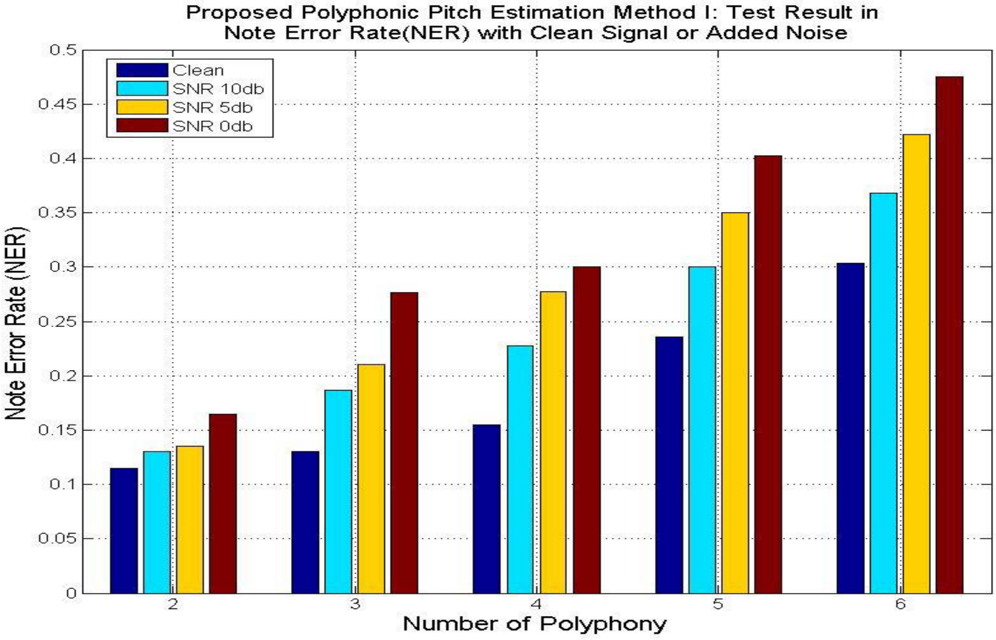

Figure 9.5, Note Error Rat (NER) of Test Results of Method I with Clean signal or Added Noise

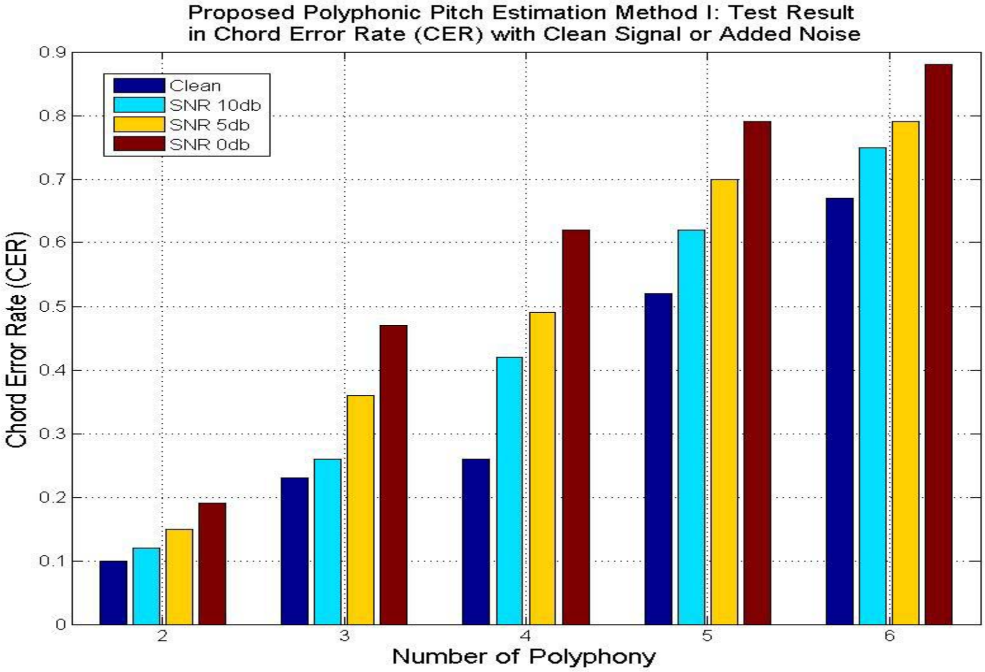

Figure 9.6, Chord Error Rate (NER) of Test Results of Method I with Clean signal or Added Noise

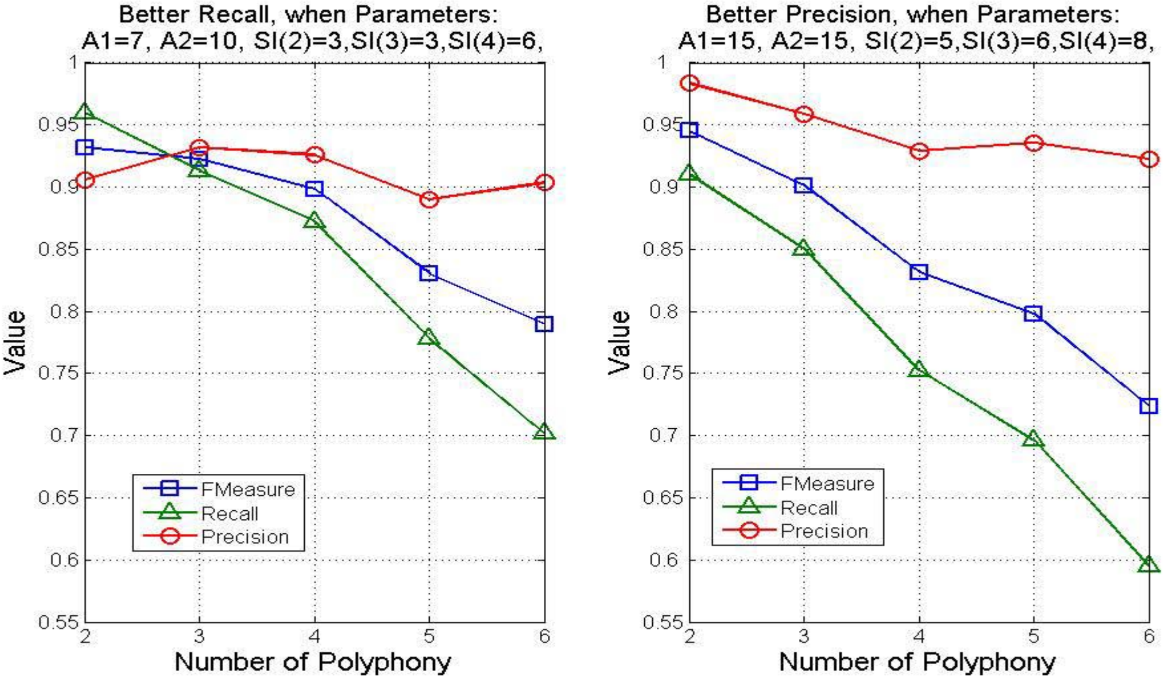

Figure 9.7, FMeasure, Recall and Precision of Test Result of Method I with different parameter values

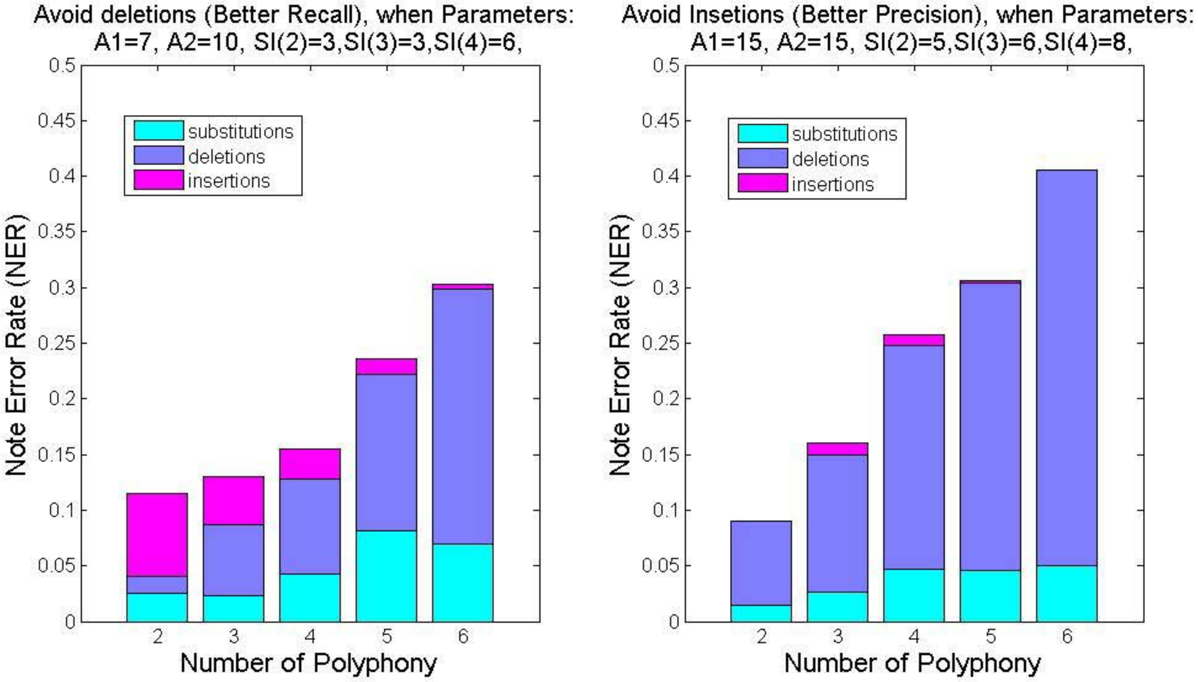

Figure 9.8, Note Error Rate (NER) of Test Result of Method I with different parameter values

9.3.2 Test Results of Method II on Polyphonic Mixtures

Figure 9.9-9.13 show the estimation performance (F-measure, Recall, Precision, Note Error Rate (NER), Chord Error Rate) of method II in cases of different pink noise levels. In this test experiment, 2000 test examples are randomly selected from Test Database 1 for every polyphony sample subset.

As indicated earlier, the polyphonic SVM estimator can also have a probability output; which can be used to achieve a trade-off between the Recall and Precision of estimation performance. When the probability outputs have been estimated, a probability threshold P can be selected. If the estimated probability of a certain note 's occurrence is greater than the threshold P, then the note is assumed to exist in the input sample. Otherwise, the note is not assumed to exist in the input sample; with a higher threshold P. The estimated results can provide better precision than increasing the missing notes (reducing the recall). Figure 9.14 shows the estimation performance F-Measure, Recall and Precision, when the estimation method selects the different probability threshold P; with the higher probability threshold (P=0.8, in the right sub-image in Figure 9.14), the method's estimation Precisions are improved and the Recalls are reduced, compared to the estimation performance of the method with the lower probability threshold (P=0.5, in the left sub-image of Figure 9.14). The similar phenomena also can be clearly seen in Figure 9.15, which shows the estimation performance in Note Error Rate. When the method selects a higher probability threshold (P=0.8, in the right sub-image), the insertion errors are reduced. However, the deletion errors are increased, compared to the estimation performance of the method with the lower probability threshold (P=0.5, in the left sub-image of Figure 9.15).

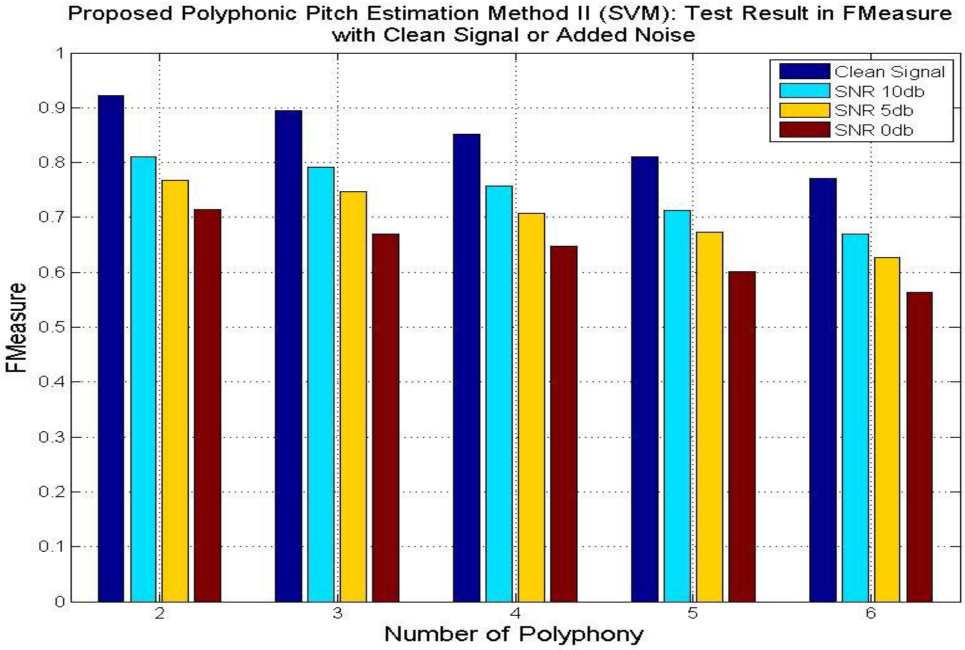

Figure 9.9, F-Measure of Test Results of Method II (SVM) with Clean Signal or Added Noise

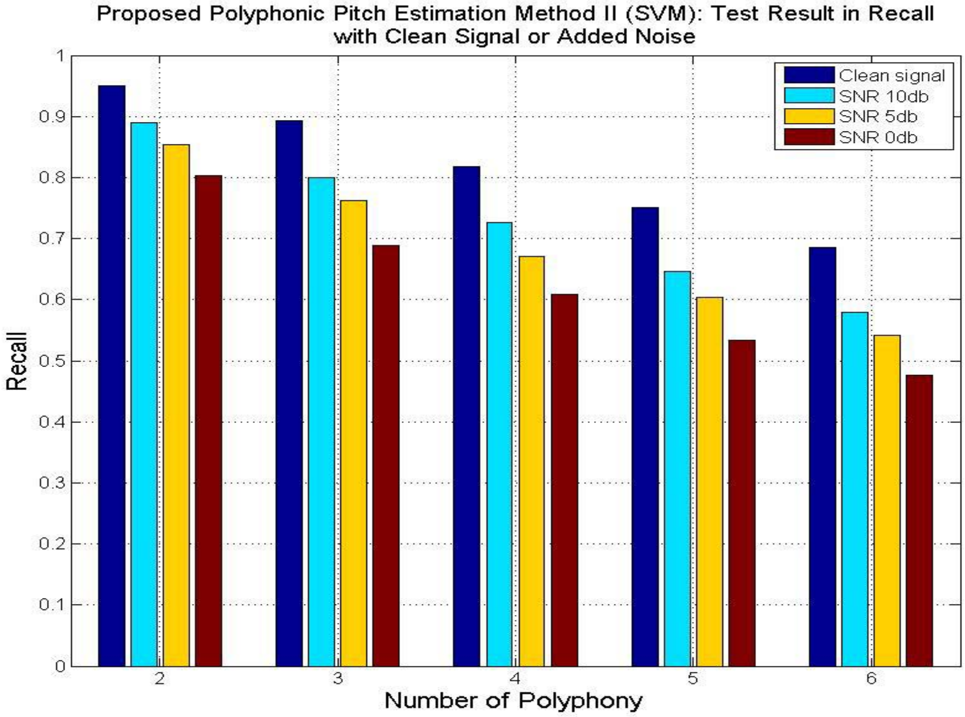

Figure 9.10, Recall of Test Results of Method II (SVM) with Clean signal or Added Noise

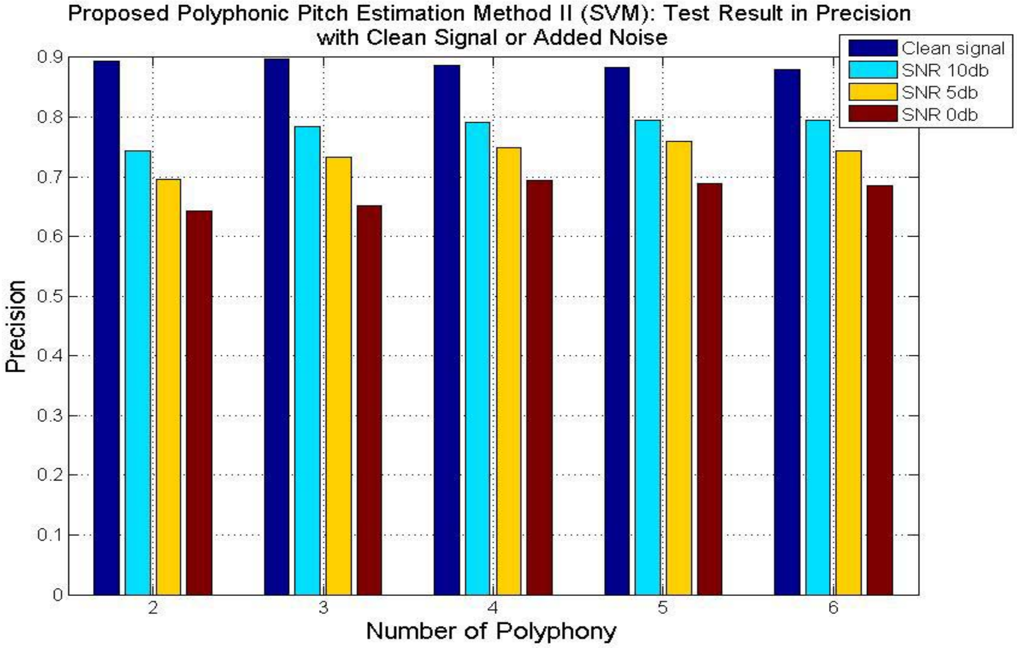

Figure 9.11, Precision of Test Results of Method II (SVM)
with Clean signal or Added Noise

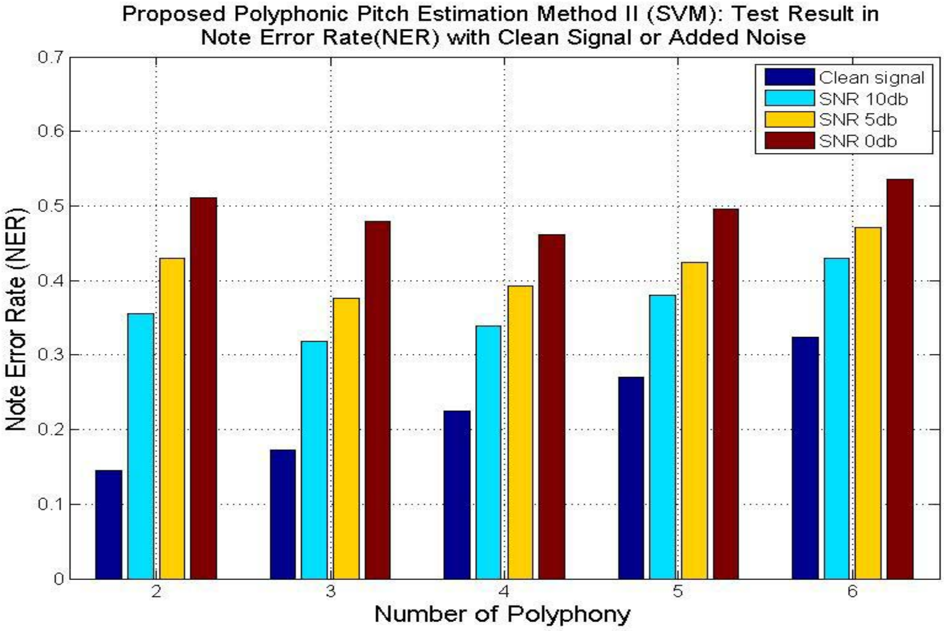

Figure 9.12, Note Error Rat (NER) of Test Results of Method II (SVM) with Clean signal or Added Noise

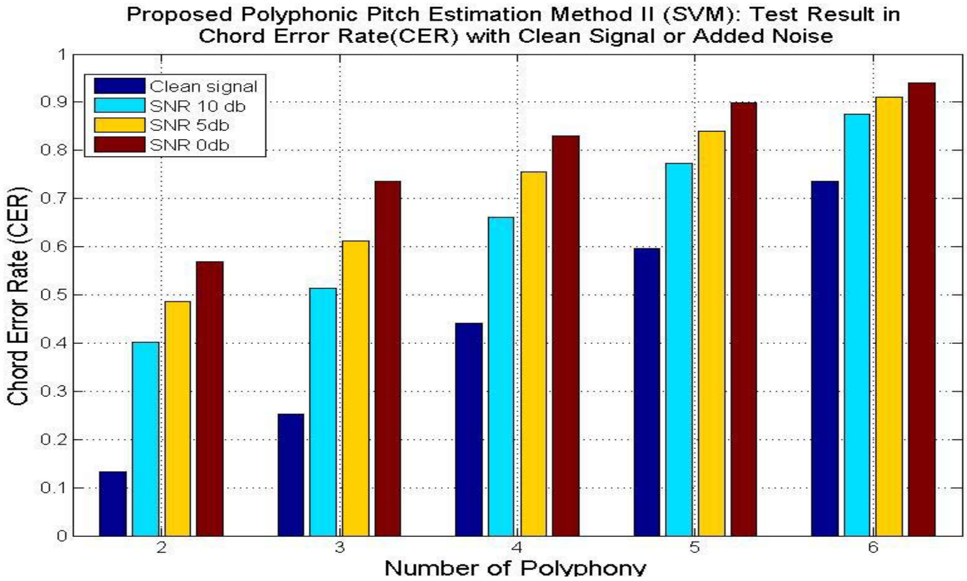

Figure 9.13, Chord Error Rate (CER) of Test Results of Method II (SVM) with Clean signal or Added Noise

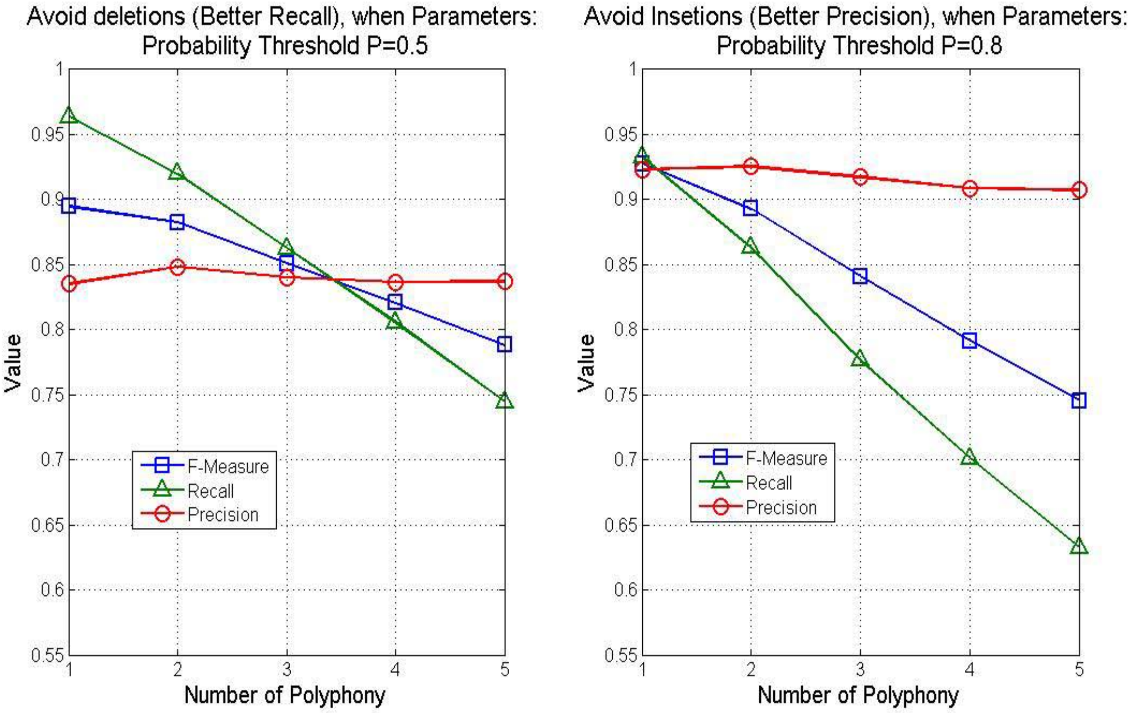

Figure 9.14, F-Measure, Recall and Precision of Test Result of Method II (SVM) with different parameter values

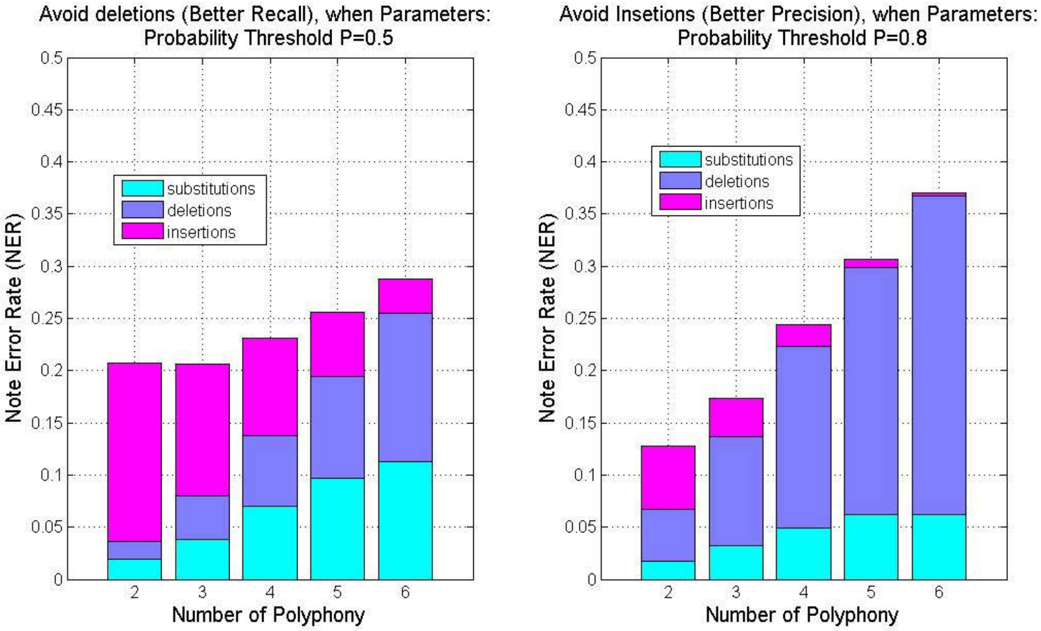

Figure 9.15, Note Error Rate (NER) of Test Result of Method II (SVM) with different parameter values

9.4 Automatic Music Transcription Systems

In order to test the estimation performance of the two proposed methods on the real music excerpts, the automatic music transcription prototype systems have been constructed with the combination of the proposed music onset detection algorithms (introduced in Chapter 5) and polyphonic pitch estimation methods. The goal of the transcription system is to detect the music notes occurring and their onset time. The sampling rate of input music signal is 44100 Hz. The onset detection algorithms are first used to separate the input real music signal into different segments according to the detected note onsets, and then pitches in each segment are estimated by the two proposed polyphonic pitch estimation methods. Finally, every estimated pitch in a certain segment must be checked if the pitch begins from a current segment or from the previous segments. For a certain segment N, if a pitch A with fundamental frequency f is estimated; then if the estimated pitches in the previous segment N-1 do not contain the pitch A, the transcription system will consider that this pitch A is a new occurring pitch in the segment N. In another case when the estimated pitches in the previous segment N-1 also contain the pitch A, then this pitch A is considered to be a new occurring pitch only on the condition that the corresponding energy spectrum of the pitch A's first or second harmonic component has been obviously increased at the starting moment of the segment N. Figure

9.16 shows the overview of an automatic music transcription system using the proposed polyphonic pitch estimation I.

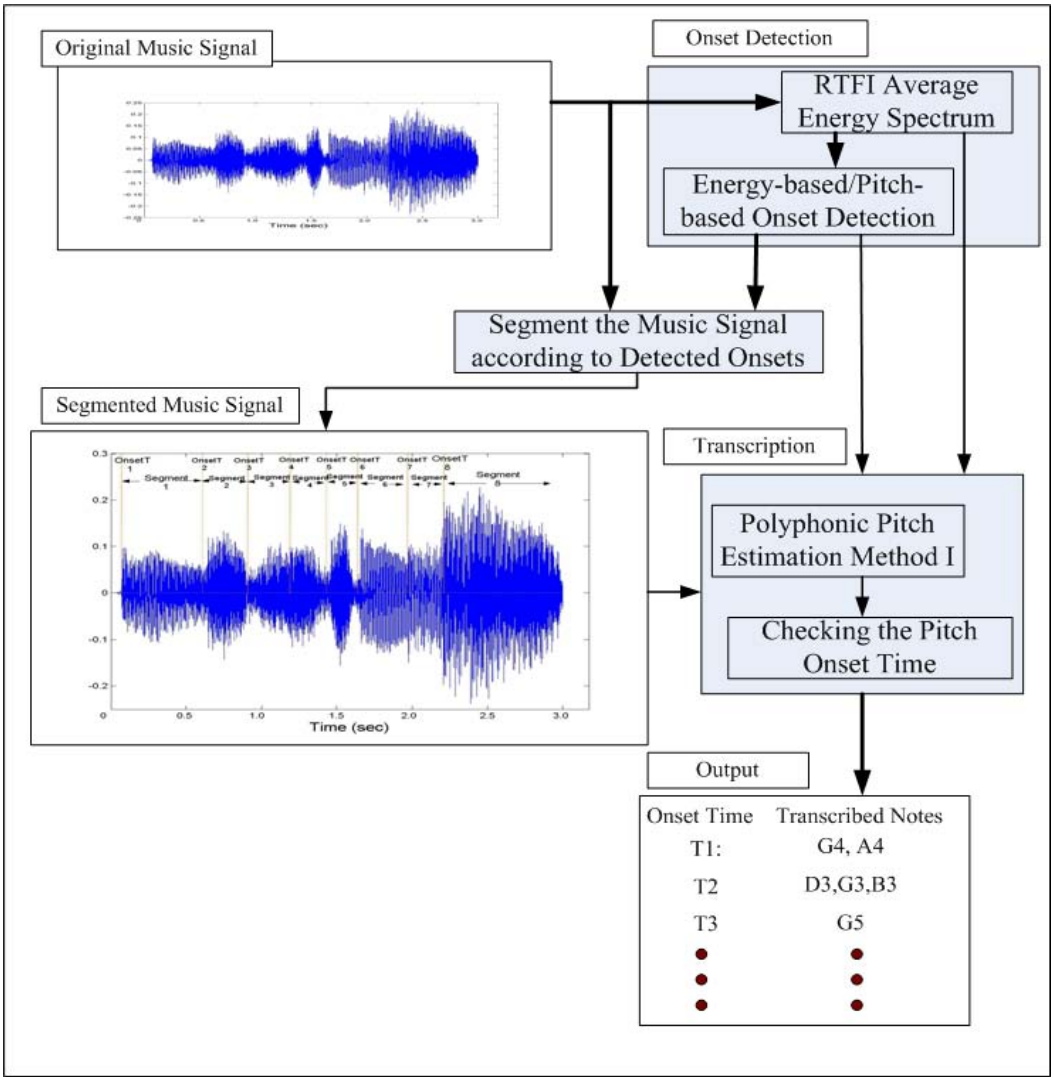
Original Music Signal
Onset Detection
RTFI Average Energy Spectrum
Energy-based/Pitch-based Onset Detection
Segment the Music Signal according to Detected Onsets
Segmented Music Signal
Transcription
Polyphonic Pitch Estimation Method I
Checking the Pitch Onset Time
Output
Onset Time
Transcribed Notes
T1:
G4, A4
T2
D3,G3,B3
T3
G5
Time (sec)
0.3
0.2
0.1
0
-0.1
-0.2
0.5
1.0
1.5
2.0
2.5
3.0
OnsetT
Segment

Figure 9.16, Automatic Music Transcription System Using the Proposed Polyphonic Estimation Method I

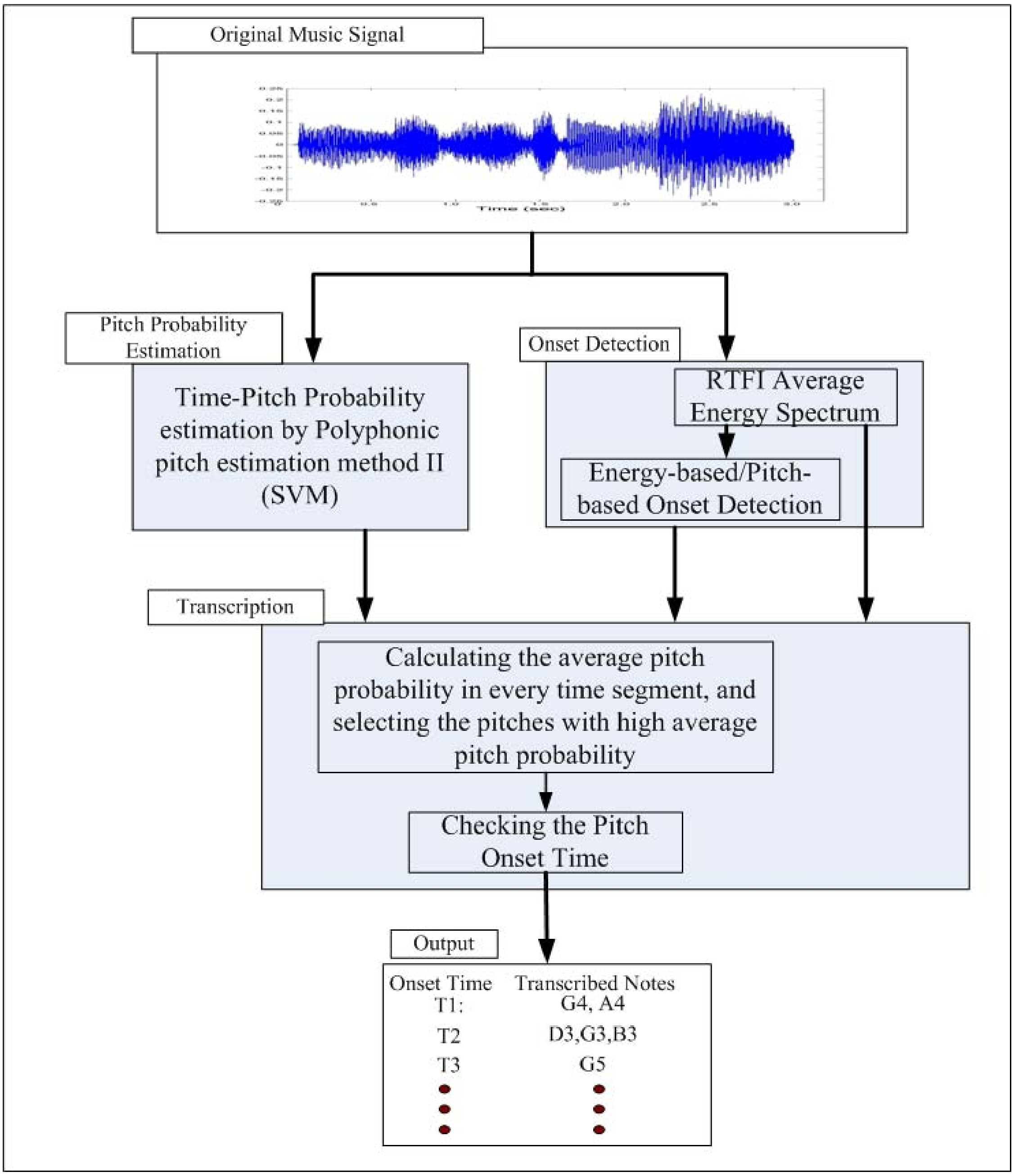
Original Music Signal
Time (sec)
Pitch Probability Estimation
Time-Pitch Probability estimation by Polyphonic pitch estimation method II (SVM)
Onset Detection
RTFI Average Energy Spectrum
Energy-based/Pitch-based Onset Detection
Transcription
Calculating the average pitch probability in every time segment, and selecting the pitches with high average pitch probability
Checking the Pitch Onset Time
Output
Onset Time
Transcribed Notes
T1:
G4, A4
T2
D3,G3,B3
T3
G5

Figure 9.17, Automatic Music Transcription System Using the Proposed Polyphonic Estimation Method II (SVM)

Figure 9.17 gives an overview of an automatic music transcription system using the proposed SVM polyphonic estimator. As shown in Figure 9.17, in the first phase, the note onsets are detected from the input music signal using the proposed onset detection algorithms (introduced in Chapter 5), and the SVM polyphonic estimator is used to produce the time-pitch probability (TPP) estimation.

For a given discrete music signal s(n) at a sampling rate 44100 Hz, the time-pitch probability estimation can be produced as follows:

$$F_T(n) = s(n + T \cdot 441), n = 1,2,3,...L \quad (9.1)$$

$$\begin{aligned} &TPP\ (k,T) = SVME\ (F_T), \\ &k = 21,22,23 \ldots 108, \qquad (9.2) \\ &T = 1,2,3,... \end{aligned}$$

In the above equations, F_T denotes an extracted signal frame beginning at the instant T_{th} in units of 0.01 seconds from the input music signal s(n) , and the duration time of the signal frame is equal to L/44100 seconds. As mentioned before, given a music signal frame, the SVM polyphonic estimator can estimate the probability that every music note occurs in the music signal frame. In the equation 9.2, k denotes the MIDI note number; the unit of the T is equal to 0.01 seconds; SVME denotes the SVM polyphonic estimator that estimates the occurring probability of 88 different music notes (from A0 to C8, in MIDI notation from 21 to 108) in the signal frame F_T, and produces a two-dimension time-pitch probability estimation TPP(k, T). For example, if the parameter L=11025, the calculated value of the TPP(60, 100) denotes the estimated probability that music note 60 occurs in segment [1sec, 1.25sec] of input music signal. Figure 9.18 illustrates the time-pitch probability output of a piano music example. In the Figure, the horizontal axis denotes time, and the vertical axis is for the 88 different music notes. The colour denotes the probability output.

As shown in Figure 9.17, in the second phase, the produced time-pitch probability (TPP) estimation and detected onset information are used for transcription. This transcription process can be expressed as follows:

Given the detected onset time: OT(m) ,m=1,2,3,... and the time-pitch probability estimation TPP(k,T), k=21,22,23,...,88, T=1,2,3,..., the time unit of both T and the detected onset time OT(m) is 0.01 second, the average time-pitch probability(ATPP) at the onset time OT(m) can be calculated as follows:

$$ATPP_{OT(m)}(k) = \frac{1}{OT(m+1) - OT(m)} \sum_{T=OT(m)}^{OT(m+1)} TPP(k,T)$$

If $ATPP_{OT(m)}(k)$ *is greater than a threshold, then the transcription process considers that the note k is a candidate which occurs at the onset time OT(m). Finally, every note candidate will be checked if it occurs in this onset time. The checking method is the same as one described in the beginning of this section.*

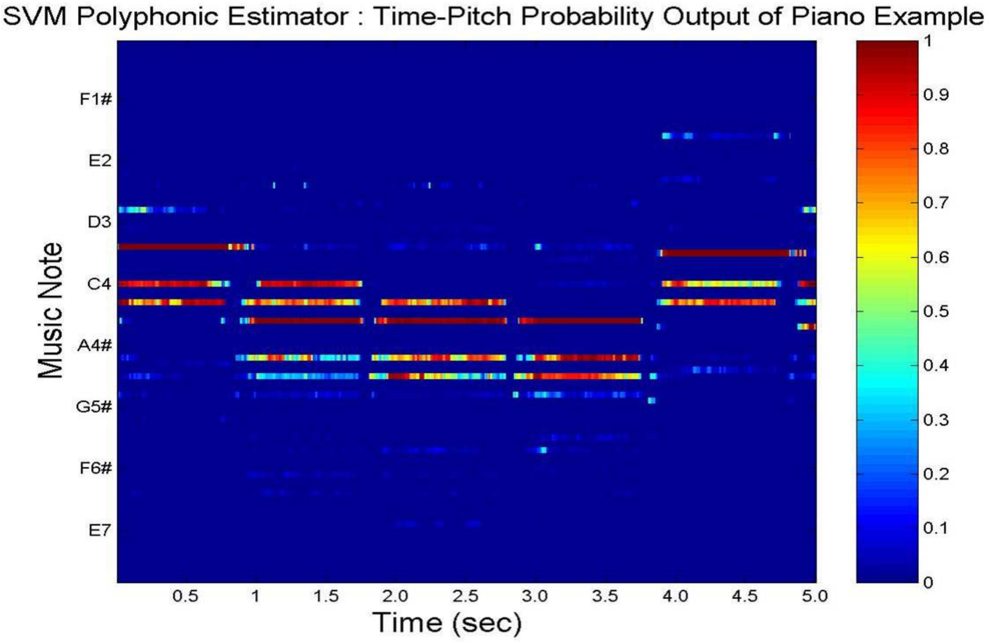

Figure 9.18, Time-Pitch Probability Output of a Piano Example

9.5 Results on the Real Music Excerpts

Using the two automatic music transcription prototype systems, the proposed two polyphonic pitch estimation methods have been tested on the real music excerpts. The test results are listed in the table 9.2.

Table 9.2 : Test Result fromTest Database 2 (Real Music Excerpts)

				Result of Proposed Polyphonic Pitch Estimation Method I			**Result of Proposed Polyphonic Pitch Estimation Method II (SVM)**		
#	Title	**Note Num**	**Average Poly**	**F-Measure**	**Precision**	**Recall**	**F-Measure**	**Precision**	**Recall**
1	Chuggin	**83**	**1.9**	**61%**	**67%**	**55%**	**53%**	**58%**	**49%**
2	Beethoven, <Egmont> Overture, op.84	**92**	**3.0**	**81%**	**89%**	**73%**	**51%**	**55%**	**48%**
3	Mozart, Rondo in D major, K.485	**261**	**1.6**	**74%**	**87%**	**65%**	**57%**	**52%**	**64%**
4	Haydn, String Quartet no.77 in C major	**137**	**2.8**	**71%**	**76%**	**66%**	**65%**	**63%**	**67%**
5	Tchaikovsky, String Quartet no.1 in D major	**108**	**2.5**	**67%**	**72%**	**62%**	**58%**	**59%**	**57**
6	Beethoven, Piano Sonata No 26 in E-flat major	**132**	**1.6**	**77%**	**76%**	**78%**	**67%**	**62%**	**69%**
Average				**72%**	**78%**	**67%**	**60%**	**59%**	**59%**

Compared to method II (SVM), method I performs better both on real music excerpts and polyphonic mixtures with different level noises.

The comparison with the other polyphonic pitch estimation methods is a difficult task because there is no standard and public distributed test database. Klapuri proposed a polyphonic pitch estimation method and achieved excellent results in this field. Here the performances of the proposed two polyphonic pitch estimation methods are compared to the Klapuri method that is introduced in section 6.2.4. It is emphasized that the comparison is approximate because the test database is similar, but not entirely the same.

For real music excerpts, the two proposed estimation methods perform much better than Klapuri's method. The results are listed in Table 9.3. When estimation methods employ a strategy of avoiding insertions, the proposed method I and Klapuri's method have approximate performances on the clean polyphonic mixtures, and Note Error Rates (NER) are listed in Table 9.4. When estimation methods employ a strategy of avoiding deletions, the proposed two methods have better performances than Klapuri's method, and the corresponding Note Error Rates (NER) are listed in Table 9.5.

Table 9.3: Recall and Precision of Different Methods on Testing Real Polyphonic Music Excerpts

Evaluation Rule	Proposed Method I	Proposed Method II (SVM)	Klapuri's Method [Ryyn05]
Average Recall	**67%**	**59%**	**39%**
Average Precision	**78%**	**59%**	**41%**

Table 9.4: Note Error Rate (NER) of Different Methods on Testing Polyphonic Mixtures (Avoiding Deletions)			
Number of Polyphony	**Proposed Method I**	**Proposed Method II (SVM)**	**Klapuri's Method** [Klapuri03]
2	12%	20%	14%
3	13%	20%	16%
4	16%	23%	18%
5	23%	26%	22%
6	30%	29%	32%

Table 9.5: Note Error Rate (NER) of Different Methods on Testing Polyphonic Mixtures (Avoiding Insertions)			
Number of Polyphony	**Proposed Method I**	**Proposed Method II (SVM)**	**Klapuri's Method** [Klapuri03]
2	9%	13%	18%
3	16%	17%	22%
4	25%	24%	27%
5	30%	30%	35%
6	41%	37%	41%

Chapter 10

CONCLUSION AND FUTURE WORK

10.1 Conclusion

10.1.1 An Original Time-Frequency Analysis Tool: Resonator Time-Frequency Image (RTFI)

Most of the music related tasks need a joint time-frequency analysis because a music signal varies with time. Chapter 2 provides an exhaustive summary of previous approaches to music signal time-frequency analysis. The existing time-frequency analysis approaches show some serious limitations for application in music signal processing. With a clear mathematical description, Chapter 4 formulates a new frequency-dependent time-frequency representation (TFR): RTFI, which is especially designed for music signal processing. A fast multi-resolution implementation of RTFI has also been proposed. As examples of practical application, all proposed methods for music onset detection and polyphonic pitch estimation in this thesis successfully exploit RTFI as the basic time-frequency analysis tool. Using the RTFI, one can select different time-frequency resolutions, such as uniform analysis, constant-Q analysis, or ear-like analysis by simply setting several parameters; and letting the RTFI generalize all these analyses in one framework.

10.1.2 Music Onset Detection

In this thesis, two music onset detection algorithms have been proposed - an energy-based detection algorithm and a pitch-based detection algorithm. Both algorithms employ the RTFI as the time-frequency analysis tool.The note onsets of the music signal can be classified into “soft” or “hard” onsets. With an appropriate time-frequency resolution, the proposed Energy-based detection algorithm works well for the music signal with hard onsets, and shows a better performance than the other existing algorithms. However, the Energy-based detection algorithm exhibits very low performance for the detection of soft onsets. In some real-life music signals with soft onsets, the energy-change in the note transition may be not noticeable. At the same time, for some music signals, the noticeable energy-change does not necessarily exist only in note transitions, but also in the stable part of the music notes. In this case, an energy-based detection algorithm probably is misdirected by such a noticeable energy change in the stable part and will cause many false positives in the detection results. This is an important reason that an energy-based detection algorithm shows very low performance on the detection of soft onsets. On the one hand, pitch change is the most salient clue for note onset detection of the music signal with soft onsets. On the other hand, most existing onset detection algorithms are based on the energy-change and/or phase-change evidence, because it is still very difficult to track a pitch change in real polyphonic music. In this thesis, I propose a Pitch-based onset detection algorithm. This Pitch-based detection algorithm is the first one, which successfully exploits the pitch change clue for onset detection in real polyphonic music, and achieves a much better performance than the other existing detection algorithms. The detailed descriptions of the two proposed onset detection algorithms can be found in Chapter 5.

10.1.3 Polyphonic Pitch Estimation

In this thesis, two polyphonic pitch estimation methods have been proposed. Polyphonic pitch estimation can be considered to be a core problem in automatic music transcription.

Based on the RTFI analysis, proposed method I primarily exploits the harmonic relation and spectral smoothing principle. The test result indicates that method I can perform well for different music sounds even if there is no available priori knowledge of these sounds. For real music excerpts, proposed method I performs better than other existing methods. A comparison of the results can be found in Table 9.3 of Chapter 9.

The proposed estimation method II involves the transformation of polyphonic pitch estimation to a pattern recognition problem. The method uses a signal processing block followed by a learning machine. Multi-resolution fast RTFI analysis is used as a signal processing component, and a support vector machine (SVM) is selected as the learning machine. The method II has a lower performance when used for real music excerpts and polyphonic mixture with the added noise. However method II is simpler and has greater potential for improvement. The possible improvement of this method is described in the following section. Another advantage of method II is its probability output, which is useful for some applications.

The detail description of the two proposed polyphonic pitch estimation methods can be found in Chapters 7 and 8.

10.2 Future Work

This section explores several interesting directions of future research by extending the work presented in the thesis.

10.2.1 Special-Purpose SVM Polyphonic Estimator

In this thesis, the goal was to develop a general-purpose polyphonic estimator that is not limited to one or several musical instrument sounds. When musical instruments of the analyzed polyphonic music sequence are known in advance, it may be better to run the polyphonic pitch analysis by a special-purpose SVM polyphonic estimator, which is trained with samples only of the corresponding instruments. For example, it may happen (and it is rather intuitive) that a better performance can be obtained by having an estimator, who was trained only with piano samples, undertake the polyphonic pitch analysis of piano music. Some preliminary experiments have been made. In these experiments, a single instrument SVM polyphonic pitch estimator was trained for piano, guitar and violin. The experimental results indicate that a special-purpose estimator performs better than does a general-purpose estimator, when the music instrument of the tested polyphonic mixtures corresponds to that used to train the special-purpose polyphonic estimator. In future work, the use of a special-purpose polyphonic estimator can be extended to different combinations of several instruments. Additionally, it may be better that training samples are extracted from the real music signal. For example, standard string quartet music is often played by violin, cello and viola, and a special-purpose polyphonic estimator for the string quartet music can be trained only with the polyphonic samples, which have been extracted from real string quartet music played by violin, cello and viola.

10.2.2 Using Temporal Features for Polyphonic Pitch Estimation

In the proposed polyphonic pitch estimation methods, the temporal features are not exploited for the estimation. The proposed pitch estimation I may be improved by utilizing the temporal features. In method I, the RTFI analysis can provide information about how the different frequency components of the analyzed signal evolve over time. This temporal information is useful for polyphonic pitch estimation. The harmonic components from the same instrument sound source often have some similar temporal features, such as a common onset time, amplitude modulation and frequency modulation. In the future, improvement, to the proposed estimation method I can make use of the temporal features, and harmonic relative frequency components with similar temporal features should be considered as a new note with more probability than the harmonic relative frequency components with different temporal features.

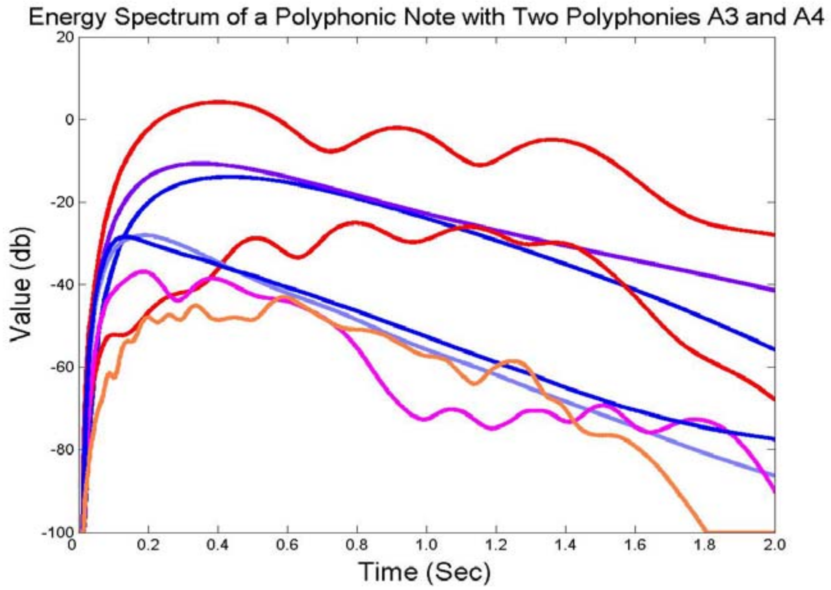

Figure 10.1 Energy Changes of Harmonic Components

For example, an analyzed polyphonic note consists of two polyphonies A3 and A4 The note A3 is played by piano and the note A4 is played by violin. It is very difficult to make a polyphonic estimation for this case, because the harmonic components of A4 are completely overlapped by the even harmonic components of A3. However, such a difficult case may become resolved by using the temporal feature. As shown in Figure 10.1, the blue lines denotes first four odd harmonic components of the note A3, and the red/magenta lines denotes the first four even harmonic components of the note A3. In Figure 10.1, it can be clearly seen that the energy spectrums of the first four even harmonic components have different temporal features than the first four odd harmonic components. This difference indicates that the even harmonic components probably are shared with another musical note A4 played by a different music instrument.

10.3 Potential Commercial Applications

An automatic music transcription system can transform recorded sound to symbolic representations, which represents important high-level features. These have some important applications. For example, the transcription system can be used as a tool to assist in music composition. A composer may play a new music piece by some music instruments, such as piano or guitar, and then obtain the corresponding musical score with the help of an automatic music transcription system. Another huge potential commercial application for transcription systems consists of Karaoke fans. The singing voice of a Karaoke fan can be recorded by a microphone. Then, the music transcription system can transform the singing voice to a musical score, which can be compared to a reference musical score of the song. The difference can be shown to the Karaoke fan to help him/her to improve his/her singing skill.

Automatic music transcription is such a difficult task that a practical general-purpose transcription system is not available at the present time. Although a few commercial transcription systems can be found in the market, the performance of the systems are not satisfactory, and the accuracies of the transcriptions are very low [Akoff01 Araki03 Innov04].

With future further improvements, the proposed onset detection algorithms and polyphonic pitch estimation methods will become very promising for commercial applications. The results of this thesis work clearly demonstrate progress. In total, the proposed solution to automatic music transcription is more systematic. Both the proposed onset detection and polyphonic estimation methods select RTFI as the same time-frequency analysis tool. The RTFI is implemented by the simple first-order complex resonator filter bank and is computation-efficient, whereas the simplicity also makes it possible to implement the faster RTFI in the future work.

The main goal of the thesis is to develop new methods for automatic music transcription. However, the original contributions in the thesis also have some other potential applications.

Firstly, the proposed RTFI can be employed as a more general time-frequency analysis tool for applications that require frequency-dependent time-frequency analysis. In other words, the RTFI is not limited only to music signal analysis, but can be extended to some other applications. The RTFI can be implemented more quickly by software and hardware optimization, and become a convenient and general time-frequency analyzer for commercial applications.

Secondly, the proposed methods can be used to extract the musical features and support content-based music retrieval. The available commercial sound retrieval systems are mainly allowing users to search only by some text criteria, such as title, name of composer, date of production, which are stored in the content header or associated descriptor. Although this approach has proven to be useful and is widely accepted, it does not make the best use of plentiful sound resources. The challenge is to develop more “intelligent” new technologies to support content-based sound and music descriptions and retrieval, which combine coding, storage and further human-like interactions. Such a system can be used to describe and retrieve sounds and music based on features, such as tempo, rhythm, melody, harmonic progression etc. For example, the user (or a higher level application) queries for piano solo waltz. The system can seek a song or composition by comparing the requirements with stored descriptions.

Thirdly, automatic music transcription can also be used to assist the high-bit rate compression coding for music signals. The easiest and still most common way to describe digital audio content is by waveform sampling encoded in pulse code modulation (PCM). This way of representing sound does not assume any “model” behind the coded signal. If the signal is represented assuming a model in it, that representation is said to be structured. The definition of a model makes assumptions about the nature of the sound and consequently defines the parameter space of the model. The more the signal can be represented by a small number of parameters. The more: the sound is structured. The more structured coding provides a higher compression ratio. As proposed in MPEG-4 audio coding, the MPEG-4 general audio coding toolset provides low-structured representations, such as perceptual coding, and the MPEG-4 Structured Audio (SA) provides a low-bitrate compression coding scheme by high-structured representations. However, in order to efficiently exploit the Structured Audio coding for music signals, two key problems must be resolved in the future. One is to define precise instrument models for a music signal. Another problem will be to automatically extract the parameter representation, such as music scores. The solution to the latter problem depends mainly on the development of automatic music transcription. The low-bitrate Structured Audio compression coding of music signals has broad practical applications. Thus, there is a large potential commercial market to develop for automatic music transcription for assisting the low-bitrate compression coding of music signals.

REFERENCES

[Akoff01] Akoff Sounds Lab, *Wav To Midi Converter Software*, 2001
URL : http://www.akoff.com/

[Araki03] Arakisoftware, *Wav To Midi Converter Software*, 2003
URL : http://www.pluto.dti.ne.jp/~araki/amazingmidi/

[Bello00] Bello J.P , Moti G. , Sandler M.B, *"Techniques for Automatic Music Transcription."* International Symposium on Music Information Retrieval (ISMIR), Plymouth, Massachusetts, USA.

[Bello03] Bello J.P , *"Towards the automated analysis of simple polyphonic music: a knowledge-based approach."* PhD thesis, Department of Electronic Engineering, Queen Mary, University of London , 2003.

[Bello03A] Bello J.P , Sandler.M, *"Phase-based note onset detection for music signals."* In Proceeding of IEEE International Conference of Acoustics, Speech, and Signal Processing (ICASSP-03), 2003

[Bello04] Bello J.P , Duxbury.C, Sandler.M, *"On the use of phase and energy for music onset detectionin the complex domain."* Journal of IEEE Signal Processing Letters Vol.11, No.6, June 2004.

[Bross05] Brossier.P.M, *" Fast onset detection using AUBIO(Brossier),MIREXx005"*
http://www.music-ir.org/evaluation/mirex-results/articles/all/short/brossier2.pdf

[Chang01] Chang.C.C, Ling C.J *"LIBSVM: a library for support vector machines"*
http://www.csie.ntu.edu.tw/~cjlin/libsvm

[Cohen96] Cohen, A Kovacevic *"Wavelets: the mathematical background"* Proceedings of the IEEE Volume 84, Issue 4, Page(s):514 – 522, April 1996

[Collins05] Collins.N, *"A change discrimination onset detector with peak scoring peak picker and time domain correction"* http://www.music-ir.org/evaluation/mirex-results/articles/onset/collins.pdf

[Collins05A] Collins.N, *"Using a pitch detector as an onset detector"* In Proceeding of International Conference of Music Information Retrieval, September,2005.

[Cortes95] Cortes.C, Vapnik .V *"Suppport-Vector networks"* Machine Learning 20 , Page(s),273-297

[Crist00] Nello Cristianini, John Shawe-Taylor *"An Introduction to Support Vector Machines and other Kernel-based Learning Methods*" Cambridge University Press, 2000.

[Daub92] Daubechies , *Ten Lectures on Wavelet., 2nd ed* Philadelphia: SIAM, 1992

[Doug92] Jones, D.L.; Parks, T.W. "*A resolution comparison of several time-frequency representations*" Signal Processing, IEEE Transactions on Volume 40, Issue 2, Feb. 1992 Page(s):413 – 420

[Dono05] J.J.O'Donovan, Dermot J.Furlong: *"Perceptually motivated time-frequency Analysis "* J. Acoust. Soc. Am. **117** (1), January 2005 page(s) 250-262

[Dorf01] M.Dörfler: *"Time-Frequency Analysis for Music Signals, a Mathematical Approach"* Journal of New Music Research, Vol 30/1, March 2001

[Duxb02] Duxbury.C, Sandler.M, Davis.M *"A hybrid approach to musical note onset detection"* In Proceeding of DAFx International Conference, 2002.

[Grim02] M. Grimaldi, P. Cunningham, A. Kokaram, *"Classifying Music by Genre Using the Wavelet Packet Transform and a Round-Robin Ensemble"* Trinity College, Dublin, CS Dep., Technical Report, TCD-CS-2002-64, November 2002. (https://www.cs.tcd.ie/publications/tech-reports/reports.02 /TCD-CS-2002-64.pdf)

[Gold 73] Goldstein.J. "*A optimum processor theory for the central formation of the pitch of complex tones* " The Journal of the Acoustical Society of America, Vol 54,No.6, pp.1496-1515, 1973.

[Goto01] Goto.M, *"An audio-based real-time beat tracking system for music with or without drum-sounds",* Journal of New Music Research, Vol 30, No 2, pp. 159-171, 2001

[Goto03] Goto.M, *"RWC Music Database : Music genre database and musical instrument sound database",* In Proceeding of the 4th International Conference on Music Information Retrieval, 2003

[Fried96] J.Friedman *"Another approach to polychotomoous classification"* JTechnical report, Department of Statistics, Stanford University,1996.

[Hains01-1] Hainsworth, S.W.; Macleod, M.D.; Wolfe, P.J. "*Analysis of reassigned spectrograms for musical transcription*" Applications of Signal Processing to Audio and Acoustics, 2001 IEEE Workshop on the 21-24 Oct. 2001 Page(s):23 – 26

[Hains01-2] Hainsworth, S.W.; Macleod, M.D.; Wolfe, P.J. "*Time-frequency Reassignment of Music Analysis* " Proceedings of Computer Music 2001 Page(s) 14-17

[Hart97] Willam M. Hartmann, *Signal, Sound and Sensation,* American Institute of Physics Press, 1997

[Hast96] Trevor Hastie, Robert Tibshirani " *Classification by Pairwise Couples*" Technical Report, Stanford University and Toronto University,1996.

[Hlaw92] Hlawatsch, F.; Boudreaux-Bartels, G.F "*Linear and quadratic time-frequency signal representations*" Signal Processing Magazine, IEEEVolume 9, Issue 2, April 1992 Page(s):21 – 67

[Hsu] Hsu.C.W, Chang.C.C,Lin.C.J "*A practical guidde to support vector machine classification*" available at http://www.csie.ntu.edu.tw/~cjlin/libsvm

[Irino97] Irino.T, Patterson.R.D *"A time-domain, level-dependent auditor filter: The gammachirp"* Journal of the Acoustical Society of America, Vol.101, pp.412-419,1997.

[Jang05] Jang, H.K., and Park, J. S. *"Multiresolution Sinusoidal Model with Dynamic Segmentation for Time-scale Modification of Polyphonic Audio Signals,.*" IEEE Trans. on Speech and Audio Signals, Vol. 13, No. 2, pp. 254-262, March 2005

[Jone04] Jones, D.L.; Parks, T.W. "*Wavelets for sparse representation of music* " A Web Delivering of Music WEDEL MUSIC 2004 Proceedings of the Fourth International Conference on 2004 Page(s):10-14

[Klapuri99] Klapuri.A, *"Sound onset detection by applying psychoacoustic knowledge.*" In Proceeding of IEEE Conference of Acoustics, Speech and Signal Processing (ICASSP 99).

[Klapuri03] Klapuri.A, *" Multiple fundamental frequency estimation bas d on harmonicity and spectral smoothness.*" IEEE Transactions On Speech And Audio Processing, Vol. 11, No,6, pp. 804-816

[Klapuri04] Klapuri.A, *" Signal Processing Method for Automatic Music Transcription.*" PhD thesis, Tampere University of Technology, 2004

[Keren98] Keren, R.; Zeevi, Y.Y.; *"Multiresolution time-frequency analysis of polyphonic music.*" Chazan, D.;Time-Frequency and Time-Scale Analysis, 1998. Proceedings of the IEEE SP International Symposium on 6-9 Oct. 1998 Page(s):565 – 568

[Lacoste05] Lacoste.A, Eck.D *"Onset detection with artificial neural network* *forMIREX2005"*http://www.music-ir.org/evaluation/mirex results/articles/onset/lacoste.pdf

[Levine98] Levine.S.N,, *" Audio representations for data compression and compressed domain processing "* PhD thesis, Stanford University, CA,USA,1998.

[Mallat89] Mallat, S.G.; **"***A theory for multiresolution signal decomposition: the wavelet representation*" Pattern Analysis and Machine Intelligence, IEEE Transactions on Volume 11, Issue 7, July 1989 Page(s):674 - 693 Volume 84, Issue 4, April 1996 Page(s):514 – 522

[Maro01] Marolt. M "*A Neural network for note onset detection in piano music*" In Proceedings of International Computer Music Conference 2002.

[Maro04] Marolt. M " *A connectionist approach to automatic transcription of polyphonic piano music*," IEEE Transactions on Multimedia, vol. 6, no. 3, June 2004.

[Mallat98] Mallat S,A *Wavelet Tour of Signal Processing* San Diego, Academic Press, 1998.

[Meddis97] Meddis.R, O'Mard. "*A unitary model of pitch perception* " The Journal of the Acoustical Society of America, Vol. 102, No..3, pp.1811-1820, 1997.

[Mell00] M.Mellody G.H Wakefield, *" The Ttime-Frequency Characteristics of Violin Vibrato: Modal Distribution Analysis And Synthesis* ." Journal of Acoustical Society of America, Vol.107,no.1,page(s): 598-611, January ,2000

[Mirex05] Information available at http://www.musicir.org/mirex2005/index.php/Audio_Onset_Detection

[Mont00] Monti,G., Sandler *"Monophonic Transcription with Autocorrelation"* Proceedings of the COST G-6 Conference on Digital Audio Effects (DAFX '00), Verona, Italy 2000.

[Patterson94] Patterson.R.D. Robinson.K, Holdsworth.J, McKeown . D,Zhang.C,Allerhand.M, "*Complex sounds and auditory images* " Auditory physiology and perception, Proc. 9th International Symposium on Hearing, Oxford, page(s) 429-446, 1992

[Piel96] William J. Pielemeier, Gregory H. Wakefield, Mary H. SIMONl "*Time-Frequency Analysis of Music Signali*" Proceedings of the IEEE Volume 84, No.9. September 1996 Page(s):1216 – 1230

[Peet02] G. Peeters, A.L Burthe and Rodet X."*Toward automatic music audio summary generation from signal analysis*" Proc. ISMIR 2002, pp. 94-100 (2002).

[Pert04] A Pertusa, Iñesta J.M. "*Pattern Recognition algorithms for polyphonic music transcripiton*" Int. Workshop on Pattern Recognition in Information Systems, PRIS 2004. Porto, Portugal. pp. 80-89. ISBN: 972-8865-01-5.

[Pert03] Pertusa A, Iñesta J.M. "*Polyphonic music transcription through dynamic networks and spectral pattern identification*" IAPR International Workshop on Artificial Neural Networks in Pattern Recognition Florence, Italy, 2003. pp. 19-25.

[Pert05] Pertua.A, Klapuri.A,Inesta.J.M "*Note onset detection using semitone bands*"http://www.music-ir.org/evaluation/mirex-results/articles/onset/pertusa.pdf

[Platt99] John C .Platt "*Probabilistic outputs for support vector machines and comparisons to Regularized Likelihood Methods*" Advances in Large Margin classifiers, MIT Press, 1999.

[Plomp64] Plomp.R "*The ear as a frequency analyzer I*" The Journal of the Acoustical Society of America, Vol. 36,No.9, pp.1628-1636, 1964.

[Plomp68] Plomp.R , Mimpen, A.M "*The ear as a frequency analyzer II* " The Journal of the Acoustical Society of America, Vol. 43,No.4, pp.764-767, 1968.

[Qian99] Shie Qian; Dapang Chen "*Joint time-frequency analysis*" Signal Processing Magazine, IEEE Volume 16, Issue 2, March 1999 Page(s):52 – 67

[Ryyn05] Ryyndnen.P.M, Klapuri.A, "*Polyphonic music transcription using note event modeling*" Proceeding of IEEE Workshop on Applications of Signal Processing to Audio and Acoustics, October, 2005.

[Ster96] Steran.A, Wakefield.G.H, "*Robust Automated Music Transcription Systemss*" Proceeding of International Computer Music Conference, Hong Kong,1996.

[Srin98] Srinivasan, P.; Jamieson, L.H.*"High-quality audio compression using an adaptive wavelet packet decomposition and psychoacoustic modeling"* Signal Processing, IEEE Transactions on [see also Acoustics, Speech, and Signal Processing, IEEE Transactions on Volume 46, Issue 4, April 1998 Page(s):1085 –1093

[Slaney93] Slaney.M, "*An Efficient Implementation of the Patterson-Holdsworth Auditory Filters*" Apple Computer Technical Report #35, Perception Group, Advanced Technology Group, Apple Computer, 1993

[Vapnik99] Vapnik.V, book, "*The nature of statistical learning theory* " , Springer-Verlag, New York1999

[Yin05] Yin.J,Sim.T,Wang.Y, "*Music transcription using a instrument models*" Proceeding of IEEE International Conference on Acoustics, Speech, and Signal Processing, March, 2005

[Tzane01] George Tzanetakis, Georg Essl, Perry Cook *"Audio Analysis using the Discrete Wavelet Transform* " In. Proc. WSES Int. Conf. Acoustics and Music: Theory and Applications (AMTA 2001) Skiathos Greece, 2001.

[West98] J.Weston, C.Watkins, *"Multi-Class Support Vector Machines"* Technical Report CSD-TR-98=04, Department of Computer Science, Royal Holloway, University of London, Egham, Surrey TW20 0EX,England,1998.

[Wu04] Ting-Fan, Chih-Jen Lin, Ruby C. Weng, *"Probability Estimates for Multi-class classification by Pairwise Coupling"* In Journal of Machine Learning Research 5 (2004) 975-1005 , 2004.

[West05] West.K, *"Mel-filter integration for onset detection"*
http://www.musicir.org/evaluation/mirexresults/articles/all/short/west.pdf

CV

1.Personal Information

Name: RuoHua Zhou
Gender: Male
Date of Birth: Jan 12,1972
Place of Birth: Zongyang County, Anhui Province, China
Marital Status: Single
Nationality: China
E-Mail: Ruohua.Zhou@epfl.ch
Phone : 021-6936989
Address : EPFL STI ITS LTS3
School of Engineering
CH-1015 Lausanne-Switzerland

2.Educational Background:

Status: PhD Degree
University: Swiss Federal Institute of Technology (EPFL)
Specialty: Signal Processing
Period: 5 Years (2001.5-Present)
Place: Lausanne, Switzerland

Degree: Master of Engineering
Academy: Chinese Academy of Sciences, Microelectronics R&D Center
Specialty: Microelectronics and Semiconductor devices
Period: 3 Years (1994.9-1997.7)
Place: Beijing, China

Degree: Bachelor of Engineering
University: Beijing Institute of Technology Electronics Engineering Department
Specialty: Microelectronics
Period: 4 Years (1990.9-1994.7)
Place: Beijing, China

3:GRE Scores

Quantitative: 790/800
Analytical: 660/800
Verbal: 610/800

4. Training:

Oct 1997, Cadence SPW(a system level design tool) training

5: Honors and Scholarships:

Excellent student scholarship(1990) in Beijing Institute of Technology
Excellent student leadership(1992,1993) in Beijing Institute of Technology
President of Chinese Student and Scholar Association in Lausanne (2002-2003)

6. Research and Development Experiences:

Period: 2001.5-present
University: Swiss Federal Institute of Technology in Lausanne
Job Title: Research Assistant
Place: Lausanne Switzerland
Contribution:

- Developing an original time-frequency analysis tool, especially for music signal.
- Research in musical instrument recognition and automatic music transcription for polyphonic music with the combination of signal processing and artificial intelligence.
- Integrating some research results of sound analysis into CTI project STILE
- Software design and implementation of MPEG4 Encoder as one part of European Project(Carrouso).
- Developing MPEG4 Structured Audio Encoder and integrating with software/hardware components from the other partners of the project.
- Design of the Server supporting MPEG4 stream Multicast transmission by network.

Period: 2000.10-2001.4
Company: Motorola (China) Suzhou Design Center
Job Title: Software Engineer
Place: SuZhou, China
Contribution :

- Took part in the development of Motorola LCA (Low Cost Architecture) Project
- Designed the embedded software for a mobile phone. The software system

design is based on the basic idea, which separates complex software into different function layers in order to accelerate product development and reduce the software maintenance cost.

Period: 1998.12-2000.10
Company: Agilent (originally named Hewlett-Packard) Technologies Software Co. Ltd
Job Title: Software Engineer
Place: Beijing, China
Contribution:

- Took part in the development of the DTV Project and provided proposals for the project.
- Research of the OFDM technology
- Developed the audio library for HP-ADS (Advance Design System, a system design EDA tool similar to Cadence-SPW and Synopsis- COSSAP)
- Developed the DTV wireless transmission library, including DVB-T and ATSC on the HP-ADS. In the software libraries design, C++ is used to do algorithms model description and the system is simulated by the ADS. The R&D results can provide the customers the system level simulation environment for supporting the audio and wireless product development.

Period: 1997.7-1998.12
Company: Chinese Integrated Circuit Design Center
Job Title: IC design engineer
Place: Beijing, China
Contribution:

- Took part in the MPEG chip project. Responsible for audio decoder chip design. The C is used as description language to complete the algorithm and architecture design on the SPW, then VHDL is used as description language to complete the logic level simulation. In the simulation process, the VHDL and C Cosimulation technology is used to reduce the simulation time based on the SPW platform.
- Took part in the design of MPEG2 Video decoder chip logic level design, using the pipeline and parallel architectures to complete DCT block design.

Period: 1995.6-1997.6
Institute: Chinese Academy of Sciences, Microelectronics R&D Center
Job Title: Research Assistant
Place: Beijing, China
Contribution:

- The smart card application system design including hardware design, embedded software and database management system design. Developed the prototype smart card application system, which can be easily adapted to different applications, such as public transport electronics tickets, hotel electronics management and electronic bank.

7.Paper:

2005	Published	R. Zhou and G. Zoia **Polyphonic Music Analysis by Signal Processing and Support Vector Machines, 20-22 September 2005** Proceedings of the 8th Conference on Digital Audio Effects, Madrid, Spain, September 2005
2004	Published	G. Zoia, R. Zhou and D. Mlynek **MPEG A multi-timbre chord/harmony analyzer based on signal processing and neural networks** Multimedia Signal Processing,2004 IEEE, 6th workshop on 29 Sept-1 Oct.2004
2002	Published	G. Zoia, R. Zhou and M. Mattavelli **MPEG Audio Coding and XML: samples, models, descriptors** IEEE, Proceedings of the Int. Conference on Musical Applications Using XML, Vol. 1, pp. 3-10, September 2002
2002	Published	S. Battista, G. Zoia, A. Simeonov and R. Zhou **Hybrid Natural and Structured Audio Coding for 3D Scenes** IEEE, Proceedings of the 3rd ICME Conference, August 2002
2002	Published	G. Zoia, A. Simeonov, R. Zhou and S. Battista **Mixing Natural and Structured Audio Coding in Multimedia Frameworks** May 2002